



Publicly Accessible Penn Dissertations


2016

The Genetic, Molecular, And Cellular Bases Of Unidentified Primary Immunodeficiencies

Ian Lamborn

University of Pennsylvania, ianl@mail.med.upenn.edu

Follow this and additional works at: <https://repository.upenn.edu/edissertations>

 Part of the [Allergy and Immunology Commons](#), [Genetics Commons](#), [Immunology and Infectious Disease Commons](#), [Medical Immunology Commons](#), and the [Virology Commons](#)

Recommended Citation

Lamborn, Ian, "The Genetic, Molecular, And Cellular Bases Of Unidentified Primary Immunodeficiencies" (2016). *Publicly Accessible Penn Dissertations*. 2410.

<https://repository.upenn.edu/edissertations/2410>

This paper is posted at Scholarly Commons. <https://repository.upenn.edu/edissertations/2410>

For more information, please contact repository@pobox.upenn.edu.

The Genetic, Molecular, And Cellular Bases Of Unidentified Primary Immunodeficiencies

Abstract

The immune system is inseparable from every part of human biology. From cell intrinsic mechanisms of pathogen recognition to multi-cellular interactions over vast ranges of time and space, the immune system is both essential for protection from infection and central to the pathogenesis of many diseases. Thus understanding it has long been a focus of biomedical research. While in vitro molecular, biochemical, and cellular techniques as well as complex genetically modified animal models have been developed, these approaches still only approximate true human disease and in vivo human biology. Primary immunodeficiencies are inborn genetic defects of immunity and present rare opportunities to observe, study, and understand how genetic perturbations impact human immunity directly. I therefore clinically and genetically analyzed three patient families with unidentified primary immunodeficiencies. Using whole exome sequencing coupled with in vitro and in vivo biochemical and cellular assays, I identified two novel genetic etiologies of primary immunodeficiency. I first identified de novo missense mutations in *GNAI2*, the gene encoding the ubiquitously expressed heterotrimeric G-protein *Gai2*, in 2 families with life-threatening multi-organ system autoimmunity and immunodeficiency to mucocutaneous infections. *Gai2* is essential for chemokine mediated leukocyte migration as well as regulating development, inflammation, and metabolism in the immune system and beyond. The heterozygous dominant gain-of-function patient proteins impaired chemokine signaling and chemotaxis in addition to augmenting T cell activation by constitutively activating costimulatory pathways and reducing the requirement for T cell costimulation. I also identified homozygous missense mutations in *IFIH1*, the gene encoding the cytosolic pattern recognition receptor of dsRNA *MDA5*, in the third family of study. The affected individual presented with recurrent severe respiratory infections with RNA viruses including human rhinovirus, coronaviruses (HKU1, OC43, NL63), influenza virus, and respiratory syncytial virus. The mutant protein lost the ability to bind dsRNA and failed to initiate antiviral interferon- β and pro-inflammatory NF- κ B responses. Using gene knockdown and gene editing in immortalized and patient derived cell lines, I demonstrated an essential role for *MDA5* in restricting rhinovirus infection in human respiratory epithelium. Thus this work demonstrates the power of human genetics to identify disease causing mutations in rare individuals and reveal how the immune system uses molecules involved in cell migration, activation, and nucleic acid sensing to robustly protect us from virus infections without causing autoimmunity.

Degree Type

Dissertation

Degree Name

Doctor of Philosophy (PhD)

Graduate Group

Immunology

First Advisor

Helen C. Su

Second Advisor

Michael J. Lenardo

Keywords

Autoimmunity, Chemotaxis, GNAI2, Immunodeficiency, Interferon, MDA5

Subject Categories

Allergy and Immunology | Genetics | Immunology and Infectious Disease | Medical Immunology | Virology

THE GENETIC, MOLECULAR, AND CELLULAR BASES OF UNIDENTIFIED PRIMARY
IMMUNODEFICIENCIES

Ian T. Lamborn

A DISSERTATION

In

Immunology

Presented to the Faculties of the University of Pennsylvania
In

Partial Fulfillment of the Requirements for the
Degree of Doctor of Philosophy

2016

Supervisor of Dissertation

Helen C. Su, M.D., Ph.D.,
Chief of Human Immunological Diseases Unit,
Laboratory of Host Defenses,
National Institute of Allergy and Infectious
Diseases.

Co-Supervisor of Dissertation

Michael J. Lenardo, M.D.
Chief of Molecular Development
of the Immune System Section,
Laboratory of Immunology,
National Institute of Allergy and
Infectious Diseases

Graduate Group Chairperson

David M. Allman, Associate Professor of Pathology and Laboratory Medicine

Dissertation Committee

Sara Cherry, Ph.D., Associate Professor of Microbiology

Pamela L. Schwartzberg, M.D., Ph.D., Chief of Genetic Disease Research Branch, Cell Signaling
and Immunity Section, National Human Genome Research Institute

Avinash Bhandoola, M.B.B.S, Ph.D., Chief of T Cell Biology and Development Unit, Laboratory of
Genomic Integrity, National Cancer Institute

Dedication

To the patients and their families without whom none of this would be possible.

ACKNOWLEDGMENT

First, I would like to thank my PhD advisors, who guided me to pursue training as a physician-scientist and without whom nothing presented here would be a reality. I thank Dr. Helen Su for her constant devotion to me and my success. Years before I even began the work presented here, she invested in the potential she saw in me and continues to do so to this day. Shortly after meeting her I recognized her as a scientist, physician, and a person that I truly wanted to be like, and I feel that way now more than ever. I thank Dr. Michael Lenardo for his enduring enthusiasm and love of science, for maintaining the highest standards in everything he does, and valuing the quality of the scientists that ultimately emerge from his lab as much or more than he values the papers that emerge from it.

I would like to thank my colleagues in the Su and Lenardo labs, especially Huie, Jing, Yu Zhang, Helen Matthews, Qian Zhang, Carrie Lucas, Moses Murdock, and Hyoungjun Ham for being great colleagues and friends. It was a privilege to work with such intelligent and hardworking individuals and to share the same passion for science. I thank Dr. Huie Jing for patiently tolerating me in the lab and teaching me everything I know about practical aspects of executing an experiment. The amount of time and energy she invested in me and the work here is tremendous.

My training and my work have benefited tremendously from generous collaborations with other labs at the NIH and outside. I would like to thank Dr. Jean-Laurent Casanova for generously opening his laboratory and expertise to me, Dr. Michael Ciancanelli for being a patient and excellent teacher, and Dr. Yamina Berchiche for hours and hard work and being so willing and interested to talk through a scientific problem at anytime.

I would also like to thank my family, especially my parents. No words I could write here or anywhere could ever begin to thank them appropriately.

I would like to thank my friends for supporting me and having faith in me in all of my endeavors even when it means my time with them is lean.

And finally I'd like to thank God for the endless blessings He has showered upon me.

ABSTRACT

THE GENETIC, MOLECULAR, AND CELLULAR BASES OF UNIDENTIFIED PRIMARY IMMUNODEFICIENCIES

Ian T. Lamborn

Helen C. Su, M.D., Ph.D.

The immune system is inseparable from every part of human biology. From cell intrinsic mechanisms of pathogen recognition to multi-cellular interactions over vast ranges of time and space, the immune system is both essential for protection from infection and central to the pathogenesis of many diseases. Thus understanding it has long been a focus of biomedical research. While *in vitro* molecular, biochemical, and cellular techniques as well as complex genetically modified animal models have been developed, these approaches still only approximate true human disease and *in vivo* human biology. Primary immunodeficiencies are inborn genetic defects of immunity and present rare opportunities to observe, study, and understand how genetic perturbations impact human immunity directly. I therefore clinically and genetically analyzed three patient families with unidentified primary immunodeficiencies. Using whole exome sequencing coupled with *in vitro* and *in vivo* biochemical and cellular assays, I identified two novel genetic etiologies of primary immunodeficiency. I first identified *de novo* missense mutations in *GNAI2*, the gene encoding the ubiquitously expressed heterotrimeric G-protein $G\alpha_i2$, in 2 families with life-threatening multi-organ system autoimmunity and immunodeficiency to mucocutaneous infections. $G\alpha_i2$ is essential for chemokine mediated leukocyte migration as well as regulating development, inflammation, and metabolism in the immune system and beyond. The heterozygous dominant gain-of-function patient proteins impaired chemokine signaling and chemotaxis in addition to augmenting T cell activation by constitutively activating costimulatory pathways and reducing the requirement for T cell costimulation. I also identified homozygous missense mutations in *IFIH1*, the gene encoding the cytosolic pattern recognition receptor of dsRNA MDA5, in the third family of study. The affected individual presented with recurrent severe respiratory infections with RNA viruses including

human rhinovirus, coronaviruses (HKU1, OC43, NL63), influenza virus, and respiratory syncytial virus. The mutant protein lost the ability to bind dsRNA and failed to initiate antiviral interferon- β and pro-inflammatory NF- κ B responses. Using gene knockdown and gene editing in immortalized and patient derived cell lines, I demonstrated an essential role for MDA5 in restricting rhinovirus infection in human respiratory epithelium. Thus this work demonstrates the power of human genetics to identify disease causing mutations in rare individuals and reveal how the immune system uses molecules involved in cell migration, activation, and nucleic acid sensing to robustly protect us from virus infections without causing autoimmunity.

TABLE OF CONTENTS

Dedication	ii
ACKNOWLEDGMENT	iii
ABSTRACT	v
CHAPTER 1: Introduction	1
1.1 Nature’s experiments in immunology: Primary immunodeficiencies, a powerful lens for understanding the immune system	1
1.2 Combined Immunodeficiencies – T cells, B cells, and more	3
1.3 Approach to Understanding Inherited Defects of Immunity	4
1.4 A Note on Studying Individual Patients and Extremely Rare Diseases	8
1.5 Gαi2, Heterotrimeric G proteins, and Immunity	9
1.6 MDA5, Pattern Recognition Receptors, and Immunity	12
1.7 Figures	16
Figure 1.1 Forward genetics approach to identifying genetic causes of PIDs.....	16
CHAPTER 2 - Dominant-activating Gαi2 mutations cause human immunodeficiency and autoimmunity by defective leukocyte migration and altered T cell activation	17
2.1 Abstract	17
2.2 Introduction	17
2.3 Results	21
2.4 Discussion	32
2.5 Tables	37
Table 2.1 Patient Characteristics.....	37
2.6 Figures	38
Figure 2.1 <i>De novo</i> mutations at the active site of G α i2.	38
Figure 2.2 T182 G α i2 mutants are activated in multiple ways.	39

Figure 2.3 Activating Gαi2 mutants impair chemokine receptor signaling and chemotaxis.	40
Figure 2.4 Impaired GPCR coupling and GPCR induced activation of T182 Gαi2 mutants.	42
Figure 2.5 Gain-of-function Gαi2 augments T cell activation.	44
Figure 2.6 Activating Gαi2 mutants stimulate translational machinery.	45
Figure 2.7 Proposed model for the effects of activating mutations of Gαi2 on T cell chemotaxis and T cell activation.	46
2.7 Supplementary Figures	47
Supplementary Figure 2.1 Patient Characteristics.	47
Supplementary Figure 2.2 Patient laboratory values.....	48
Supplementary Figure 2.3 WT and mutant DNA, RNA, and protein levels.	49
Supplementary Figure 2.4 T182 Gαi2 mutants abrogate RGS-binding.	50
Supplementary Figure 2.5 Activating Gαi2 mutants impair chemotaxis <i>in vitro</i> and <i>in vivo</i>	51
Supplementary Figure 2.6 Determination of BRET _{max} and acceptor/donor expression levels in BRET experiments	53
Supplementary Figure 2.7 Patient T cell cytokine production and activation.	55
2.8 Supplementary Tables	57
Supplementary Table 2.1 Summary of WES Variants found at each filtering stage for P1.....	57
Supplementary Table 2.2 P1 candidate gene list by genetic model.	58
Supplementary Table 2.3 CRISPR targeting <i>Gnai2</i> in mouse embryos.	59
2.9 Supplementary Notes	60
Supplementary Note 2.1 P1 clinical course.....	60
Supplementary Note 2.2 P2 clinical course.....	65
2.10 Materials and Methods	67
2.11 Contributions	90
CHAPTER 3 - Recurrent rhinovirus infections in a child with inherited MDA5 deficiency	92
3.1 Abstract	92
3.2 Introduction	92
3.3 Results	94
3.4 Discussion	98
3.5 Tables	102
Table 3.1 Summary of WES Variants found after each filtering stage.	102
Table 3.2 Non-synonymous rare genetic variants found in the patient by WES.	103
3.6 Figures	104
Figure 3.1 Infection history in a human with recurrent respiratory tract infections.	104
Figure 3.2 Autosomal recessive, homozygous <i>IFIH1</i> mutation in the proband.	105
Figure 3.3 Loss-of-function <i>IFIH1</i> mutation.	106

Figure 3.4 Loss of MDA5 function results in increased replication of HRV in respiratory epithelial cells.	107
Figure 3.5 MDA5 effects on IFN during HRV infection of respiratory epithelial cells.	108
Figure 3.6 Loss of MDA5 function results in increased replication of HRV in respiratory epithelial cells.	109
Figure 3.7 Loss of MDA5 function does not affect replication of flu or production of pro-inflammatory cytokines in respiratory epithelial cells.	110
Figure 3.8 Loss of MDA5 function does not affect flu replication, or flu-induced IFN production or cytotoxicity, in respiratory epithelial cells or fibroblasts.	111
Figure 3.9 Loss of MDA5 function does not affect RSV replication while affecting RSV-induced IFN-regulated transcripts.	112
3.7 Supplementary Notes	113
Supplementary Note 3.1 Patient clinical course.	113
3.8 Materials and Methods	114
3.9 Contributions	137
 CHAPTER 4 – Discussion and Future Experiments	 139
4.1 Dominant-activating mutations in Gαi2 cause MAGIS Syndrome - Discussion and Future experiments	139
4.2 Human MDA5 Deficiency - Discussion and Future experiments	144
 BIBLIOGRAPHY	 148

CHAPTER 1: Introduction

1.1 Nature's experiments in immunology: Primary immunodeficiencies, a powerful lens for understanding the immune system

“Nevertheless, human immunodeficiency disease is still the best source of insight into normal pathways of host defense against infectious diseases in humans.”[1]

Janeway's Immunobiology

Human primary immunodeficiencies (PIDs) are genetic inborn errors of immunity that result in a wide range of immunological and sometimes non-immunological presentations. Since O.C. Bruton's seminal description of the first recognized primary immunodeficiency in 1952, patients with PIDs have been identified as providing invaluable insight into the essential workings of the immune system in humans.[2, 3] Methods for determining the underlying genetic cause of PIDs have dramatically evolved since the origin of this field. It is founded on a principle of “forward genetics” involving first clinically observing a phenotype and then working to identify the underlying genetic cause. These diseases are extremely rare; many have been identified in <10 affected individuals (several in only 1 individual thus far) and the most common PID, selective IgA deficiency, has been observed at a rate of only 1 in 800 in the general population. The number of identified PIDs is rapidly growing (and expected to keep growing). Today over 300 PIDs are causally linked with single-gene defects.[4] While any individual PID is very rare, we now recognize that individuals with primary immunodeficiencies are far more common than once thought. In fact, the massive increase in the proportion of

newly identified PIDs arising from extremely rare *de novo* mutations has led some to hypothesize that most life-threatening infection seen in the general population is actually evidence of latent primary immunodeficiency within the global population which is now largely masked by advances in modern medicine and public health.[5, 6]

The process of investigating naturally-occurring PIDs to understand the immune system has consistently and significantly impacted our understanding of immunology and medicine over six decades for several reasons.[7] First, studying PIDs allows for direct genotype-phenotype observations in humans, bypassing the limitations of *in vitro* and animal models of human disease. Secondly, patients with PIDs reveal the identity of the immunodeficiency *in natura*, highlighting the specific pathogens the genetically altered pathways have evolved to protect against. The advantages of observing a natural course of infection has been increasingly appreciated as more and more PIDs are being identified with a very narrow infectious susceptibility (1-3 organisms), a finding which often contrasts to wide infectious susceptibility seen in the disease-analogous mouse models subjected to laboratory infections.[8]

The similarity of studying PIDs (and other genetic diseases in humans) to various forward genetics approaches in mice (ENU mutagenesis, etc.) has led many to refer to PIDs as “experiments of nature.” These experiments have provided groundbreaking insight into the development of the immune system, novel T helper cell subsets, new processes of establishing peripheral tolerance, and much more.[9-11] Additionally, the study of PIDs has spearheaded major medical advances by providing unique medical needs, opportunities for novel treatment, and proof-of-principle demonstration for novel therapies such as immunoglobulin replacement therapy, hematopoietic stem cell transplantation, and gene therapy.[12]

1.2 Combined Immunodeficiencies – T cells, B cells, and more

Combined immunodeficiencies (CID) are a class of PIDs that impair both the cellular and humoral arms of the adaptive immune response.[13] Severe combined immunodeficiency (SCID) is the most severe form of CID and typically manifests with a severe defect in T cell numbers (T- SCID) or function and may also present with an absence of B and/or natural killer (NK) cells (B- and/or NK- SCID). SCID is often differentiated from less severe CID by the fact that it results in fatal infection within the first year of life without treatment.[14] While SCID had long been recognized as a clinical entity (most commonly via X-linked recessive inheritance presenting in males), it was not until 1972 when Dr. Elo Giblett discovered two patients who completely lacked protein bands known to be adenosine deaminase (ADA) on red blood cell electrophoresis that the first molecular diagnosis of PID was made.[15]

The association between the SCID phenotype and ADA-deficiency in these two boys was clear; however the idea that ADA-deficiency caused SCID was immediately questioned. Commentary co-published with the Giblett's original article stated that ADA, an enzyme known at the time to be required for the catabolism of purines, was unlikely to be essential for the development or "division of T cells in carrying out their function." [16] In the decades since this sentinel discovery, mutations of many other "non-immune" genes have been shown to cause SCID. Currently more than 49 recognized genetic causes comprise the CID disease family.[4] The genes that make up this list encode proteins involved in a vast range of cellular processes including cytokine sensing, DNA repair, metabolism, chemotaxis, antigen receptor signaling, and more.[17-22] Thus, it has become clear that T cell development and function relies on a complex network of molecules and processes, many of which are not intrinsic to the T cell (but

are essential for T cell mediated immunity *in vivo*), and many which are likely still unidentified.

The work put forth here represents an initial investigation into the genetic and molecular mechanism of three families who presented with CID and susceptibility to virus infections. As the differences in their clinical presentations suggest, the underlying molecular bases for their diseases are widely varied, a finding that supports and adds to the complex network of essential genes for protective B and T cell function in humans.

1.3 Approach to Understanding Inherited Defects of Immunity

For many of the reasons discussed in **Chapter 1.1** regarding the success and impact of forward genetic studies of primary immunodeficiencies on the field of immunology and medicine, the work described in **Chapter 2** and **Chapter 3** largely represent a modernized strategy for exploring the genetic causes and molecular mechanisms of PIDs.

Over the past 8 years the number of identified genetic causes of PIDs has more than doubled the total number of those identified over the first 56 years following Bruton's description of congenital agammaglobulinemia.[2, 4, 23, 24] This dramatic increase in the rate of discovery is notable for two reasons. First, it is largely a reflection of advances in and accessibility of massively parallel or next generation DNA sequencing (NGS) in the setting of molecular biology techniques such as polymerase chase reaction (PCR), cloning, RNA interference (RNAi), and Clustered regularly interspaced short palindromic repeats (CRISPR) which can accurately validate gene candidates. Secondly it is notable because in the years prior to this surge in genetic discovery it was commonly thought the field was nearing the point of having described

most PIDs.[5] This was clearly not the case, and recent trajectory of the field lends credence to those who endorse the hypothesis that rare, personalized genetic mutations (now uncovered by NGS and present in all individuals) underlie most, if not all, life-threatening infections.

My approach to understanding novel genetic immunodeficiencies can be broken down into three major stages: (1) information gathering – a synergistic effort combining clinical history of affected individuals and their family members, a laboratory workup based on their clinical history, and whole exome or whole genome sequencing (WES and WGS, respectively); (2) functional validation of candidate genes – a wet bench demonstration of *in vitro* cellular abnormalities with a complementary demonstration of the candidate genetic mutation's sufficiency to recapitulate the patient's cellular phenotype in otherwise normal cells; and (3) information synthesis – an experimental and intellectual effort to understand the mutant gene product's role in normal immunity and how its perturbation results in disease (Figure 1.1).

The information gathering stage (stage 1) first involves the selection of patients to work with and the collection of extensive clinical and laboratory data for those patients. When selecting patients to study, I consider the likelihood that the patient's disease is due to a genetic cause. Multiple affected individuals over multiple generations within the pedigree is the strongest indicator; however early (<1 year of age), severe onset is also a positive indicator of a likely genetic etiology.[6] Additionally, it is critical to rule out all known potential causes of the patient's disease in order to enrich the studied patient population for novel etiologies. I also consider the williness of the patient and family to cooperate with the often rigorous demands of our research. This is particularly important during the second stage of my approach when I am

dependent upon the availability of patient tissue (blood, skin, saliva, etc.) to identify patient-specific cellular abnormalities.

The second half of the information gathering stage is WES or WGS on the patient(s) and unaffected family members. In this work, I employed WES, which generates an extensive (hundreds to thousands) list of candidate gene mutations. The synergy of the clinical and genetic data is critical for appropriately ranking candidate genetic lesions. To pare down and prioritize the list of candidates, I fit the genetic data to the patient pedigree assuming different potential models of inheritance. For instance, if the patient has two unaffected parents, I assume either recessive inheritance (compound heterozygous in the absence of observed consanguinity or homozygous recessive if consanguinity is present) or a *de novo* mutation. I next consider the expression profile of the gene in light of what we know clinically about the patient. For example, if the patient has extensive developmental or non-immune abnormalities, I prioritize genes that are expressed during development as well as in non-immune tissues. If the patient has a specific absence of antibodies and recurrent sinopulmonary bacterial infections, I would prioritize genes expressed in B cells and T cells. Lastly I consider a host of bioinformatic information about each candidate mutation including the frequency of the mutation in the general population, the type of mutation (coding vs. non-coding, missense vs. non-sense, etc.), the predicted effect on RNA and protein expression and function (e.g. via databases such as PolyPhen2), and the degree of conservation (both DNA and protein) at the site of mutation. Together, the genetic and clinical information is integrated to create a ranked list of candidate genetic mutations.

The second stage of my approach is the functional validation of candidate genes. The goal is to determine whether a candidate mutation is contributing to or causing a

patient's disease. This is accomplished by first identifying a functional cellular abnormality in the patient's cells and subsequently demonstrating the sufficiency of the patient's mutations to cause the *in vitro* cellular phenotype. The experiments performed are heavily guided by both the clinical presentation of the patient (what lab values are affected in the patient? What infections has the patient suffered from?) and the identity and function (if known) of the top gene candidates. Once an *in vitro* cellular abnormality is demonstrated with the patient cells, I attempt to phenocopy the patient's cellular abnormality by genetically mimicking the patient (i.e. gene knockout, knockdown, overexpression, etc.) using cells from healthy individuals. For instance, small molecule inhibitors, small interfering RNA (siRNA) gene silencing, short-hairpin RNA (shRNA), and CRISPR are used to suppress gene expression/function in primary cells from healthy individuals, mimicking loss-of-function (LOF) mutations in recessively inherited diseases or diseases of haploinsufficiency. Similarly, overexpression and knock-in studies are used to model dominant negative and gain-of-function (GOF) mutations. Ultimately, the goal of these experiments is to demonstrate the sufficiency of a candidate gene mutation to recapitulate a disease-relevant cellular phenotype in healthy control cells.

The third stage of my approach is an intellectual and experimental period of synthesizing what I have observed in clinical history of the affected individuals with the identity of the candidate gene shown to be sufficient to elicit diseased behavior in cells. What can I infer about the role of this gene product in normal human immunity? How does the mutation in this gene product result in disease? The degree of insight into normal human immunity at this stage is wide-ranging. Often the mutated gene is not known to regulate the abnormal cellular processes observed in the patient cells. Other

times, however, the pathways are better understood and immediate efforts can be made to therapeutically intervene.

1.4 A Note on Studying Individual Patients and Extremely Rare Diseases

It has long been held that identifying multiple affected individuals with a given genetic lesion is necessary evidence for defining a causative relationship between an identified mutation and a new genetic disease; however it is now possible to convincingly demonstrate the relationship between a given candidate gene mutation and a novel immunodeficiency in an individual patient.[25] This is largely due to the advent of WES and WGS as well as major advances in genetic manipulation of primary cells from healthy individuals (i.e. gene silencing, advances in transfection methods/overexpression, and CRISPR) that are used to validate the sufficiency of a genetic lesion to cause disease-related dysfunction in relevant cell types. The ability to identify and rigorously establish a causal relationship between a novel genetic lesion and a disease phenotype in single patients has been a significant contribution to the recent explosion in the number of newly identified PIDs. However, strict criteria must be met in order make this conclusion.[26, 27]

Criteria for establishing causality of a genetic lesion in a single patient has been thoroughly described by Casanova, et al.[27] Similar criteria employed by our lab are summarized here.

1. The patient's candidate genotype must be unique to the patient (i.e. not present in other unaffected family members) and present within the population at rate less than or equal to the prevalence of the disease. As

such, this criterion precludes the sufficient establishment of causality of a mutation in a disease that is not highly penetrant.

2. Experimental studies must demonstrate that the candidate genetic mutation impairs, destroys, or alters gene expression or protein function.
3. The genetic mutation must be sufficient to recapitulate the disease feature(s) of the patient or patient cells when introduced into healthy control cells or an animal model.

The massive increase in DNA sequencing over the past decade revealed much greater genetic variation among individuals than was generally thought to exist.[28] Every individual harbors extensive genetic variation, a significant amount of which is unique to an individual's 'clan' or nuclear family (and distinct from the general population) and additional variation that is unique to the individual entirely (and distinct even from his/her parents).[29, 30] Thus extremely rare, sporadic diseases likely exist throughout the population, and NGS efforts coupled with investigation into patient phenotypes is confirming this.[31] The establishment of guidelines for implicating a genetic lesion in the causality of a novel disease is thus critical for ensuring that extremely rare patients are identified and published as it may be years before the identification of another patient.

1.5 G α i2, Heterotrimeric G proteins, and Immunity

Heterotrimeric G proteins are an evolutionarily conserved protein family and one of the longest studied protein families in biomedical research. Decades before the advent of molecular cloning and genetics, Sutherland and others observed that stimulating cells with a range of hormones resulted in the production of cyclic adenosine monophosphate

(cAMP), the first identified second messenger.[32, 33] Although it would be years until this was shown to be a GTP-dependent process (thus requiring G proteins), Sutherland received the Nobel Prize in Medicine or Physiology for his work in 1971.[34] Subsequent work studying the effects of cholera toxin, a product of *Vibrio cholerae*, revealed constitutive production of cAMP in targeted cells. Surprisingly the target of cholera toxin was not the cAMP-generating enzyme adenylyl cyclase (AC), but rather a heterotrimer of 45, 25, and 8-10 kDa proteins intermediaries that became ADP-ribosylated. The work of Martin Rodbell and others in 1970's demonstrated the role of GTP in hormone receptor signaling and that GTP was bound by the trimeric target of cholera toxin. Thus these proteins became known as the heterotrimeric 'G proteins' $G\alpha$, $G\beta$, and $G\gamma$, and Rodbell received the Nobel Prize in Medicine or Physiology in 1994 for the discovery of G proteins.[35-38]

Extensive sequencing efforts and bioinformatics analysis has demonstrated that heterotrimeric G proteins are expressed and highly conserved throughout eukaryotes from excavates to animals.[39] Their conservation and centrality to eukaryotic biology is evidenced by the co-evolution of multiple toxins from other organisms that directly target these proteins. Notably pertussis toxin (PTX) and the related cholera toxin (CTX) are ADP-ribosylases that catalyze the addition of NAD^+ to C-terminal residues within $G\alpha_i$ and $G\alpha_s$ family subunits, respectively. This results in the inactivation (PTX) or constitutive activation (CTX) of $G\alpha$ proteins ($G\alpha_i/o$ and $G\alpha_s$ family members, respectively) leading to cellular pathology.[40, 41] Furthermore, the wasp venom component mastoparan allosterically activates $G\alpha_i/o$ family proteins, demonstrating that eukaryotes have also evolved mechanisms of targeting these proteins.[42, 43]

The primary identified function of heterotrimeric G proteins is their function as molecular switches, activating intracellular signaling cascades in response to extracellular ligands sensed by G-protein coupled receptors (GPCRs). To date, there are nearly 800 GPCRs identified in humans, and, as such, they influence nearly every aspect of eukaryotic cellular biology. GPCRs also serve as the principle target of ~30% of drugs available today, underscoring their importance in medicine.[44-46] Despite the vast diversity of the GPCR superfamily, these receptors rely on a relatively tiny repertoire of heterotrimeric G proteins to transmit signals within the cell. 16 $G\alpha$, 5 $G\beta$, and 12 $G\gamma$ genes in humans form hundreds of different potential trimer combinations, providing specificity and the capacity for unique regulation of the GPCRs. Still many heterotrimeric G-proteins must be widely expressed and service multiple GPCRs within a given cell type.

The $G\alpha$ subunits provide the molecular switching function of heterotrimeric G proteins (overview of this and the GTPase cycle are provided in the introduction of **Chapter 2**) and are sub-divided into four $G\alpha$ families: $G\alpha_s$, $G\alpha_i/o$, $G\alpha_q$, and $G\alpha_{12}$ based on their primary effectors.[47] The inhibitory $G\alpha_i$ subunits were named because of their inhibition of cAMP production by adenylyl cyclase, and consists of four members in humans: $G\alpha_i1$, $G\alpha_i2$, $G\alpha_i3$, and $G\alpha_o$. Of these, $G\alpha_i2$ and $G\alpha_i3$ are highly expressed in lymphocytes. $G\alpha_i1$ is also expressed in lymphocytes, but at much lower levels.[48, 49]

There is considerable co-regulation of $G\alpha_i$ -coupled GPCR signaling by $G\alpha_i2$ and $G\alpha_i3$ in lymphocytes, however $G\alpha_i2$ appears to serve a much broader non-redundant role in immune function and elsewhere in the body. In particular, $G\alpha_i2$ is the principle

G α subunit regulating chemokine receptor signaling and leukocyte migration.[50, 51] Consistent with this, mice lacking G α i2 are immunodeficient while G α i1 or G α i3 deficient mice do not exhibit any overt phenotype.[47, 52] As would be expected from a ubiquitously expressed protein regulating dozens of different receptors, G α i2 knockout mice exhibit a wide range of defects including abnormal T cell and B cell development, loss of glucose regulation, failure of cancer suppression, aberrant cardiac function, abnormal bone growth and fusion, and develop spontaneous colitis.[47, 53-57] Thus G α i2 functions as a critical regulator of the immune system as well as a non-redundant component of the endocrine, cardiac, skeletal, and gastrointestinal systems.

1.6 MDA5, Pattern Recognition Receptors, and Immunity

Pattern recognition receptors (PRRs) are genetically encoded, non-variable receptors that recognize microbially generated (non-self) products, or pathogen-associated molecular patterns (PAMPs). Thus, these are distinct from heterogenous T cell and B cell receptors that are products of gene rearrangements and genomic editing. PRRs are expressed all throughout the body and, upon binding their cognate ligand(s), they immediately initiate an anti-microbial inflammatory response. It is now appreciated that this innate immune response is necessary for priming the adaptive immune response.[58, 59]

The seeds of the idea that microbial products resulted in inflammation can be traced all the way back to descriptions by Koch and Pasteur of the germ theory of disease. Throughout the decades that followed, many investigators extracted purified components of infection secretions and studied their effects on uninfected hosts. The extracted components were sufficient to recreate many aspects of infectious

inflammation such as fever, pus, and immune cell infiltration, however they were not sufficient to propagate infection[58] It was not until the 1960s that lipopolysaccharide (LPS), likely the predominant PAMP studied in the purifications efforts of the 19th, and early 20th centuries, was chemically characterized and identified as a major component of the cell wall of gram negative bacteria.[60-63]

Despite these advances in innate immunology, the decades of immunological research that followed were defined by major advances in our understanding of the adaptive immune system, furthering our understanding of the adaptive immune response. The idea that unique T cell receptors enabled education of self and non-self in the thymus coupled with convincing demonstrations of the clonal selection theory and the generation of immunologic memory via long-lived memory cells were elegant and revolutionary. As a result, the study of LPS and the effects of other PAMPs on the immune system shifted out of focus [64-67].

However, throughout the many immunizations and infectious challenges that took place during these decades of research, it became increasingly apparent that non-self antigen alone was not sufficient to generate an adaptive immune response, but rather microbial products needed to be co-inoculated with non-self antigen for immunization to occur. Perhaps most famously put forth in 1989 by Charles Janeway Jr., he and others hypothesized that sensing of microbial products by the innate immune system provided a second necessary signal for the initiation of the adaptive immune response.[68] In close succession, discoveries in the mid 1990s conclusively revealed a family of receptors, now known as mammalian Toll-like receptors (TLRs), as the link between pathogenic microbial products and the full activation of costimulatory antigen presenting cells.[69-72]

The first Toll-like receptor identified in mice and humans was Toll-like receptor 4 (TLR4), now known to bind and signal LPS.[69-72] Subsequent investigation into other Toll-related genes reveal an entire family of Toll-like receptors whose ligands included a broad range of bacterial, fungal, and viral products. Stimulation through these receptors was sufficient to transition innate immune cells into a state which enable them to provide necessary costimulation to the adaptive immune system. Genetic deletion of these receptors resulted in impaired recognition and infectious susceptibility to classes of pathogens expressing associated TLR-activating molecules.[73]

Not only was it amazing that one family of receptors could recognize such a diverse range of PAMPs, it suggested that cells may have alternative PRRs for directly recognizing pathogens and their byproducts. In 2004, Yoneyama, et al. first described a role for a cytosolic RNA-helicase that could recognize double-stranded RNA (a replicative byproduct of many viral infections) and induce an interferon (IFN) mediated antiviral response.[74] This receptor, retinoic acid inducible gene I or RIG-I, is the first member of what is now known as the RIG-I like receptors (RLRs). This discovery prompted investigation into similar functions in the RIG-I paralog, melanoma differentiation antigen 5 (MDA5), where it too was found to sense dsRNA and initiate an IFN-mediated antiviral response.[75] Initially it seemed RIG-I and MDA5 had redundant function; however work by Kato, et al. and others clearly demonstrated that these receptors had differential roles in the recognition of RNA viruses.[76-78]

We now know that RIG-I recognizes the ends of uncapped 5' triphosphorylated and 5' diphosphorylated RNAs, while MDA5 is preferentially stimulated by long double stranded RNAs[77, 78]. There is still considerable uncertainty about exactly what the identity and scope of the *in vivo* ligands are for these receptors, but is clear that they

recognize different RNA structures and distinct but overlapping sets of viruses. Elegant work by Sun Hur and others, has demonstrated that MDA5 can bind and oligomerize along the shank of dsRNAs in a dynamic process that is regulated by the length of the dsRNA and hydrolysis of ATP by MDA5. Stabilized dsRNA-bound MDA5 oligomers then interact with mitochondrial antiviral protein (MAVS) on the surface of the mitochondria, initiating an antiviral gene response through the activity of the transcription factors IRF3 and NF- κ B. While RIG-I has been demonstrated to have antiviral functions towards a large range of infections, the role of MDA5 appears to be somewhat more limited. Many studies on the recognition and antiviral function of RIG-I vs. MDA5 have clarified a non-redundant role for murine MDA5 in restricting the murine picornavirus, encephalomyocarditis virus (EMCV) while RIG-I appears to be the predominant RLR in initiating antiviral responses to parainfluenzaviruses, orthomyxoviruses, and others [76, 79-89] Still many studies have conflicting results that appear to be highly dependent on virus strain, cell type/species of organism, and the experimental system used.[90, 91] Common human pathogens related to EMCV (picornaviridae) are enteroviridae and the closely related human rhinovirus (HRV, common cold) as well as the coronaviridae family viruses which have an increasingly recognized role in human disease.[92] [93] Because of decades of research innate immune sensing, we have a broad base of information about the interactions between the innate immune and adaptive immune systems, the role of PRRs, RLRs, and what these receptors recognize and signal. However, the fundamental question of what role MDA5 plays in human immunity remains unanswered.

1.7 Figures

Figure 1.1 Forward genetics approach to identifying genetic causes of PIDs

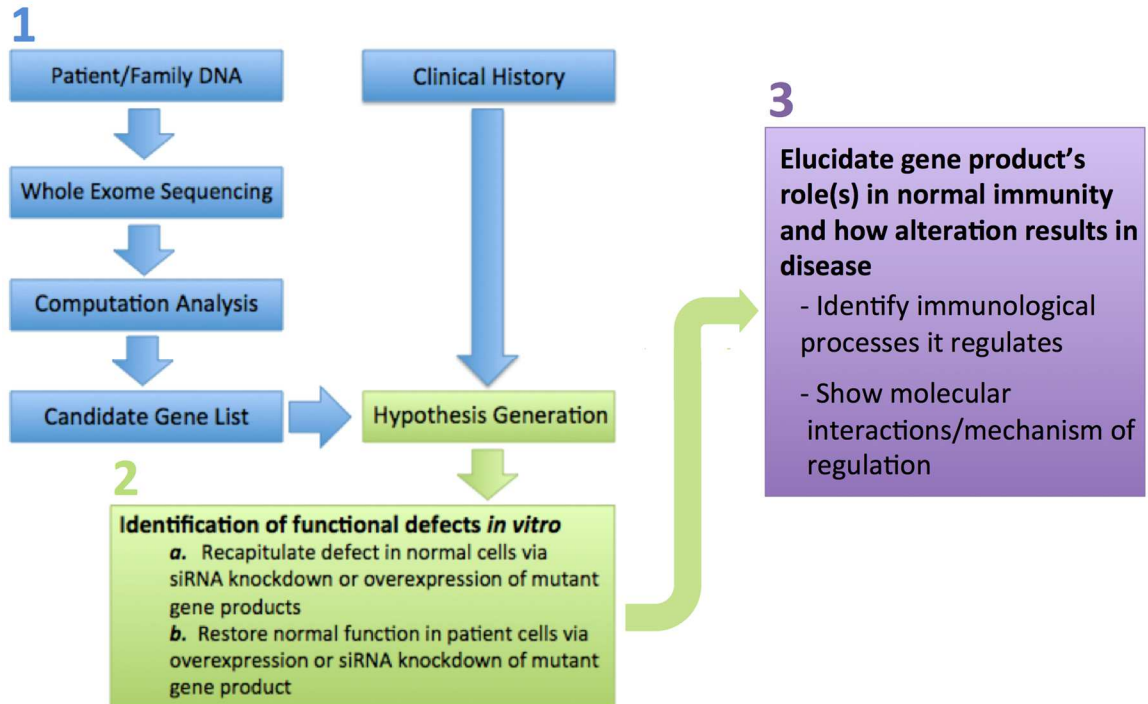


Figure 1 Forward genetics approach to identifying genetic causes in patients with primary immunodeficiencies.

CHAPTER 2 - Dominant-activating G α i2 mutations cause human immunodeficiency and autoimmunity by defective leukocyte migration and altered T cell activation

2.1 Abstract

The ubiquitously expressed heterotrimeric G-protein, G α i2, relays signals for dozens of G-protein-coupled receptors throughout the body and is critical for leukocyte biology. We found dominant missense mutations in *GNAI2*, the gene encoding G α i2, in patients with life-threatening, multi-organ system autoimmunity and susceptibility to mucocutaneous bacteria and virus infections. The mutant proteins impaired immunity by uncoupling chemokine receptor signaling and thereby interfering with leukocyte chemotaxis *in vitro* and to sites of inflammation *in vivo*. They also augmented T cell effector responses and diminished the requirement of costimulation for T cell activation by constitutively signaling downstream costimulatory pathways. These results identify essential roles of G α i2 in maintaining immune-competence and self-tolerance in humans and highlight G α i2-responsive pathways as potential candidates for new therapeutics for autoimmune diseases.

2.2 Introduction

Heterotrimeric G-proteins are the molecular switches that activate intracellular signaling programs in response to ligand activated G-protein-coupled receptors. As such, they serve essential roles in a broad range of cellular processes including development, hormone signaling, neurotransmission, metabolism, inflammation, and chemotaxis.[95-100] Each heterotrimer is composed of three subunits in a 1:1:1 ratio: a guanine

nucleotide-binding $G\alpha$ subunit and a $G\beta\gamma$ dimer (composed of $G\beta$ and $G\gamma$). $G\alpha$ proteins enable the molecular switch function. In the basal, GDP-bound state, $G\alpha$ is “off” (inactive) and complexed tightly with $G\beta\gamma$, poised for activation by GPCRs. Upon ligand binding, GPCRs catalyze the release of GDP allowing uptake of GTP by $G\alpha$. The GTP-bound $G\alpha$ is “on” (activated) and dissociates from $G\beta\gamma$ to initiate distinct downstream signaling from both $G\alpha$ and $G\beta\gamma$. Ultimately, GTP hydrolysis by $G\alpha$ returns $G\alpha$ to its GDP-bound, $G\beta\gamma$ -complexed “off” state. To ensure the switch is efficiently regulated, Regulator of G-protein Signaling (RGS) proteins function as GTPase Activating Proteins (GAPs) to accelerate the intrinsic GTPase activity of $G\alpha$ and rapidly stop further signaling.[46, 101, 102] The human genome encodes 16 $G\alpha$ subunits responsible for the signaling of nearly 800 GPCRs, thus each $G\alpha$ subunit couples to a wide range of GPCRs.[94] $G\alpha_i2$ (encoded by *GNAI2*) is ubiquitously expressed and, along with $G\alpha_i3$, is one of two $G\alpha_i$ -family subunits highly expressed in lymphocytes[48, 49] where knock-out studies have demonstrated its non-redundant role in nearly all chemokine signaling in addition to regulating thymocyte egress[54, 103, 104], inflammatory cytokine production,[105, 106] and B cell and lymph node development.[51, 53, 104] Studies utilizing RGS-insensitive $G\alpha_i2$ mutants, which cause prolonged GPCR dependent $G\alpha_i2$ signaling, also revealed defects in cell migration, hematopoietic development, and immunity, emphasizing the importance of tightly regulating $G\alpha_i2$ activity[107] [108]. Despite decades of research on heterotrimeric G-proteins, the fundamental question of how $G\alpha_i2$ activity modulates human immunity remains unanswered.

The integrity of the immune response depends upon leukocytes' ability to precisely respond to chemokine gradients to exit the circulation into sites of

inflammation, retain protective immune cell populations in non-inflamed tissues, and downregulate retentive chemokine signaling to respond to infection elsewhere.[109-111] Severe bacterial infections and periodontal disease affect humans with leukocyte adhesion deficiency (LAD) due to loss of integrin- β 2 (CD18, LAD I)[112], its ligands (fucosylated selectins, LAD II)[113, 114], or the ability to activate integrins in response to endothelial displayed chemokines (Kindlin-3 deficiency, LAD III).[115] Each of these defects impairs chemokine-mediated leukocyte exit from the blood stream resulting in massive accumulation of circulating leukocytes, deficient leukocyte numbers at the site of infection, and recurrent mucocutaneous bacterial infections.[116] The immune system's ability to respond to chemokines is also critical for controlling chronic infections through the maintenance of lymphocyte populations at barrier sites.[117] Human DOCK8 deficiency impairs the lymphocyte migration machinery essential for normal cell movement creating deficient resident T cell numbers in the skin.[118] These patients suffer from uncontrolled human papillomavirus (HPV), molluscum contagiosum, herpes simplex virus (HSV), and herpes zoster infections.[110] Equally important, is turning off chemokine signaling to allow cells to leave resident sites in order to respond to infection elsewhere. Warts, hypogammaglobulinemia, infection, and myelokathexis (WHIM) syndrome is caused by heterozygous mutations in the cytoplasmic tail of the chemokine receptor CXCR4 which impair receptor downregulation.[119] Constitutive signaling from CXCR4 causes retention of B cells and neutrophils in the bone marrow and a paucity of circulating neutrophils leading to recurrent bacterial infections.[120] Although these and other diseases of cell migration emphasize the importance of precisely regulating chemotaxis, WHIM syndrome is the only known disease of cell migration caused by mutations to a chemokine receptor. Furthermore, no disease of cell migration is known

to result from mutations in a heterotrimeric G protein. Thus it remains unknown how disrupting chemotaxis at the level of the heterotrimeric $G\alpha$ subunit would affect cell migration and effector responses in humans.

The sensitivity of the T cell receptor (TCR) to various types, strengths, and durations of stimulation determine which signals generate effector responses and which will not. Mechanisms both enhancing T cell activation and preventing it ensure T cell effector responses are only unleashed against appropriate stimuli at the correct time. A fundamental mechanism increasing the specificity of T cell activation is the requirement of a second costimulatory signal (signal 2) in addition to the TCR signal (signal 1) for full activation (metabolic shift, proliferation, cytokine production). Signal 1 occurs when the TCR encounters an activating peptide-MHC (major histocompatibility complex) complex on an antigen presenting cell (APC). Signal 2 is a verification signal canonically mediated through CD28 (on the T cell) via interaction with CD80 or CD86 (on APCs) that ensures the T cell should be fully activated and is not simply responding to self-peptide-MHC complexes. Because potent costimulatory molecules are restricted to APCs activated by microbial products or inflammatory cytokines, a highly specific set of immunological events must occur for T cell activation.[121] CD28 and dozens of other costimulatory receptors regulate full T cell activation by amplifying TCR signaling by recruiting Src and phosphatidylinositol-3-OH kinases (PI(3)K), sustaining intracellular Ca^{2+} levels, promoting interleukin-2 (IL-2) production, stimulating protein synthesis, and shifting cellular metabolism to glycolysis for rapid cellular proliferation although the exact requirements for sufficient costimulation are still unknown.[122-124] Chemokine stimulation activates many of the same pathways via $G\alpha_i2$ and its co-regulated $G\beta\gamma$ subunits, including Src and PI(3)K activity, Ca^{2+} flux, and increased protein synthesis via

phosphorylation of ribosomal protein S6, in addition to actin cytoskeleton rearrangements important for the formation of the immunological synapse.[95, 125, 126] Thus increased $G\alpha i2$ signaling during T cell activation would be expected to augment proliferation and effector responses, and indeed this occurs when T cells are activated in the presence of $G\alpha i2$ activating chemokines CXCL12 and CCL21.[127, 128] However, chemokine mediated $G\alpha i2$ activation is quickly turned off following receptor stimulation, limiting its costimulatory effect on T cell activation.[129] Human T cell lymphomas as well as cells exogenously expressing the constitutively activating R179C $G\alpha i2$ mutant exhibit activation of key costimulatory pathways and characteristics of malignant transformation highlighting the importance of downregulating $G\alpha i2$ activity.[130, 131] Still the consequences of constitutive $G\alpha i2$ activity on T cell activation and human immunity are unknown. Here we describe two patients with combined immunodeficiency and life-threatening autoimmunity who share gain-of-function mutations in *GNAI2*. These mutations dominantly impaired chemokine signaling causing impaired cell migration to sites of inflammation and simultaneously altered T cell activation, reducing the requirement for costimulation to elicit effector function.

2.3 Results

Life-threatening autoimmunity and immunodeficiency

We studied two patients with life-threatening multisystem autoimmunity and combined immunodeficiency (**Table 2.1** and **Supplementary Note 2.1 and 2.2**). Both presented in the first year of life with recurrent sinus, lung, and middle ear infections (**Supplementary Fig. 2.1a**). Immunoglobulin replacement therapy and antibiotic prophylaxis only partially reduced the infection rate (**Supplementary Fig. 2.2m-p**). Among the recurrent

infections, were bacterial and viral skin infections including *Staphylococcus aureus*, herpes zoster, and surgically refractive human papillomavirus driven warts on the arms, hands, and feet of P1 (**Supplementary Fig. 2.1b**).

Early in life, both patients developed autoimmune thrombocytopenia and hemolytic anemia with anti-red blood cell antibodies (DAT⁺). Despite splenectomy (P1), treatment with corticosteroids, and B cell depletion (rituximab), both manifested recurrent hemolytic crises requiring transfusions (**Supplementary Fig. 2.1a and 2.2h**). At age six P1 was diagnosed with autoimmune arthritis of her knees, which later involved her ankles, wrists, fingers, and jaw. The arthritis caused “Swan neck” finger deformities (**Supplementary Fig. 2.1c**) and required right knee replacement surgery. By age 21 she had developed plaque psoriasis of her arms and legs (**Supplementary Fig. 2.1a**). Following an episode of bacterial meningitis at age 4, P2 developed a progressive leukodystrophy with diffuse T cell infiltration (**Supplementary Fig. 2.1d**). By age 5 he developed recurrent seizures and lost the ability to walk and speak before passing away at age 8 due to declining brain function. Extensive testing revealed no viral or metabolic etiology.

Longitudinal laboratory testing revealed mildly low absolute CD4⁺ and CD8⁺ T cell counts (normalized following splenectomy in P1) with a normal ratio of CD4⁺ to CD8⁺ T cells (**Supplementary Fig. 2.2a,b,c**). The relative numbers and percentages of CD45RA⁺CCR7⁺ naïve T cells within the CD4⁺ and CD8⁺ compartments were decreased (P1; peripheral blood no longer available for P2) (**Supplementary Fig. 2.2i-l**). P1 exhibited normal percentages of senescent (CD57⁺), exhausted (PD-1⁺), and recent thymic emigrants (CD31⁺) (**Supplementary Fig. 2.1h,i**). Both patients developed a progressive leukocytosis, with expansion of neutrophils, monocytes, and B cells pre-

rituximab treatment (**Supplementary Fig. 2d,f,g**). Non-immune abnormalities included intrauterine growth restriction with slow post-natal growth, mild dysmorphism, clubfeet, congenital hip dislocations, butterfly vertebrae (P1), hemivertebrae (P2), and small bowel malrotation (P1) (**Table 2.1**).

***De novo* mutations of the active site of G α i2**

Both patients' severe, early-onset disease suggested a genetic etiology. As all family members were healthy and without history of consanguinity, we suspected an autosomal dominant disease from *de novo* mutations or an autosomal recessive disease with compound heterozygous mutations. We carried out whole exome DNA sequencing (WES) on both patients and their immediate family members which revealed novel heterozygous missense mutations of threonine 182 (T182) in *GNAI2* (P1: c.544A>G, p.T182A; P2 c.545C>T, p.T182I), the gene encoding the ubiquitously expressed heterotrimeric G-protein G α i2 (**Fig. 2.1a**). These mutations were not present in any parent, the sibling, 13,006 exomes from publically available databases^[132], or >700 previously sequenced exomes from our immunodeficiency cohort. WES and confirmatory Sanger dideoxy sequencing confirmed equal copy number of the wild-type (WT) and mutant alleles in the patients' leukocytes (**Fig. 2.1b** and **Supplementary Fig. 2.3a**) and dermal fibroblasts (**Supplementary Fig. 2.3b** and data not shown), suggesting it arose in the germ cell or early during embryonic development.[31] This mutation was the only non-synonymous *de novo* mutation found in either patient. We identified several compound heterozygous mutations, but none was biallelic, predicted to be damaging (PolyPhen2 > 0.8), nor expressed in immune and non-immune tissues (**Supplementary Table 2.1** and **2.2**). G α i2 is a 355 amino acid protein composed of a helical domain and a highly conserved GTPase domain shared by the entire GTPase

superfamily (**Fig. 2.1c**).[45] T182 is evolutionary constrained (GERP, 5.0) and highly conserved within the eukaryote GTPase superfamily (PhastCons, 1) as the central amino acid of a Mg^{2+} binding element (RXXTXGI) in first of three flexible 'Switch regions' (**Fig. 2.1c, d**). In the GTP-bound state, T182 interacts directly with the Mg^{2+} ion at the active site, coordinating the γ -phosphate of GTP (**Fig. 2.1e**)[133, 134], and mutagenesis studies using the rat ortholog of $G\alpha i2$ or human $G\alpha s$ have previously demonstrated a critical role for T182 in efficient GTP hydrolysis.[135, 136] Thus, overall it seemed likely that these novel T182 mutations were contributing to disease.

Hyperactivation in T182 $G\alpha i2$ mutants

The activation and inactivation of $G\alpha$ proteins is tightly regulated. Activation (GTP binding) first requires release of GDP from the nucleotide binding pocket, the rate-limiting step imposed by the high affinity of $G\alpha$ for GDP. Since the patients' cells expressed normal total levels of $G\alpha i2$ protein compared to healthy controls (**Fig. 2.2a** and **Supplementary Fig. 2.3c**) and a 1:1 ratio of WT to mutant transcripts (**Supplementary Fig. 2.3d**), we hypothesized that the T182 $G\alpha i2$ mutations might alter GDP:GTP exchange to favor the active, GTP-bound state. We therefore purified recombinant $G\alpha i2$ proteins and conducted *in vitro* GTP-binding assays, by co-incubating non-hydrolyzable BODIPY-GTP γ S with GDP-bound WT, T182A, and T182I $G\alpha i2$ and monitored GTP γ S uptake in real time. The known partially activating RGS-insensitive G184S mutant, and constitutively active, GTPase-deficient Q205L $G\alpha i2$ were included for comparison.[107, 137] We found that T182 mutant proteins bound GTP γ S significantly faster than WT $G\alpha i2$ and the activating G184S and Q205L mutants (**Fig. 2.2b,c**). These data implied that the T182 mutant proteins rapidly shed GDP, thus

opening the binding site for GTP and spontaneously accelerating transition into the active GTP-bound state, an observation consistent with similar studies of this threonine in other G-proteins[135, 136].

Once activated, G α i family subunits are further controlled by two methods of inactivation: self-inactivation via intrinsic GTPase activity, and accelerated extrinsic inactivation (10 to 100 fold) through RGS mediated GAP activity.^[45, 138] We hypothesized that mutating T182 impaired the intrinsic and/or RGS accelerated inactivation of G α i2 and tested this via *in vitro* GTP hydrolysis assays. We found that the T182 mutants markedly impaired intrinsic GTP hydrolysis compared to WT (**Fig. 2.2d** dotted lines, and **Fig. 2.2e**) although to a lesser extent than the constitutively active, GTPase deficient Q205L mutant. We also found that adding RGS16, a RGS family protein highly expressed in immune cells, greatly accelerated GTP hydrolysis by WT G α i2 but did not affect RGS-insensitive G184S, GTPase-deficient Q205L, or patient-derived T182A or T182I mutants (**Fig. 2.2d** solid lines, **Fig. 2.2e**). Furthermore, we conducted RGS-binding assays to test the ability of purified RGS proteins to bind each G α i2 mutant. Consistent with the results of the GTP hydrolysis assays, WT G α i2 but neither T182A nor T182I G α i2 stably complexed with RGS proteins (**Supplementary Fig. 2.4a,b**). Thus, the T182A and T182I mutations impaired both intrinsic and extrinsic modes of inactivation. Taken together, these data suggested that T182A and T182I G α i2 are dominant gain-of-function mutants and might contribute to disease through overactive G α i2 effector function.

Defective leukocyte chemotaxis *in vitro* and *in vivo*

G α i2 couples to most chemokine receptors and is a critical mediator of chemokine signaling in the immune system.[54, 103, 104] Given its altered GTP hydrolysis and nucleotide binding, we tested the migration of the patient's cells *in vitro*. Compared to healthy controls, patient T cells and neutrophils showed impaired chemotaxis towards increasing doses of CXCL12 and CCL21 (T cells) or fMLP, IL-8, and leukotriene B₄ (neutrophils) but normal responses to C5a. (**Fig. 2.3a** and **Supplementary Fig. 2.5a**). We stimulated patient T cells with CXCL12, CCL19, CCL21, CCL3, CCL4, and CCL5 and found reduced chemokine induced Ca²⁺ fluxes (**Fig. 2.3b,c** and data not shown) and normal or slightly low surface expression of chemokine receptors (**Supplementary Fig 2.5b,c**). To determine the sufficiency of T182 mutations to inhibit chemokine receptor signaling and chemotaxis, we expressed T182A G α i2 in healthy control T cells via lentiviral transduction and examined chemokine-induced migration and Ca²⁺ flux. T182A and the constitutively active Q205L G α i2 but not WT G α i2, RGS-insensitive G184S G α i2 or a control protein (Luciferase) impaired both chemotaxis and Ca²⁺ flux without altering receptor levels (**Fig 2.3d,e,f** and **Supplemental Fig. 2.5d,e**). Thus, recapitulating results from patient cells, overexpressed T182A G α i2 was sufficient to disrupt chemotaxis and proximal chemokine receptor signaling *in vitro* supporting our hypothesis that these mutations are dominantly causing disease.

The patients' recurrent sinopulmonary and chronic skin infections are similar to that seen in other inherited diseases of defective leukocyte migration[116, 118, 119]. To determine if T182 mutations affected T cell homing *in vivo*, we used retroviral transduction (green fluorescent protein positive, GFP⁺) to stably express WT or T182A G α i2 in murine T cells (Thy1.1⁺CD45.2⁺) and co-transferred the cells with an equal number of transduced T cells stably expressing WT G α i2 (Thy1.1⁺CD45.1⁺) into a WT

recipient (Thy1.2⁺). Upon examining the ratio of transduced CD45.2⁺ to CD45.1⁺ cells in various target organs, we observed a significantly decreased proportion of T182A Gαi2 expressing cells in the splenic white pulp and lymph nodes (**Fig. 2.3e,f**) but not in circulation (**Supplementary Fig. 2.5f**). We further confirmed this defect by *in vivo* measurements of leukocyte migration into the P1's skin. To do this, small blisters were placed on the skin of the patient and healthy controls, thereby creating a chemoattractant source via sterile inflammation. Despite >10 times normal circulating leukocyte counts (**Supplementary Fig. 2.2g**), the patient's skin blisters contained <5% healthy control leukocyte concentration (**Supplementary Fig. 2.5g**). Additionally, we isolated and enumerated leukocytes migrating into the oral cavity and observed reduced numbers in the patient compared to healthy controls, a finding consistent with her early-onset periodontal bone loss[139] (**Supplemental Fig. 2.5i**). Taken together, these findings show a clear deficit in leukocyte migration.

Activating Gαi2 mutations uncouple chemokine receptor signaling

The ability of patient derived Gαi2 to impair chemokine receptor signaling in healthy control cells suggested a dominant interfering mechanism of action. This was surprising because it also exhibited RGS-insensitivity and a deficiency in GTPase activity (**Fig. 2.2b,c**), both hallmarks of constitutively active Gα subunits (e.g. Q205L Gαi2).^[140] We reasoned that T182 mutants might be uncoupled from chemokine receptors due to constitutive activation, and therefore unable to respond to receptor ligation, a situation that causes receptor hypo-responsiveness for other activating mutations.[141] Alternatively T182 mutants might stably bind GPCR cytoplasmic tails, blocking them from activating WT Gα proteins ("GPCR sequestration").[142, 143] We tested the ability of Gαi2 mutants to bind with chemokine receptors in living cells using bioluminescence

resonance energy transfer (BRET). This technology measures protein-protein interactions (<10 nm) between a photon donor (*Renilla* luciferase, RLuc91) embedded within G α i2 that excites a photon acceptor (yellow fluorescent protein, YFP) on the GPCR cytoplasmic tail (**Fig. 2.4a**).[144] G184S G α i2 bound CXCR4 and CCR7 with similar affinity (BRET_{max}, **Supplementary Fig. 2.6a,b**) to WT G α i2, however the constitutively active Q205L G α i2 and patient derived T182A G α i2 mutants showed minimal interaction, suggesting these mutations impaired GPCR-G α i2 coupling (**Fig. 2.4b,c**) without affecting receptor expression or localization (**Supplementary Fig. 2.6c-h**). GPCR-induced G α activation results in large conformational shifts within both proteins resulting in a loss of the baseline BRET signal (**Fig 2.4a**).[44] Using BRET, we tested the ability of T182A G α i2 to be activated by receptor stimulation. GPCR stimulation resulted in a dose-dependent reduction in BRET signal from WT and G184S G α i2-coupled GPCRs, but no change in BRET intensity from the constitutively activated Q205L G α i2 or patient derived T182A G α i2-coupled GPCRs (**Fig. 2.4d,e**). Notably, full-activation of WT and G184S G α i2 resulted in a BRET signal comparable to the pre-stimulation BRET signal of Q205L and T182A G α i2, suggesting these mutants spontaneously adopt an active conformation with respect to GPCRs. Together these data provided strong evidence that T182A G α i2 exists in an active conformation with respect to GPCRs and thereby disrupts chemokine signaling as its activity cannot be induced upon receptor ligation.

Hyper-responsive T Cell Phenotype

Although the patient's chemokine receptor signaling defects leading to impaired leukocyte migration could explain her immunodeficiency, the etiology of her

autoimmunity was less clear. To better understand this, we examined T cell functions *in vitro*. Compared to normal controls, we observed elevated IL-17 producing CD4⁺ T cells, reduced IFN- γ producing T cells, but normal percentages of CD4⁺CD25⁺CD127^{lo}FoxP3⁺ T_{reg} cells (**Supplementary Fig. 2.7a,b,c**). The patient's T cells exhibited augmented induction of activation markers CD69 and CD25 and increased cell proliferation in response to TCR stimulation (soluble anti-CD3 and anti-CD28), a difference that could be masked by using more potent TCR stimulation (immobilized anti-CD2, anti-CD3, anti-CD28). Similar results were obtained in purified T cells stimulated with soluble anti-CD3 without additional costimulation (**Fig. 2.5a,b,c** and **Supplementary Fig. 2.7d,e**), supporting the notion that the patient's T cells had a lower threshold for activation. To ensure that this effect was not due to heterogeneity within the T cell preps, we purified patient, parent, and healthy control naïve and memory CD4⁺ T cells by flow cytometry and observed marked hyper-responsiveness in her naïve and memory T cells compared to the other specimens. Notably, naïve CD4⁺ cells from healthy controls only responded to the strongest stimulation (immobilized anti-CD2, anti-CD3, and anti-CD28); by contrast, patient naïve CD4⁺ T cells proliferated in response to much weaker stimulation (soluble anti-CD3 and anti-CD28) and even upregulated CD69 in response to anti-CD3 only (**Supplementary Fig. 2.7 f,g,h,i**). We next examined if the patient's hyper-responsive T cell phenotype reflected more proximal events in TCR signaling. Following TCR ligation we saw no consistent differences in the magnitude or kinetics of TCR induced phosphorylation of CD3 ζ , ZAP70, LAT, or PLC γ 1 (data not shown), however, patient T cells exhibited increased cytosolic Ca²⁺ fluxes following TCR crosslinking compared to healthy controls (**Fig. 2.5d**). G α i2 and other G α -subunits are known to modulate T cell activation, but exactly how they influence activation remains unclear.

[145, 146] To determine the sufficiency of activating G α i2 mutants to augment T cell Ca²⁺ responses, we stably expressed WT, T182A, G184S, or Q205L G α i2 in T cells from healthy controls and examined TCR-mediated Ca²⁺ fluxes. Prolonged expression (21-35 days), but not short term expression (7-10 days), resulted in elevated TCR-induced Ca²⁺ fluxes in T182A and Q205L G α i2 expressing cells but not cells expressing WT or G184S G α i2 or a control protein (luciferase) (**Fig. 2.5e,f**). Thus exogenous expression of activating G α i2 mutations was sufficient to augment TCR-induced Ca²⁺ fluxes as seen in patient cells, supporting our hypothesis that activating G α i2 mutants augment TCR activation, reducing the requirement for costimulation.

Activating G α i2 mutations stimulate translational machinery

G α i family subunits, including G α i2, are direct inhibitors of cyclic adenosine monophosphate (cAMP) production by adenylyl cyclase (AC). Since cAMP is a potent inhibitor of T cell activation and proliferation, we hypothesized that T182 G α i2 mutants might constitutively lower cAMP levels resulting in T cell hyperactivation.[147] To determine if activating G α i2 mutants constitutively inhibit AC, we expressed WT, T182A, G184S, and Q205L G α i2 along with a BRET mediated cAMP reporter in cells and monitored drug induced cAMP levels. We found the activating T182A and Q205L G α i2 mutants inhibited drug induced cAMP production compared to WT and G184S G α i2 (**Fig. 2.6a**). However we did not detect differences in baseline or drug induced cAMP levels in patient T cells compared to healthy controls (**Fig. 2.6b**). Additionally pharmacological elevation of cAMP levels via phosphodiesterase inhibitor (Piclamilast) treatment did not normalize the patient T cell hyperactivation compared to healthy controls (**Fig. 2.6c**).

The activation of $G\alpha i2$ co-regulates the activation of $G\beta\gamma$. [100] Since a primary effector of $G\beta\gamma$ in lymphocytes is the $p110\gamma$ subunit of PI(3)K, we hypothesized that increased $p110\gamma$ activity in patient's T cells may be promoting T cell activation and effector function as demonstrated by activating mutations in other components of the PI(3)K pathway. [148-151] We therefore treated healthy control and patient T cells with increasing doses of the $p110\gamma$ inhibitor (AS605240), assessed T cell activation, and found that $p110\gamma$ inhibition did not normalize patient T cell activation relative to healthy controls (**Fig. 2.6d**). Additionally, baseline and TCR-induced phosphorylation of AKT (PKB), a downstream consequence of increased PI(3)K activity, was not increased in patient T cell relative to healthy controls (**Fig. 6e**).

A critical component of T cell activation and proliferation is the mobilization of translational machinery necessary to meet the increased protein synthetic demand. Activated 70 kDa ribosomal S6 kinase (p70S6K) phosphorylates ribosomal protein S6. This enhances translation of ribosomal proteins and elongation factors and permits rapid cellular proliferation. [152] We assessed S6 phosphorylation at residues S235/S236 and S240/S244 before and after TCR stimulation and found increased levels of phosphorylated S6 in patient T cells compared to healthy controls (**Fig. 2.6f**). To determine the sufficiency of activating $G\alpha i2$ mutations to induce S6 phosphorylation, we stably expressed WT, T182A, G184S, and Q205L $G\alpha i2$ in a human acute T cell leukemia line and observed increased phosphorylation of S6 in T182A and Q205L $G\alpha i2$ expressing cells compared to cells expressing WT $G\alpha i2$ (**Fig. 2.6g**). These data demonstrate that T182 $G\alpha i2$ mutants constitutively activate the translational machinery necessary for rapid proliferation, likely contributing to the hyper-responsiveness of patient T cells to TCR ligation. Together these data support the hypothesis that

activating mutations in *Gαi2* decouple *Gαi2*-associated GPCRs resulting in impaired chemokine signaling and susceptibility to mucocutaneous infections while simultaneously reducing the requirements for full T cell activation by augmenting costimulatory pathways (**Fig. 2.7**).

2.4 Discussion

Genetic immunodeficiencies in humans frequently co-present with autoimmunity, but how individual gene products simultaneously regulate immune-competence and prevent autoimmunity is not well understood.[153, 154] *Gαi2* knockout mice are susceptible to bacterial and viral infections; they also develop autoimmune colitis and adenocarcinomas on some genetic backgrounds but not on others.[54, 155] Knock-in mice bearing the partially activating RGS-insensitive G184S *Gαi2* are mildly immunodeficient, but do not develop autoimmune disease.[108, 156] These studies place *Gαi2* at the nexus of immunodeficiency and autoimmunity, but do not provide a simple explanation where a lack of *Gαi2* activity leads to immunodeficiency and increased *Gαi2* activity leads to autoimmunity. Recently the two activating mutations found here (T182A and T182I *Gαi2*) and two other constitutively activating *Gαi2* mutations were found to be overrepresented in somatic mutations in T cell lymphomas.[130] This corroborates earlier findings of activating *Gαi2* mutations in other tumors and the idea that the pathways driven by activating *Gαi2* promote tumorigenesis possibly through promoting mitogenesis and cell cycle dysregulation.[131] Despite growing evidence of the importance of *Gαi2* in immune regulation and development among other functions, the full phenotypic effect of *GNAI2* mutations in humans has not been described. We have now reported the identification of two patients with

heterozygous *de novo* activating mutations affecting multiple organ systems resulting in a novel immunodysregulation disorder comprising life-threatening immunodeficiency and autoimmunity.

The patients described here presented early in life with combined immunodeficiency of T and B cells and recurrent sinopulmonary tract infections. A distinguishing feature of this disease is recurrent mucocutaneous bacteria and viral infections with a progressive neutrophilia and monocytosis. This phenotype is reminiscent of the LADs and consistent with the role of $G\alpha i2$ in leukocyte chemotaxis and extravasation from the circulation.[52] The presentation of severe recurrent human papillomavirus and herpes zoster infections (chronic cutaneous DNA virus infections) without concomitant cytomegalovirus or Epstein-Barr virus viremia (chronic lymphocyte DNA virus infections), is tightly associated with impaired T cell chemotaxis and effector function in solid tissues (e.g. DOCK8).[110] Thus the immunodeficiency has features of defects of both neutrophil migration (e.g. LAD)[113, 114, 116] and lymphocyte migration (e.g. DOCK8)[110] such as Wiskott-Aldrich syndrome (WAS)[157, 158] or WHIM.[119, 120] Both patients exhibited decreased antibody production (IgM and IgG); however, thorough analysis of the B cell compartment was not possible due to therapeutic B cell ablation for treatment of autoimmune cytopenias. We have shown impaired neutrophil and T cell chemotaxis and chemokine signaling in patients with activating $G\alpha i2$ mutations as well as the sufficiency of exogenously expressed GOF $G\alpha i2$ to impair chemotaxis in healthy control cells. Of note, our clinical observations and *in vitro* and *in vivo* experiments demonstrate the migration defect is partial compared to severe forms of LAD and DOCK8 deficiency.[116, 118] This is likely due to the heterozygous state of *de novo* mutations as the mutant proteins tested in isolation showed severely impaired

GTP hydrolysis and GPCR coupling/responsiveness. Furthermore, we have shown in living cells that activating mutations in G α i2 decouple G α i2-chemokine receptor interactions, breaking the signaling circuit necessary for chemokine responsiveness. This observation is similar to the reduced effectiveness of drugs/stimuli on their targets after repeated stimulation (i.e. tachyphylaxis), and consider it “genetic tachyphylaxis” from the perspective of chemokine signaling. Through this mechanism, activating G α i2 mutations represent the first human disease of cell migration due a mutation in a heterotrimeric G-protein.

Autoimmunity is commonly observed in Mendelian forms of immunodeficiency, however the features of autoimmunity are highly diverse and often difficult to explain.[153] While defects in cell migration such as WAS and DOCK8 deficiency may be associated with autoimmune cytopenias, impaired chemotaxis alone is infrequently associated with severe multi-organ system autoimmunity as seen in our patients.[159] Defects in TCR signaling, thymic selection, and peripheral tolerance, in addition to activating germline mutations in cytokine signaling proteins such as STAT3 and STAT1, all cause life-threatening multi-organ system autoimmunity.[141, 160, 161] We therefore focused on the patient T cells and demonstrated a reduced requirement for T cell costimulation (a necessary mechanism of peripheral tolerance), augmented TCR mediated Ca²⁺ fluxes (a fundamental part of TCR signaling and a critical determinant of thymic selection), and hyperactivation of translational machinery necessary for cell growth and division. While significant dysregulation of any one of these processes can result in life-threatening autoimmune disease[153, 159], we propose that augmented TCR signaling, constitutive activation of downstream translational machinery, and likely

other, yet unidentified, processes are working together to permit otherwise suboptimal TCR signals to result in full T cell activation and proliferation.

We have shown exogenous expression of activating $G\alpha i2$ mutants in control T cells is sufficient to impair chemokine signaling and augment TCR mediated Ca^{2+} fluxes. Short term expression of activating $G\alpha i2$ mutants immediately impaired chemokine signaling; however, prolonged expression of activating $G\alpha i2$ over multiple cell divisions was required to phenocopy the augmented TCR-mediated Ca^{2+} responses observed in patient T cells. That we could recapitulate this behavior in healthy control peripheral T cells demonstrates that the patient T cell phenotype is not simply a result of aberrant selection in the thymus, however our results cannot rule out that abnormal thymic selection does not occur in patients. $G\alpha i2$ knockout mice have been reported to have defects in thymic egress and some have postulated that this contributes to the autoimmune colitis they exhibit on the 129SvEv background.[54, 155, 162] Interestingly, T cells from these mice exhibit augmented TCR mediated Ca^{2+} fluxes and reduced costimulatory requirement; however, this may be an effect of T cells developing in the absence of $G\alpha i2$ rather than a reflection of the role of $G\alpha i2$ in normal T cells.[146] Because $G\alpha i2$ mutations constitutively inhibit cAMP production *in vitro* and phosphorylation of S6 in patient cells, our results suggest the patients' T cell hyper-responsiveness is not simply the result of deficient $G\alpha i2$ -dependent GPCR signaling, but rather that enhanced $G\alpha i2$ signaling reprograms T cells overtime, altering their response to TCR stimulation and reducing their requirement for costimulation. The inability of acute pharmacological inhibition of PDEs or p110 γ to normalize patient T cell responses supports the hypothesis of a more permanent hyper-responsive state being established by activating $G\alpha i2$ mutants over time.

These observations supported the rationale for generating a knock-in mouse bearing a highly active G α i2 (T182I), however our efforts suggested *in utero* selection against T182I G α i2 expressing embryos (**Supplementary Table 2.3**). While G184S G α i2 knock-in mice are viable even as homozygotes, both heterozygous and homozygous mice are born below Mendelian frequencies.[108] Therefore, it is likely that more activating T182 mutations are also subject to *in utero* selection. As sequencing efforts expand worldwide, it will be important to determine the incidence of this disease compared to the spontaneous mutation rate at the *GNAI2* locus. If *in utero* selection is occurring, understanding the genetic variation that permits survival of these patients will be important for understanding the pathogenesis of this disease.

In conclusion, we have identified a previously unknown human immunodysregulation disorder we call 'MAGIS syndrome' (Myelocytosis, Autoimmunity, Gain-of-function G α i2, Immunodeficiency, and Short stature). This disease is characterized by dominant, gain-of-function mutations in *GNAI2*, and results in developmental abnormalities, immunodeficiency due to chemotaxis and chemokine signaling, and autoimmunity characterized by hyper-responsive T cell activation and a reduced requirement for T cell costimulation.

2.5 Tables

Table 2.1 Patient Characteristics.

	P1	P2
Gai2 mutation	T182A	T182I
Age, Sex	28, F	8 (†), M
Sinupulmonary Bacterial Infections	✓	✓
Skin Infections (DNA viruses)	✓	No
Skin Infections (Bacteria)	✓	✓
Bacterial infections	Mastoiditis	Meningitis
Otitis media (recurrent)	✓	✓
Autoimmune Cytopenias	✓, DAT+	✓, DAT+
Psoriatic Arthritis	✓	No
CNS Infiltrates	No	✓
Intrauterine Growth Restriction	✓	✓
Short Stature (<3rd percentile)	✓	✓
Gut Malrotation	✓	No
Vertebral Malformation	T4, T6	T5, T7
Dysmorphism	✓ (mild)	✓ (mild)
Splenomegaly	✓	✓
Monocytosis	✓	✓
Neutrophilia	✓	✓
T Cell Subsets	CD4+ ↓* CD4+ naïve ↓ CD4+ memory nl CD8+ ↓* CD4+ naïve ↓ CD4+ memory ↑	CD4+ ↓ ND ND CD8+ ↓ ND ND

Infections, autoimmunity, developmental abnormalities, and immunological phenotypes of patients. M, male; F, female; †, deceased; ✓, present; ↓, decreased abundance; ↑, increased abundance; ND, not determined; DAT+, direct antiglobulin test positive; T4-T7, thoracic vertebrae 4 through 7. *normalized following splenectomy.

2.6 Figures

Figure 2.1 *De novo* mutations at the active site of Gαi2.

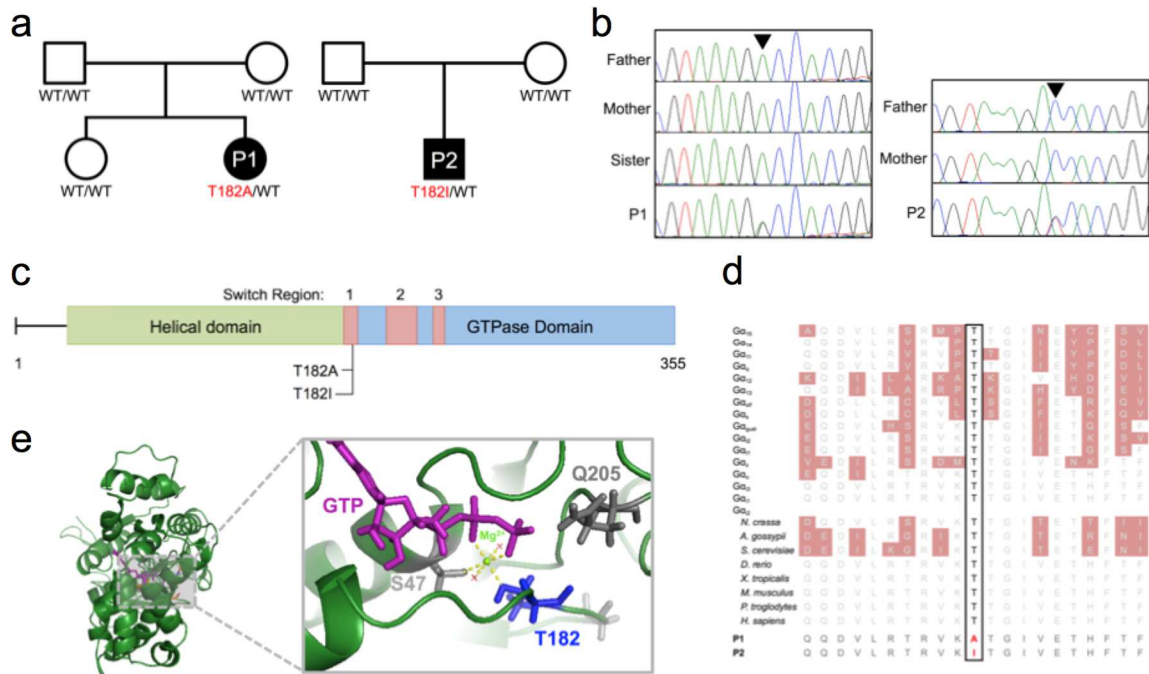


Figure 2.1 *De novo* mutations at the active site of Gαi2. (a) Patient pedigrees showing *de novo* mutations c.544A>G, p.T182A (P1) and c.545C>T, pT182I (P1), WT = wild type (b) Sanger sequencing electropherograms of genomic DNA (isolated from blood leukocytes) bases corresponding to the mutations indicated by the inverted triangle; green = adenine, red = thymine, black = guanine, blue = cytosine. P1 family (left); P2 (right) (c) Schematic representation of Gαi2 showing the helical domain (green) and GTPase domain (blue) containing three switch regions (red). Black line indicates location of patient mutations. (d) Amino acid sequence alignment of corresponding protein region from all human heterotrimeric Gα subunits and selected Gαi2 sequences from other species. Amino acids not conserved with human Gαi2 are shown in red; the affected threonine is boxed and bolded. (e) Structural ribbon representation of Gαi2 (dark green) bound to GTP (left) with zoomed view (right) showing GTP (purple) bound by GTPase binding domain and threonine 182's (T182, blue) role in the octahedral coordination shell of Mg²⁺ (bright green sphere). Additional ionic bonds (yellow dashes) are with the β-phosphate of GTP, γ-phosphate of GTP, serine 47 (S47, light gray), glutamine 205 (Q205, dark gray), and two with free water molecules (red X's). Mentioned amino acids are shown in 'tube' format. Structures represent fitting primary amino acid sequence of Gαi2 onto the structure of Gαi3 (Protein Data Bank accession code 2V4Z). Standard single amino acid code is employed throughout.

Figure 2.2 T182 Gai2 mutants are activated in multiple ways.

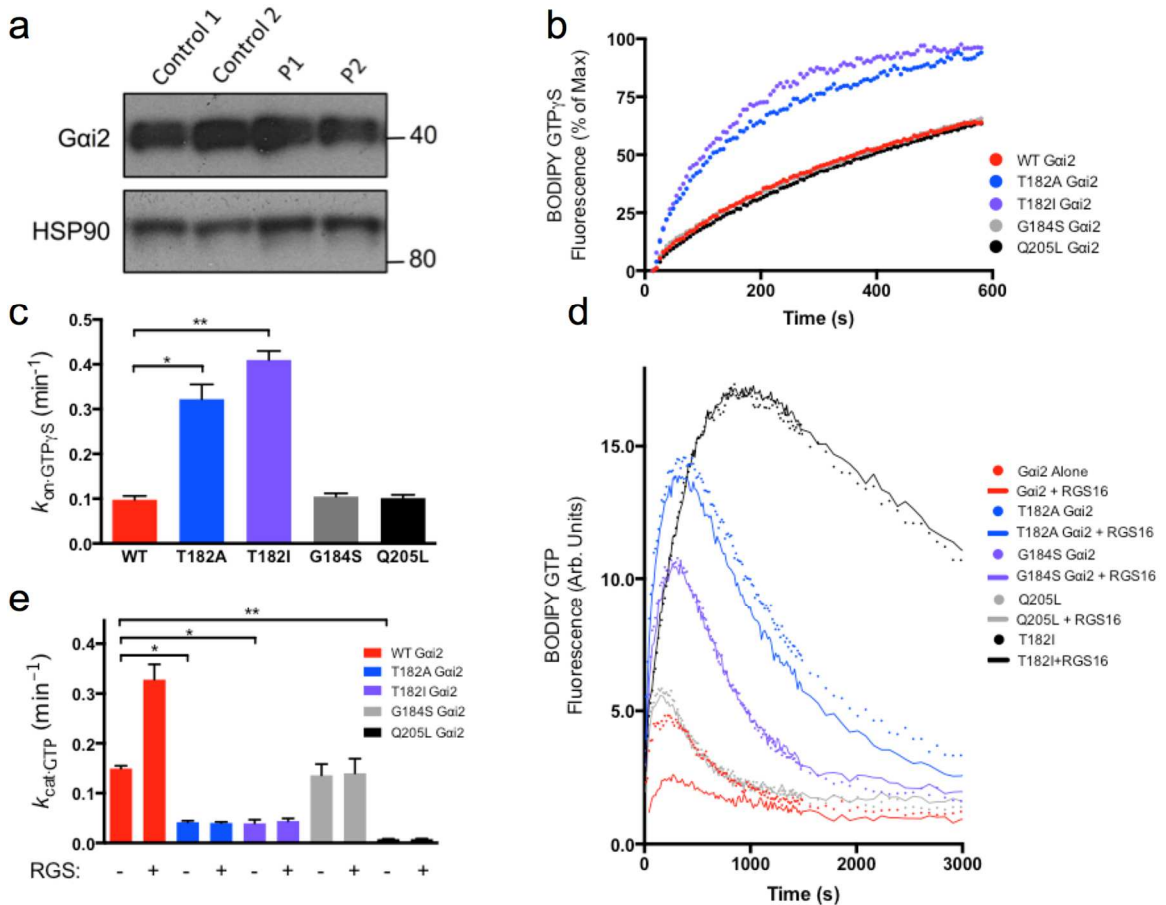


Figure 2.2 T182 Gai2 mutants are activated in multiple ways. (a) Immunoblot analysis of Gai2 and heat shock protein 90 (HSP90) loading control from whole cell extracts from patient and healthy control fibroblasts (b,c,d,e) *In vitro* biochemistry comparing WT, T182A (P1's mutation), T182I (P2's mutation), G184S (RGS-insensitive only), and Q205L (GTPase deficient, RGS-insensitive). BODIPY-GTP analogs increase fluorescence upon G-protein binding and fluorescence is lost upon GTP hydrolysis.[163] (b) *In vitro* GTP binding assay. Purified WT or various mutant Gai2 proteins were incubated with non-hydrolyzable GTP analog BODIPY-GTP γ S. Changes in fluorescence were measure in real time. (c) Quantification of the binding rate constant ($k_{on-GTP\gamma S}$) from (b) as described in Methods. (d) *In vitro* GTP hydrolysis assay. Hydrolysis of BODIPY-GTP was measured in the presence of purified WT or various mutant Gai2 proteins with (solid lines) or without (individual points) purified RGS16. (e) Quantification of hydrolysis rate constant ($k_{cat-GTP}$) from (d) as described in Methods. Data representative of three independent experiments (a,b,d) or means \pm SD of three independent experiments (c,e). * $p < 0.05$, ** $p < 0.01$, by Kruskal-Wallis test (c,e).

Figure 2.3 Activating Gai2 mutants impair chemokine receptor signaling and chemotaxis.

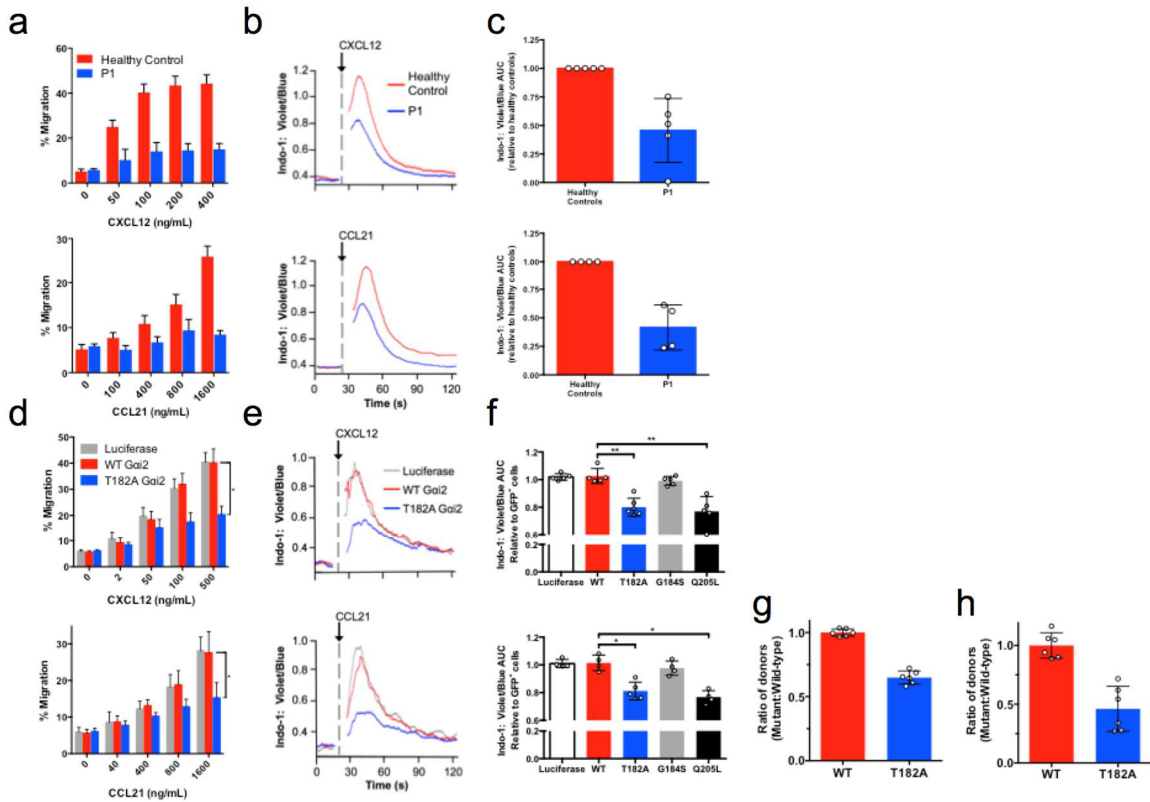


Figure 2.3 Activating Gai2 mutants impair chemokine receptor signaling and chemotaxis. (a) Proportion of healthy control or patient activated T cells migrating through transwell inserts in response to CXCL12 (upper) or CCL21 (lower). (b) Representative Ca²⁺ fluxes from healthy control and patient activated T cells stimulated with 500 ng/mL CXCL12 (upper) or 1 µg/mL CCL21 (lower) measured as the ratio of violet to blue fluorescence intensity of Indo-1 AM; see Methods for details. (c) Quantification of repeated Ca²⁺ fluxes from (b) as area under curve measurements normalized to healthy controls assessed in each experiment. (d) Same as (a) using activated healthy donor T cells stably expressing luciferase, WT Gai2, or T182A Gai2. (e) Same as (b) using activated healthy donor T cells stably expressing luciferase, WT Gai2, or T182A Gai2. (f) Quantification of repeated Ca²⁺ fluxes in (e) as area under curve measurements normalized to Ca²⁺ fluxes of untransduced cells in each culture. G184S and Q205L Gai2 were included as additional controls. (g, h) Ratio of transduced (GFP+) murine T cells stably expressing WT or T182A Gai2 (CD45.2+Thy1.2+) to transduced (GFP+) T cells stably expressing WT Gai2 (CD45.1+Thy1.2+) 36 hours after co-transfer into a WT (Thy1.1+) recipient and recovered from splenic white pulp (g, red pulp T cells were excluded via intravascular labeling, see Methods for details) or inguinal lymph nodes (h). Data show means ± SD (a,c,d,f,g,h) or representative data (b,e) from five independent experiments (d,e,f, upper), four independent experiments (d,e,f, lower), 2 independent experiments with three mice per group (g,h, open circles represent

individual mice), or five independent experiments with 10 (**a,b,c**, upper), 9 (**a**, lower), or 8 (**b,c**, lower) healthy controls. * $p < 0.05$, ** $p < 0.01$, by Kruskal-Wallis test in (**d**, comparing area under curve for each overexpression) and (**f**).

Figure 2.4 Impaired GPCR coupling and GPCR induced activation of T182 Gai2 mutants.

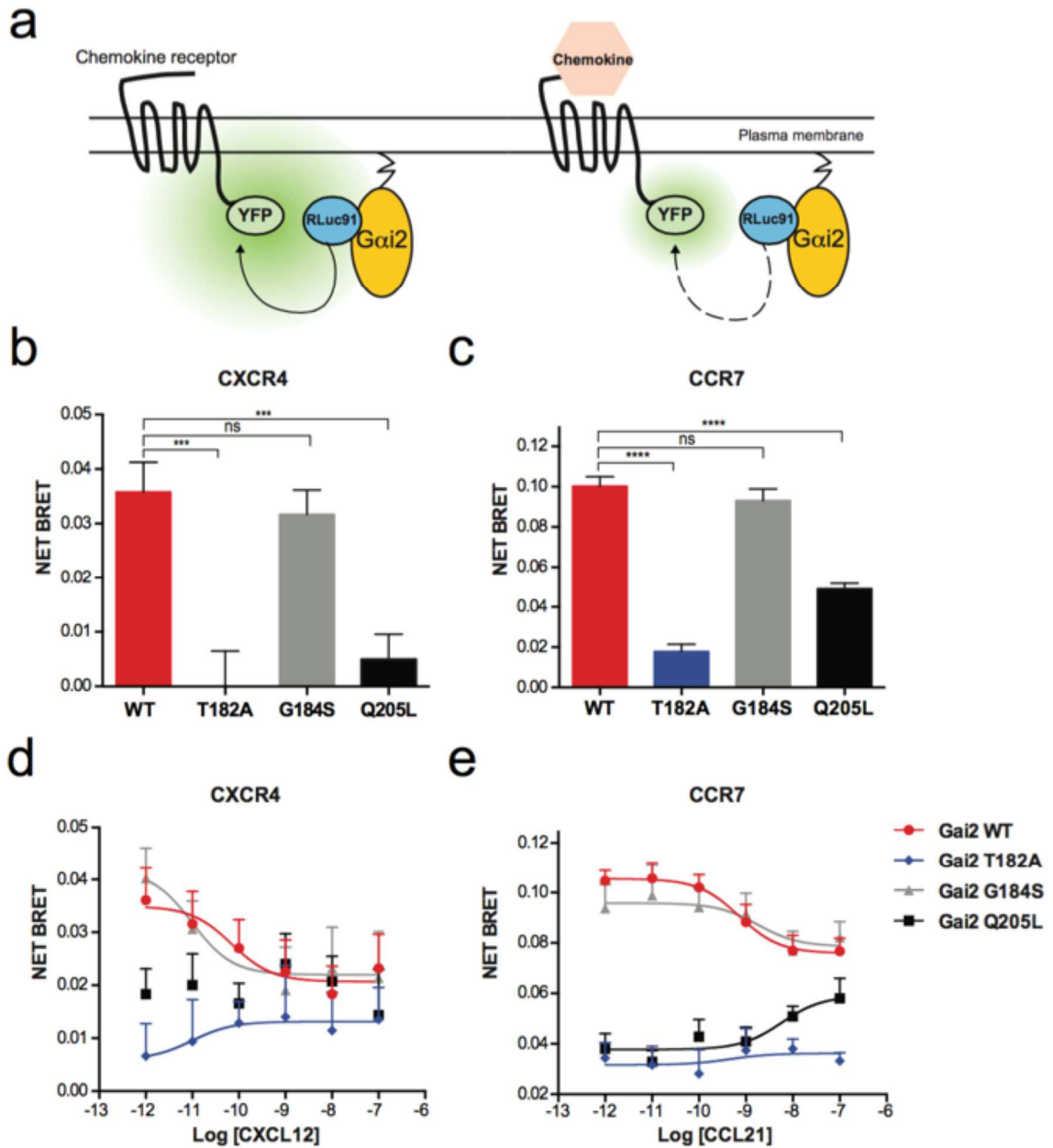


Figure 2.4 Impaired GPCR coupling and GPCR induced activation of T182 Gai2 mutants. (a) Schematic of BRET reaction between the photon donor Gai2-RLuc91 and photon acceptor GPCR-YFP. Ligand binding (right) results a conformational shift of the GPCR cytoplasmic tail, activation of WT Gai2, and a reduction of pre-ligand (left) BRET signal (green). RLuc91 = *Renilla* luciferase. (b,c) Net BRET signal of WT, T182A, G184S, or Q205L Gai2-RLuc91 and CXCR4-YFP (b) or CCR7-YFP (c) co-expressed in 293T cells without exogenous ligand. (d,e) Net BRET signal of WT, T182A, G184S, or Q205L Gai2-RLuc91 and CXCR4-YFP (d) or CCR7-YFP (e) co-expressed in 293T cells

after stimulation with increasing doses of CXCL12 and CCL21, respectively. Data show means \pm SEM of three to four independent experiments performed in triplicate. Statistical significance of the differences between BRET signal measured with WT G α i2-RLuc91 and mutant G α i2-RLuc91 constructs: ***, $p < 0.001$, ****, $p < 0.0001$ by Bonferroni's multiple comparison test in (d,e).

Figure 2.5 Gain-of-function $G\alpha i2$ augments T cell activation.

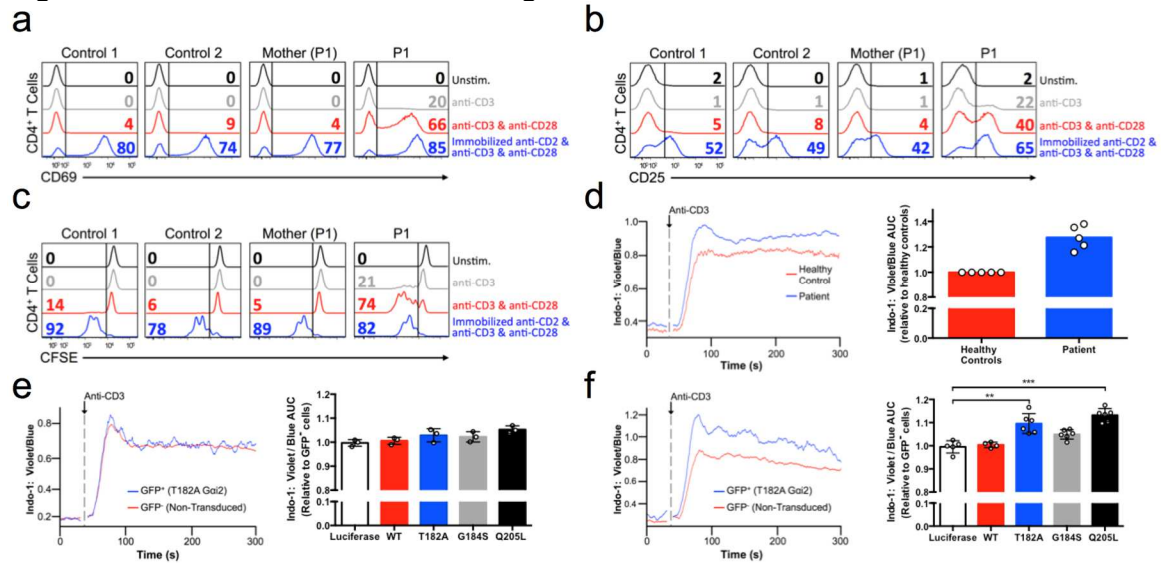


Figure 2.5 Gain-of-function $G\alpha i2$ augments T cell activation. **(a,b)** CD69 expression **(a)** or CD25 expression **(b)** on purified CD4⁺ T cells after 20 hours stimulation with anti-CD2 + anti-CD3 + anti-CD28 immobilized on beads (Miltenyi biotech, bead to cell ratio = 1:1), 1 μ g/mL of anti-CD3 and anti-CD28, 1 μ g/mL anti-CD3 only, or unstimulated (Unstim.). **(c)** CFSE dilution in purified CD4⁺ T cells after 96 hours stimulation as in **(a,b)**. **(d)** Representative T cell receptor mediated Ca²⁺ fluxes (left) with quantification (right, independent experiments showing area under curve calculations normalized to healthy controls from each) of patient and healthy control activated CD4⁺ cells stimulated with 10 μ g/mL anti-CD3 cross-linked with 200 ng/mL protein A. **(e,f)** Representative T cell receptor mediated Ca²⁺ fluxes (left) of healthy control CD4⁺ T cells stably expressing T182A $G\alpha i2$ (GFP⁺) and co-cultured non-transduced cells (GFP⁻) with quantification (right) of independent experiments showing area under curve for cells stably expressing luciferase or WT, T182A, G184S, or Q205L $G\alpha i2$ (GFP⁺) normalized to co-cultured non-transduced cells (GFP⁻) and stimulated as in **(d)** after short term (7-10 days) expression **(e)** and long term (21-35 days) expression **(f)**. All fluxes were measured as the ratio of violet to blue mean fluorescent intensity of Indo-1 AM; see Methods for details. Data show means \pm SD **(d,e,f** right side) or representative data **(a,b,c** and **d,e,f** left side) from four independent experiments with 15 healthy controls **(a,b)**, three independent experiments with 11 healthy controls **(c)**, five independent experiments with 10 healthy controls **(d)**, three independent experiments **(e)** or four to six independent experiments **(f)**. ** $p < 0.01$, *** $p < 0.001$ by Kruskal-Wallis test **(e,f)**. See **Supplementary Fig. 2.7 d,e** for full quantification of **(a,b,c)**.

Figure 2.6 Activating G α i2 mutants stimulate translational machinery.

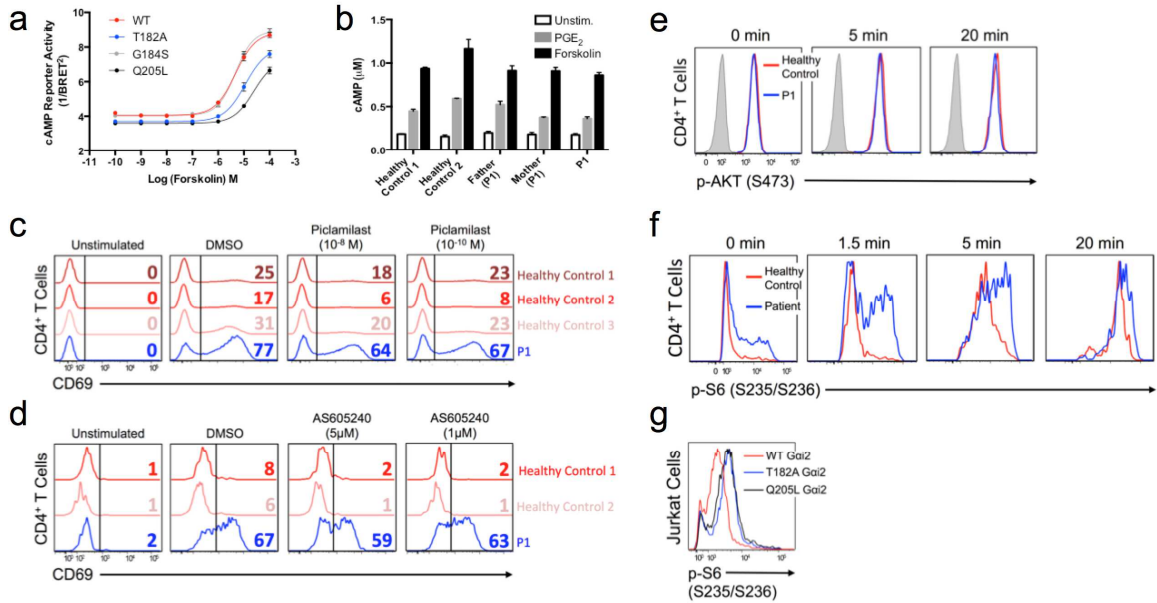


Figure 2.6 Activating G α i2 mutants stimulate translational machinery. **(a)** cAMP BRET reporter Rluc3-EPAC-GFP10 activity in 293T cells expressing WT, T182A, G184S, or Q205L G α i2 upon treatment with increasing doses of forskolin (adenylyl cyclase agonist). **(b)** cAMP levels determined by competitive ELISA of patient, parent, and healthy control T cell lysates either unstimulated (Unstim.) or stimulated with PGE₂ or Forskolin. **(c,d)** CD69 expression of purified patient and healthy control CD4⁺ T cells pretreated for 6 hours with vehicle control (DMSO) or different doses of the PDE4 inhibitor, Piclamilast **(c)**, or the p110 γ inhibitor, AS605240 **(d)**, and activated with 1 μ g/mL anti-CD3 and anti-CD28 for 20 hours. **(e,f)** Phosphorylation of AKT at Ser473 (p-AKT(S473)) **(e)** or S6 at Ser235/S236 (p-S6(S235/S236)) **(f)** in patient and healthy control T cell blasts either unstimulated or stimulated with anti-CD3 (10 μ g/mL) plus protein A (200ng/mL) for indicated time. **(g)** Phosphorylation of S6 at Ser235/S236 (p-S6(S235/S236)) in unstimulated Jurkat cells (rested and fixed in serum free media) stably expressing WT, T182A, or Q205L G α i2. Data show means \pm SEM from representative experiment done in triplicate **(a)** (n=2), or representative data from four independent experiments **(b,e,f)** or two independent experiments **(c,d,g)**.

Figure 2.7 Proposed model for the effects of activating mutations of Gai2 on T cell chemotaxis and T cell activation.

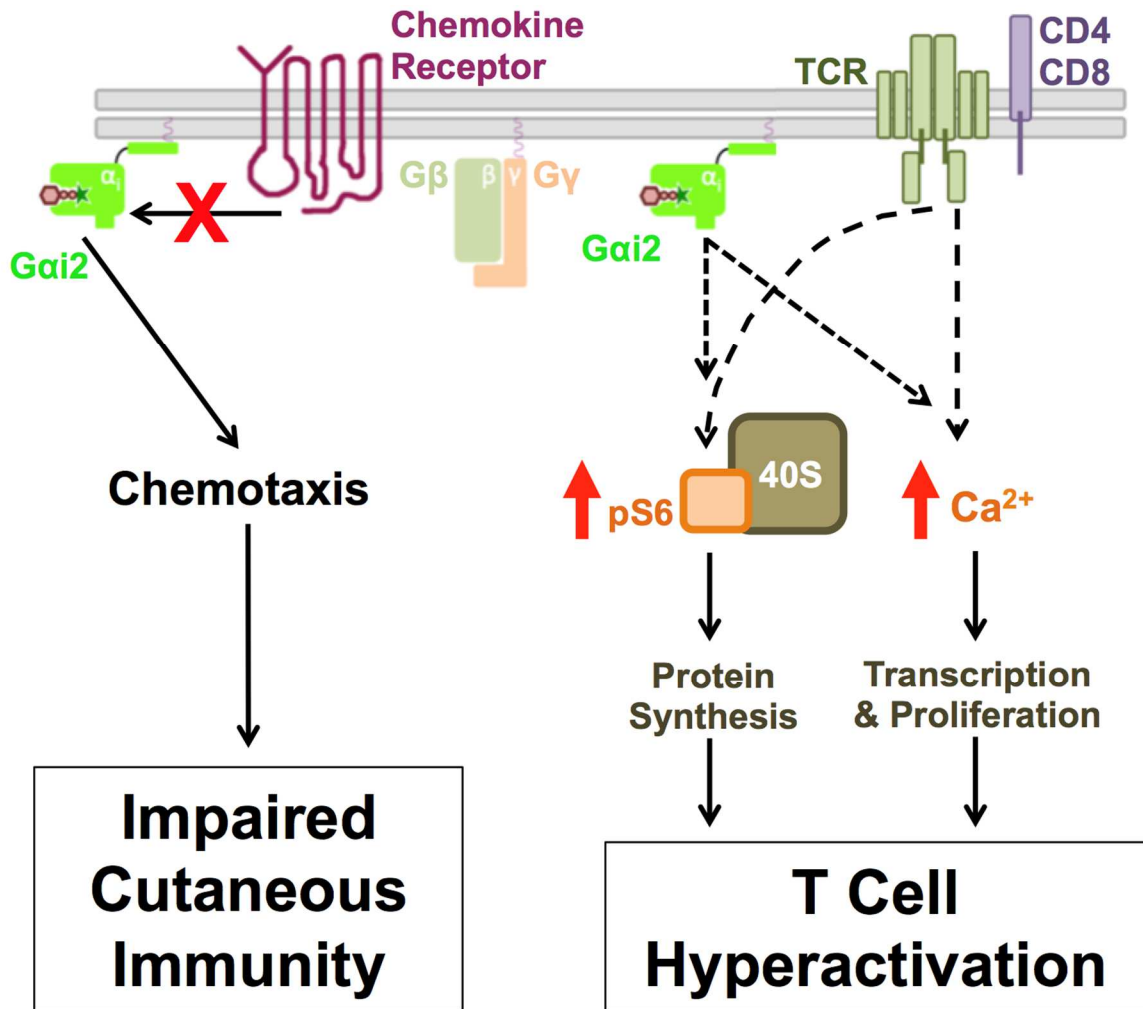
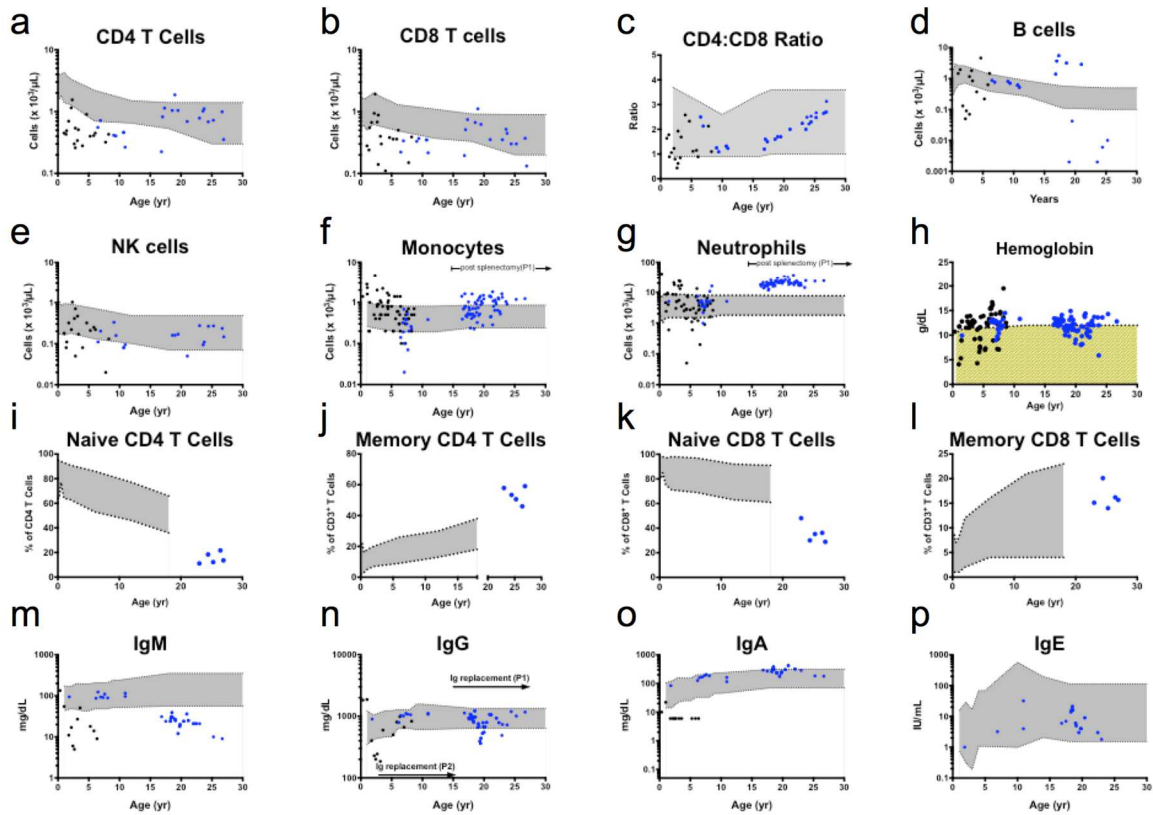


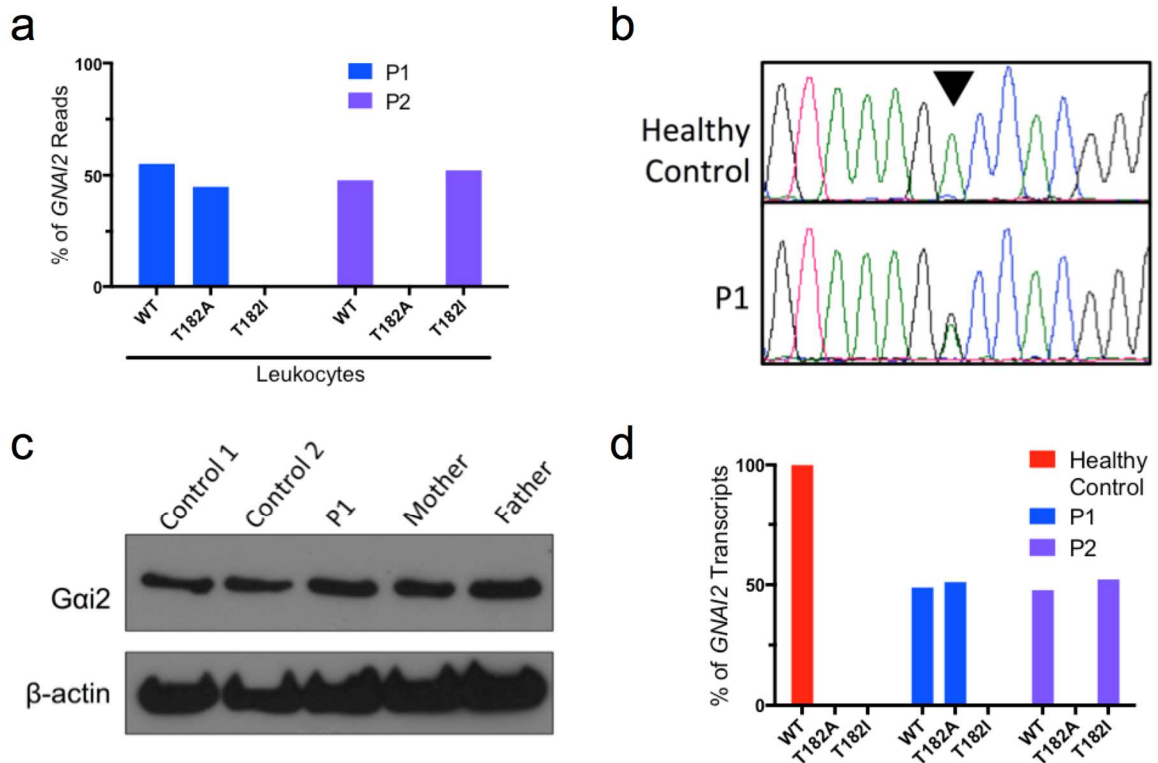
Figure 2.7 Proposed model for the effects of activating mutations of Gai2 on T cell chemotaxis and T cell activation. Activating mutations in Gai2 uncouple Gai2 from chemokine receptors resulting in blunted chemokine signaling, defective chemotaxis, and impaired cutaneous immunity. Activating Gai2 mutations augment TCR mediated Ca²⁺ and activate translational machinery promoting T cell hyperactivation.

Supplementary Figure 2.2 Patient laboratory values.



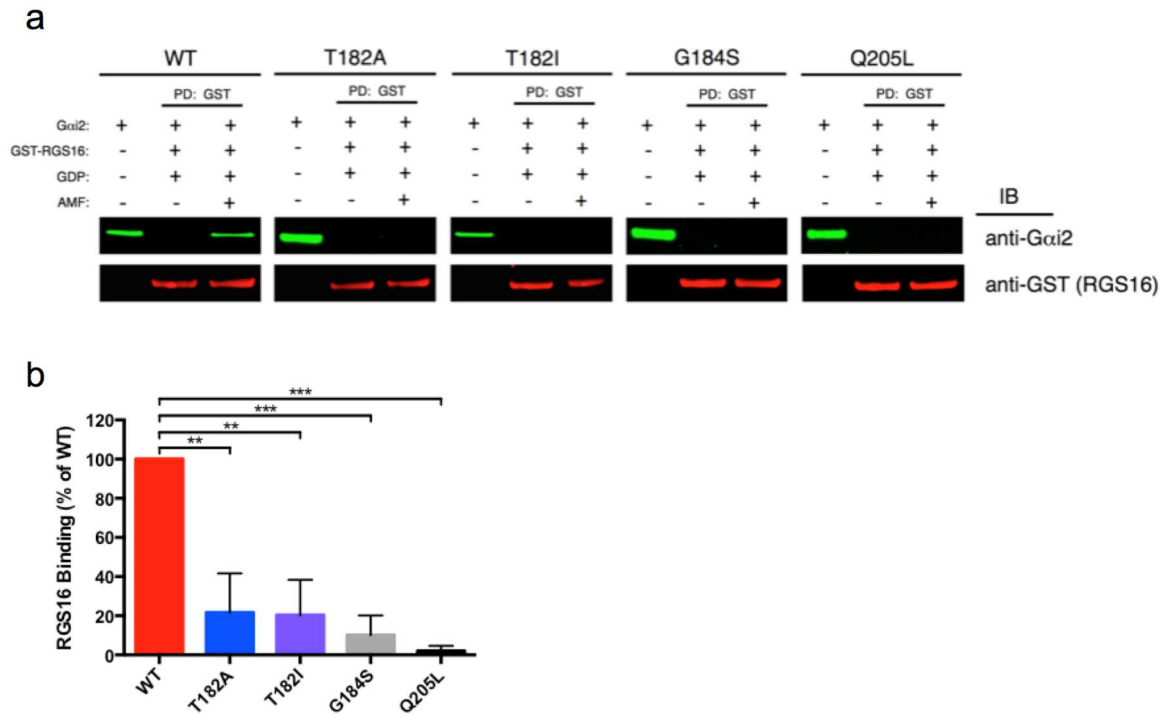
Supplementary Figure 2.2 Patient laboratory values (a-p) Patient laboratory values measuring the peripheral blood for absolute CD4⁺ (a) and CD8⁺ (b) T cell count; the ratio of CD4⁺ to CD8⁺ T cells (c); absolute B cell (d), natural killer (NK) cell (e), monocyte (f), and neutrophils (g); hemoglobin concentration (h); the percentages of naïve CD4⁺CD45RA⁺ (i) and naïve CD8⁺CD45RA⁺ (k) T cells among CD4⁺ and CD8⁺ T cells, respectively; the percentages of memory CD4⁺CD45RO⁺ (j) and memory CD8⁺CD45RO⁺ (l) T cells among all CD3⁺ T cells; serum immunoglobulin concentrations: IgM (m), IgG (n), IgA (o), and IgE (p). Gray range indicates 5th to 95th percentile of normal values vs. age. Blue circles represent P1. Black circles represent P2.

Supplementary Figure 2.3 WT and mutant DNA, RNA, and protein levels.



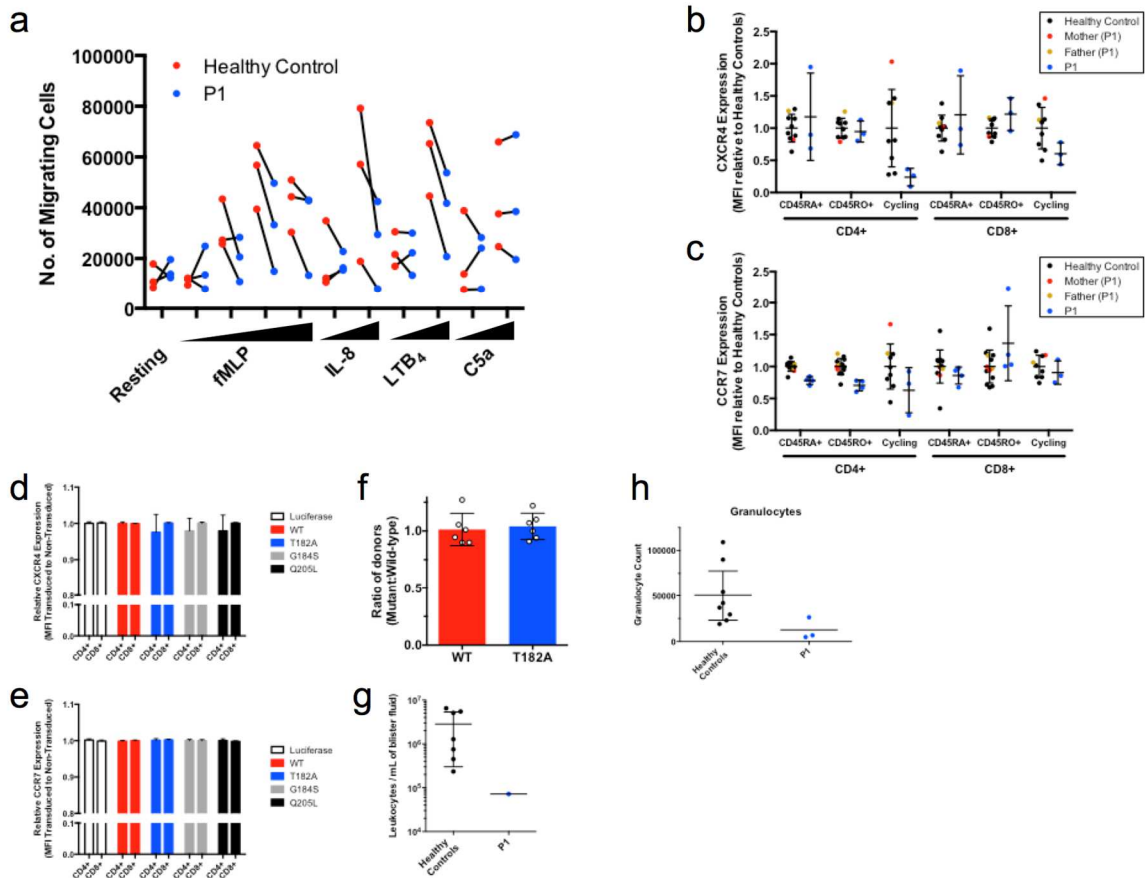
Supplementary Figure 2.3 WT and mutant DNA, RNA, and protein levels (a) Percentage of WT and mutant (c.544A>G, p.T182A = "T182A" or c.545C>T, pT182I = "T182I") WES DNA sequencing reads from blood leukocytes. Data represent WES reads as percent of reads mapping to aforementioned point mutation site (coverage >100X at this site for all samples). (b) Sanger sequencing electropherograms of genomic DNA (isolated from dermal fibroblasts) base corresponding to the mutations indicated by the inverted triangle. P1 and healthy control; P2 (data not shown); green = adenine, red = thymine, black = guanine, blue = cytosine. (c) Immunoblot analysis of Gai2 and β-actin loading control from whole cell extracts from P1, parent, and healthy control activated T cells. (d) Quantification of wild-type (WT) and mutant (c.544A>G, p.T182A = "T182A" or c.545C>T, pT182I = "T182I") transcripts from control and patient T cells (P1) or patient fibroblasts (P2). Messenger RNA was reverse transcribed into cDNA. *GNAI2* transcripts were PCR amplified and sub-cloned into pCR4-TOPO vector (Life Technologies). Individual clones (96 control, 96 from each patient) were selected and sequenced. Data are representative of three independent experiments (c).

Supplementary Figure 2.4 T182 Gαi2 mutants abrogate RGS-binding.



Supplementary Figure 2.4 T182 Gαi2 mutants abrogate RGS-binding (**a**) RGS-binding assay. Purified recombinant His-Gαi2 (WT, T182A, T182I, G184S, or Q205L), purified recombinant GST-RGS16, and glutathione sepharose beads were co-incubated together with GDP with or without aluminum magnesium fluoride (AMF), which mimics the pre-transition state of GTP hydrolysis, the stabilized state during RGS binding.[164] Beads were washed, bound proteins were eluted, and pull-down (PD) contents were separated by SDS-PAGE. Immunoblot for pulled down RGS16 (anti-GST) and associated Gαi2 (anti-Gαi2) is shown. Gαi2 only lane (left lane for each blot) shows 20% of input Gαi2 protein. (**b**) Quantification of Gαi2 pull-down signal from AMF+ (right lane for each blot) compared to the amount of WT Gαi2 bound to RGS16 (100%). Representative data (**a**) or means ± SD of 3-4 independent experiments (**b**), **p = 0.002; ***p < 0.0004, one-way ANOVA with Dunnett's multiple comparison test.

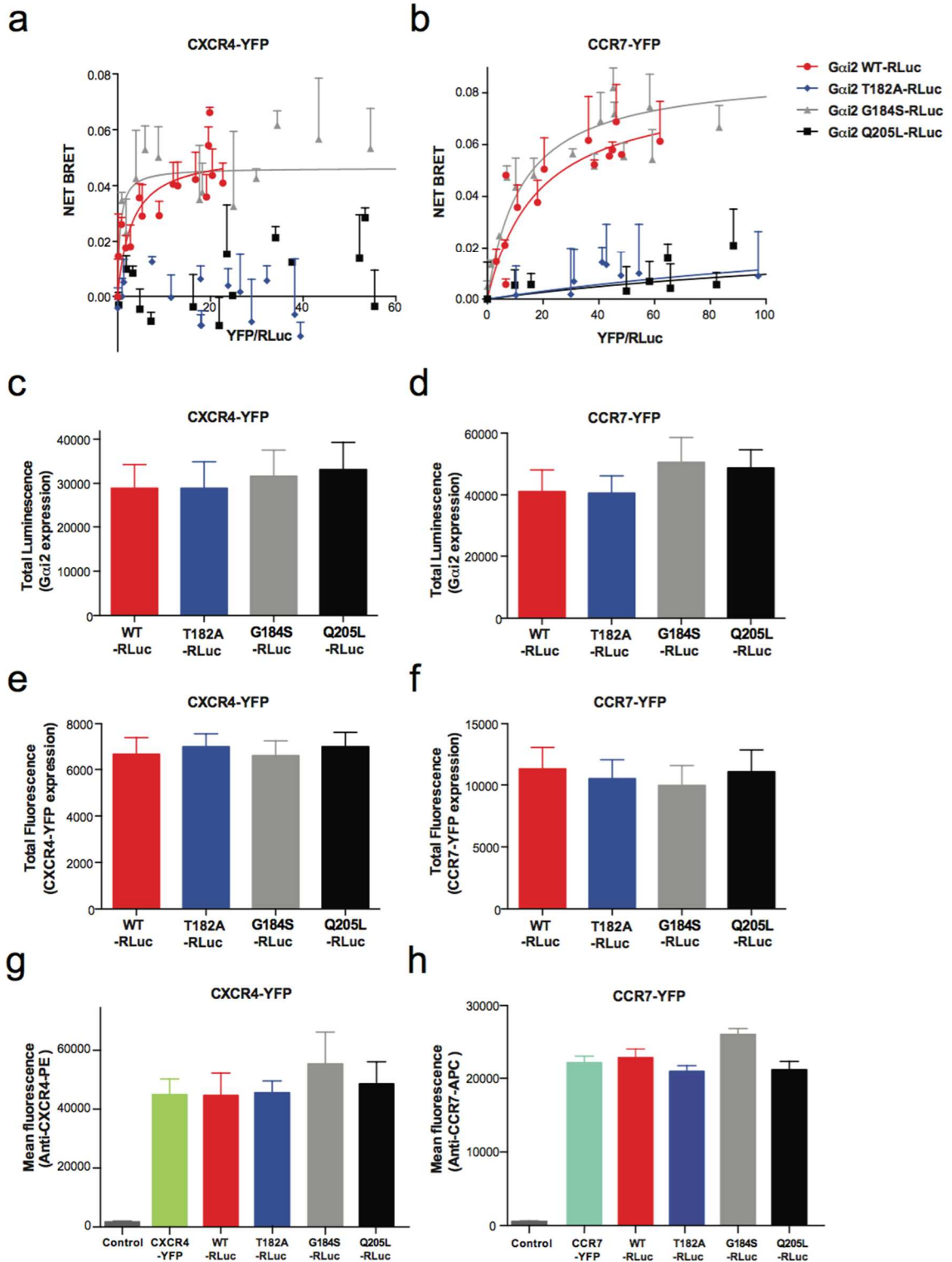
Supplementary Figure 2.5 Activating $G\alpha i2$ mutants impair chemotaxis *in vitro* and *in vivo*.



Supplementary Figure 2.5 Activating $G\alpha i2$ mutants impair chemotaxis *in vitro* and *in vivo*. **(a)** Neutrophil chemotaxis assay from P1 and healthy controls in response to indicated chemokines. Connected data points indicate samples purified and analyzed together. All measurements done using the NeuroProbe chemotaxis system; see Methods for details ($n=3$). **(b,c)** Flow cytometry staining for surface expression of CXCR4 **(b)** and CCR7 **(c)** on healthy control and patient (P1) naive (CD45RA⁺), memory (CD45RO⁺), or cycling CD4⁺ or CD8⁺ T cell blasts. Mean fluorescence intensity (MFI) of patient is shown relative to the healthy control MFI from each experiment. Data shows mean \pm SD of 3 or 4 independent experiments. **(d,e)** Flow cytometry staining for surface expression of CXCR4 **(d)** and CCR7 **(e)** in healthy donor T cells stably expressing luciferase or WT, T182A, G184S, or Q205L $G\alpha i2$. MFI of transduced cells is shown relative to non-transduced cells in the same culture. **(f)** Ratio of transduced (GFP⁺) murine T cells stably expressing WT or T182A $G\alpha i2$ (CD45.2+Thy1.2+) to transduced (GFP⁺) T cells stably expressing WT $G\alpha i2$ (CD45.1+Thy1.2+) 36 hours after co-transfer into a WT (Thy1.1+) recipient and recovered from the blood. **(g)** Concentration of leukocytes in blister fluid from *in vivo* chemotaxis assay from healthy controls (mean and 95% CI) and P1 ($n = 1$). **(h)** Absolute number of granulocytes recovered from oral cavity

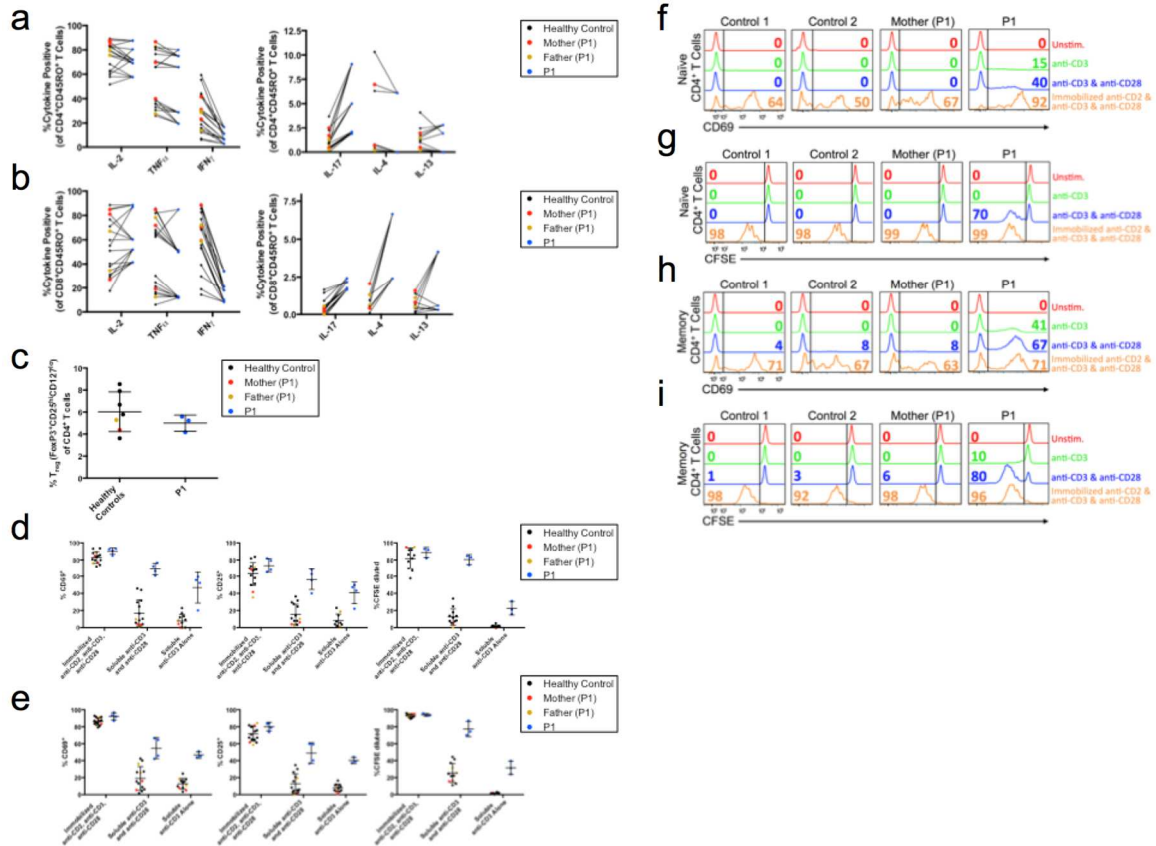
from healthy controls (mean and 95% CI) and P1 (n = 3) by oral rinse and quantified by flow cytometry. Data representative of mean \pm SD of 3 independent experiments (**a,b,c,d,e**) or 2 independent experiments with 3 mice per experiment (**f**, individual data points represent individual mice).

Supplementary Figure 2.6 Determination of BRET_{max} and acceptor/donor expression levels in BRET experiments



Supplementary Figure 2.6 Determination of BRET_{max} and acceptor/donor expression levels in BRET experiments. **(a,b)** Acceptor/donor titration curves for determination of BRET maximum (BRET_{max}). 293T cells were transfected with WT, T182A, G184S, or Q205L Gai2-RLuc91 (donor) and increasing amounts of CXCR4-YFP **(a)** or CCR7-YFP **(b)** (acceptors). The net BRET signal was determined and graphed as a function GPCR-YFP fluorescence (acceptor) to Gai2-RLuc91 chemiluminescence (donor) ratio (YFP/RLuc). **(c,d)** Total WT, T182A, G184S, or Q205L Gai2-RLuc91 expression in the presence of CXCR4-YFP **(c)** or CCR7-YFP **(d)** measured by total *Renilla* luciferase expression from transfections in **Fig. 4b-e** (at BRET_{max}). **(e,f)** Total CXCR4-YFP **(e)** or CCR7-YFP **(f)** expression measured by YFP fluorescence in transfections in **Fig. 4b-e** (at BRET_{max}). **(g,h)** Cell surface expression of CXCR4-YFP **(g)** or CCR7-YFP **(h)** measured by flow cytometry in transfections in **Fig. 2.4b-e** (at BRET_{max}). Data shows means ± SEM of triplicate measurements of one representative experiment of four independent experiments **(a,b)** or means ± SEM of four independent experiments performed in triplicate **(c-h)**.

Supplementary Figure 2.7 Patient T cell cytokine production and activation.



Supplementary Figure 2.7 Patient T cell cytokine production and activation. **(a,b)** Unstimulated *ex vivo* purified T cells were stimulated with PMA and ionomycin for 8 hours in the presence of Brefeldin A and then stained intracellularly for the indicated cytokines. Data shown are the percentages of cytokine expressing cells within the CD45RO⁺ memory population for CD4⁺ **(a)** or CD8⁺ **(b)** T cells. Lines connecting healthy controls (or parents) and P1 indicate samples processed and analyzed together (an independent experiment). **(c)** Unstimulated *ex vivo* T cells stained for CD4⁺CD25⁺CD127^{lo}FoxP3⁺ regulatory T helper cells (T_{reg}) shown as a percentage of CD4⁺ T cells. **(d,e)** CD69 expression (left), CD25 expression (center), or percent CFSE diluted (≥ 1 cell division) of purified *ex vivo* pan T cells either CD4⁺ gated **(d)** or CD8⁺ gated **(e)** following 20 hours (CD69 and CD25) or 96 hours (CFSE dilution) stimulation with anti-CD2 + anti-CD3 + anti-CD28 immobilized on beads (Miltenyi biotech, bead to cell ratio = 1:1), 1 μ g/mL of anti-CD3, or anti-CD28, or 1 μ g/mL anti-CD3 only. **(f,h)** CD69 expression on flow cytometry purified naïve (CD4⁺ CD45RA⁺ CD45RO⁻ CCR7⁺) **(f)** or memory T cells (CD4⁺ CD45RO⁺ CD45RA⁻) **(h)** 20 hours after stimulation. **(g,i)** CFSE dilution of naïve **(g)** or memory **(i)** CD4⁺ T cells after stimulation with either anti-CD2 + anti-CD3 + anti-CD28 immobilized on beads (bead to cell ratio = 1:1), 1 μ g/mL of anti-CD3, or anti-CD28, or 1 μ g/mL anti-CD3 only. Data represent two to five independent experiments with eight to sixteen healthy control or parent samples per cytokine **(a,b)**, three independent experiments and seven healthy controls **(c)**, three to four independent

experiments with ten to fifteen healthy control or parent samples (**d,e**), or 1 independent experiment with 3 healthy controls (**f-i**).

2.8 Supplementary Tables

Supplementary Table 2.1 Summary of WES Variants found at each filtering stage for P1.

	Patient
Total variants from WES (SNP/indels)	80213
Nonsynonymous variants	10906
Novel or Rare variants	2551
Genes which fit genetic model	5
Candidate causal gene (deleterious, expressed, etc)	1

Supplementary Table 2.1 Summary of WES variants found at each filtering stage for P1. Total number of variants (single nucleotide polymorphisms, i.e. SNPs, and insertion/deletions, i.e. indels) found by WES. The number of remaining variants after each filtering stage of bioinformatics analysis is shown.

Supplementary Table 2.2 P1 candidate gene list by genetic model.

Genetic model	chr	position	referenceBase	Proband	Father	Mother	Sister	accession
De-novo variants	3	50293703	A	R	A	A	A	NM_001166425.1
	5	178413492	G	R	G	R	G	NM_000843.3
Autosomal recessive - Compound Heterozygous variants	5	178413684	G	R	R	G	R	NM_000843.3
	7	151884485	C	S	C	S	S	NM_170606.2
	7	151945334	T	Y	Y	T	Y	NM_170606.2
	15	41815528	G	K	K	G	G	NM_015540.2
	15	41815547	G	K	G	K	G	NM_015540.2
	19	42795029	C	S	S	C	C	NM_015125.3
	19	42796573	T	Y	T	Y	Y	NM_015125.3
Autosomal recessive - Homozygous variants	7	100385561	GGCTTCAGCTACCGCTTCAAGGCCGATGACCTAT	G/G	GGCTTCAGCTACCGCTTCAAGGCCGATGACCTAT/G	G/G	GGCTTCAGCTACCGCTTCAAGGCCGATGACCTAT/G	NM_003386.1
	14	74041748	A	R	R	R	R	NM_006821.5
	17	39274069	G	C	S	S	S	NM_013059.3
	17	45234420	T	G	S	K	K	NM_00114091.1
	20	1895950	C	G	S	S	S	NM_001040022.1
	20	1895951	C	T	Y	Y	Y	NM_001040022.1
	20	1895952	T	C	Y	Y	Y	NM_001040022.1
	20	1895963	A	G	R	R	R	NM_001040022.1
	20	1895965	C	A	M	M	M	NM_001040022.1
	20	1895984	C	A	M	M	M	NM_001040022.1
	20	1895990	G	A	R	R	R	NM_001040022.1
	20	1896059	G	A	R	R	R	NM_001040022.1
	20	1896060	T	C	Y	Y	Y	NM_001040022.1

Table 2.2 continued

Genetic model	functionGVS	rsID	aminoAcids	proteinPosition	cDNAPosition	polyPhen	granthamScore	scorePhastCons	consScoreGERP	scoreCADD	geneList	genomesESP	genomesEXAC
De-novo variants	missense	0	THR,ALA	145/319	433	0.999	58	1	5	28.3	GNAI2	A=13006	unknown
	missense	142780395	PRO,LEU	588/878	1763	0.119	98	0.002	-2.06	0.019	GRM6	A=4/G=12964	A=60/G=112108
Autosomal recessive - Compound Heterozygous variants	missense	143491269	PRO,LEU	524/878	1571	1	98	0.865	4.63	24.1	GRM6	A=5/G=12991	A=76/G=118232
	missense	0	GLY,ARG	1624/4912	4870	0.998	125	0.923	3.6	15.94	KMT2C	C=13006	unknown
	missense	4639425	ASN,ASP	729/4912	2185	0.094	23	0	0.317	3.864	KMT2C	T=13006	unknown
	missense	0	LEU,ILE	821/1394	2461	1	5	1	5.7	19	RPAP1	G=13006	T=10/G=116618
	missense	0	SER,ARG	814/1394	2442	0.005	110	0.009	2.51	5.456	RPAP1	G=13006	T=28/G=110186
	missense	370962921	ASP,GLU	703/1609	2109	0.064	45	0.987	2.34	12.71	CIC	G=1/C=12987	G=1/T=1/C=108272
	missense	0	SER,PRO	1044/1609	3130	0.396	74	0.996	4.08	14.19	CIC	T=12988	C=17/T=117817
Autosomal recessive - Homozygous variants	frameshift	72364644	none	NA	NA	unknown	unknown	1	4.63	unknown	ZAN	unknown	unknown
	missense	149033118	HIS,ARG	328/484	983	0.001	29	0.001	-2.2	0.016	ACOT2	A=12694	unknown
	missense	349771	ARG,GLY	167/195	499	0.253	125	0.948	2.95	12.44	KRTAP4-11	G=4564	unknown
	missense	78493795	TYR,SER	234/831	701	0.003	144	0.999	5.44	13.53	CCZ2	T=12926	unknown
	missense	1135200	ASP,GLU	95/505	285	0.804	45	0.007	-2.65	11.32	SIRPA	C=12978	unknown
	missense	149634649	LEU,PHE	96/505	286	0.852	22	0	-8.38	3.243	SIRPA	C=12972	unknown
	missense	146163282	LEU,PRO	96/505	287	0.003	98	0	-7.65	3.586	SIRPA	T=12962	unknown
	missense	17855613	ASN,ASP	100/505	298	0.022	23	0	-5.69	10.72	SIRPA	unknown	unknown
	missense	17855614	ASN,LYS	100/505	300	0.407	94	0.002	0.771	11.08	SIRPA	unknown	unknown
	missense	17855615	ARG,SER	107/505	319	0.964	110	1	3	15.32	SIRPA	C=12994	unknown
	missense	17855616	GLY,SER	109/505	325	0.001	56	0.994	1.43	1.961	SIRPA	G=12994	unknown
	missense	115287948	VAL,MET	132/505	394	0.188	21	0	-2.28	9.326	SIRPA	G=12976	unknown
missense	114499682	VAL,ALA	132/505	395	0.03	64	0.001	-4.1	12.17	SIRPA	T=12978	unknown	

Supplementary Table 2.2 P1 candidate gene list by genetic model. Candidate gene mutations, found by WES, their status in immediate family members, and bioinformatics analysis (type, frequency, prediction of functional effect, etc.) are shown for P1 and grouped by the genetic model they fit (*de novo*, autosomal recessive - compound heterozygous, or autosomal recessive – homozygous).

Supplementary Table 2.3 CRISPR targeting *Gnai2* in mouse embryos.

	Intended <i>Gnai2</i> mutation	
	T182I	G184S
Total Mice Born	63	25
# Modified (any modification)	10	
# with HR-mediated modification	1*	1
# with correct KI	0	1
# embryos screened (~8 cell)	20	
# Modified (any modification)	14	
# with correct KI	1	

*This mouse included the silent mutations from the HR donor template, but excluded the T182I *Gnai2* missense mutation

Supplementary Table 2.3 CRISPR targeting *Gnai2* in mouse embryos. Clustered, regularly interspaced, short palindromic repeat (CRISPR)-Cas9 technology was used to target mouse embryos along with homologous recombination (HR) donor to induce knock-in (KI) of the indicated mutations (T182I or G184S *Gnai2*). Total numbers of screen mice and or early embryos (~8 cell) with any modification, an HR mediated recombination event, and those with the intended (correct) HR-mediated KI event.

2.9 Supplementary Notes

Supplementary Note 2.1 P1 clinical course.

This 28-year old Caucasian female has a combined immunodeficiency with recurrent sinopulmonary and viral skin infections, as well as autoimmunity with autoimmune hemolytic anemia and psoriatic arthritis. She also has developmental abnormalities involving gastrointestinal tract, bone, and vasculature.

Parents are nonconsanguineous, and neither they nor her older sister have a history of immunodeficiency or autoimmunity. She was born by repeat cesarean at 39 weeks and 5 days gestational age. Pregnancy was complicated by intrauterine growth restriction. Her birth weight was 4 pounds and 9 ounces. Congenital hip dysplasia and clubfeet were corrected with a Pavlik harness and casting. Throughout childhood she remained at < 3rd percentile for age in height and weight, although these were proportional until she gained weight from chronic corticosteroids. Bone age was consistent with chronological age on multiple examinations.

Mild dysmorphic features include hypotelorism with reduced inner canthal distance, small ears, and plagiocephaly. She was suspected of having autosomal dominant spondylocostal dysostosis, with scoliosis, spondylolithesis, occult spina bifida, and short stature present in her mother, and scoliosis in maternal grandfather. She has dextroscoliosis of 35° from T10 to L2, butterfly vertebrae at T8, and osteopenia secondary to chronic corticosteroid use with vitamin D deficiency, which was complicated by a compression fracture at T12.

At six months of age, she began to develop recurrent upper respiratory tract infections. This was followed by several episodes of mostly clinically diagnosed pneumonia associated with reactive airways disease exacerbations, including a hospitalization for respiratory syncytial virus at 18 months. She had recurrent otitis media, complicated by mastoiditis and mild conductive hearing loss, which required placement of eight sets of tympanostomy tubes and hearing aids. She also developed recurrent sinusitis, confirmed radiographically, which required nine sinus surgeries with polypectomies. She has received antibiotics every few weeks for most of her life for sinusitis, bronchitis, or otitis media. A trial of rotating prophylactic antibiotics was marginally effective in controlling her sinus infections. At 14 years of age, she was started on Ig replacement therapy, which was associated with a reduction in sinopulmonary infections. Periodontal examination revealed generalized moderate bone loss around teeth unexpected for her age, and mild gingival inflammation.

She received all recommended vaccinations during her childhood without adverse effect including oral polio vaccination. While 4 years of age, she had a mild case of chicken pox; varicella vaccination was not standard of care at that time. At 7 years of age, she began to develop progressively worsening warts (> 400), most extensive on her antecubital fossa, hands, and soles; these worsened before she started receiving chronic corticosteroids, and have recurred despite surgical removal under general anesthesia. At 16 years of age, she had herpes zoster which recurred at 23 years of age. She never developed recurrent yeast or fungal infections.

Standard immune evaluations completed in early childhood did not reveal a known cause of immunodeficiency. She had normal sweat chloride, cilia ultrastructure, neutrophil oxidative burst, complement levels, 22q11 FISH, and 46XX karyotype.

Directional and random chemotaxis of neutrophils were decreased when evaluated at age 6 years of age. Quantitative immunoglobulins were initially normal; while receiving IgG for infection prophylaxis, she developed decreased IgG, decreased IgM, and occasionally increased IgA. Post-immunization tetanus and pneumococcal titers were normal, as were titers post-infection or post-immunization to parvovirus B19, varicella, and rubeola. Isohemagglutinins were present at normal titers. Mitogen proliferation responses to concanavalin A (Con A), pokeweed mitogen (PWM), and phytohemagglutinin A (PHA) ranged from moderately decreased to within normal values. Antigen stimulation studies to *Candida* and tetanus toxoid also varied from normal to low back to normal on subsequent assessment. CTL and NK cell cytotoxicity were normal. Although absolute lymphocyte count was normal during infancy, she later developed intermittent lymphopenia involving T cells and NK cells or lymphocytosis involving B cells. She has naïve T cell lymphopenia but normal numbers of effector/memory phenotype T cells. T-cell Receptor V beta repertoire clonogram was normal.

Splenomegaly was first noted at 4 years of age while she had chickenpox. She developed autoimmune hemolytic anemia (DAT⁺) when 6 years of age. She also had rare thrombocytopenia with her massive splenomegaly. Bone marrow biopsy showed trilineage maturation without findings suggestive of Gaucher's or other storage diseases. Antinuclear antibodies and autoantibodies (rheumatoid factor, anti-mitochondrial, anti-centromere, anti-smooth muscle, anti-liver/kidney microsomal, anti-cardiolipin, anti-thyroglobulin antibodies) were negative. At 10 years of age, oral corticosteroids were started for falling hemoglobin and platelet counts and need for transfusions. She had multiple hemolytic crises, particularly in the couple of days following surgical procedures. At 11 years of age, she underwent splenectomy and cholecystectomy because of

splenic infarction and cholelithiasis. Histopathology showed infarction, fibrosis, and chronic inflammation of the spleen, with Gama-Gandy bodies and lymphocytosis in the red pulp consisting of a mixture of scattered B cells, a few polyclonal plasma cells, and more numerous T cells, as well as chronic inflammation of the gallbladder. Following splenectomy, she developed baseline leukocytosis (~20 K/ μ L) reflecting neutrophilia and monocytosis, but her hemolytic anemia did not improve. Rituximab was started at 14 years, along with IVIG, which has improved control of her hemolytic anemia. She continues to have intermittent softening of her skull bones suggestive of extramedullary hematopoiesis. She has not had persistent lymphadenopathy.

She developed arthritis with effusion of the knees starting at 6 years. Arthritis progressed to involve ankle joints. By 12 years of age, MCP joints were involved, with progressive multi-articular arthritis, affecting knees, ankles, MCP, DIP and toe joints. She developed avascular necrosis of ankles and knees, osteochondritis dissecans of knees, and underwent right knee replacement at 20 years of age. At age 21 years, she developed red plaques on the skin on her extremities, leading to a diagnosis of psoriatic arthritis for which she currently takes mesalamine (did not tolerate plaquenil). She has also developed arthritis of the TMJ joints, which at time of manuscript are her most painful joints. She takes NSAIDs and has received corticosteroid joint injections which have provided some relief.

Immunologic history is also notable for mild eczema limited to early childhood and persistent asthma treated with theophylline in early life, later improving to become intermittent in adulthood. Skin testing for common aeroallergens at 16 years of age was negative. In childhood, she also had an episode of suspected alopecia areata partialis of the scalp that lasted for a year.

Non-immunologic history is notable for chronic intermittent non-bloody diarrhea and abdominal pain that began around 7 years of age, with negative infectious and malabsorption studies. Intestinal malrotation was detected on abdominal/pelvic CT performed as an adult and confirmed by upper gastrointestinal series. She underwent surgical correction by Ladd's procedure with appendectomy at 23 years of age, with resolution of chronic gastrointestinal symptoms. She subsequently developed hepatomegaly and coarsened echogenicity on ultrasound. Liver biopsy showed nodular regenerating hyperplasia. Transjugular wedge pressures revealed portal hypertension, but EGD and colonoscopy showed no varices. Histopathology of biopsied gut showed duodenitis, cryptitis and chronic colitis in the ascending and transverse colon, and prominent lymphoid nodules with mild architecture distortion in the descending colon.

She has primary amenorrhea with menses that can be triggered by various oral contraceptives. She had decreased IGF-1 and received human growth hormone starting at age 12 for 5 years for short stature.

She was found to have unusual brachiocephalic vessels with anomalous course of draining systemic vein from left upper extremity and unusual branching pattern from left-sided aortic arch with aberrant right subclavian artery and common origin for carotid arteries. Echocardiogram was normal.

In summary this 28-year-old female has a combined immunodeficiency manifesting with recurrent sinopulmonary and viral skin infections, as well as autoimmunity comprised of autoimmune hemolytic anemia and psoriatic arthritis. She also has developmental abnormalities involving gastrointestinal tract, bone, and vasculature.

Supplementary Note 2.2 P2 clinical course.

This deceased 8-year-old Caucasian male had a combined immunodeficiency manifesting with recurrent sinopulmonary infections, E. coli meningitis with empyema, and macrophage activation syndrome in response to viral gastroenteritis, and autoimmunity manifesting with autoimmune hemolytic anemia, mild to moderate thrombocytopenia, and progressive leukodystrophy. He also had global developmental delay and fetal developmental abnormalities involving bone and the genitourinary tract.

Parents were nonconsanguineous and neither they nor his 3 half-siblings had any evidence of immunodeficiency. The father has inflammatory bowel disease and no other immediate family member has evidence of autoimmunity. He was born by at 37 weeks. Pregnancy was complicated by asymmetric intrauterine growth restriction. Postnatal growth continued to be slow with height <1st percentile and weight at the 3rd percentile. He had global developmental delay. He had mild facial dysmorphism. Other non-immune abnormalities included short stature, small hands and feet, hemivertebrae T5 and T7, bilateral hip dysplasia, talipes, micropenis and bifid scrotum, and bilateral vesico-ureteric reflux.

He had recurrent respiratory infections from the first year of life, with an admission to the intensive care unit at 10 months of age with RSV bronchiolitis complicated by apneas. Reactive airways and suppurative bronchiolitis were evident by 15 months and nocturnal oxygen was instituted. Bilateral bronchiectasis was present by 2 ½ years of age. He also had multiple episodes of otitis media and externa and one episode of E.coli meningitis with empyema at 4 years of age.

Hypogammaglobulinemia was diagnosed at 2 years of age and he commenced replacement intravenous gammaglobulin. Gammaglobulin levels were high (IgG > 15 g/L) early in his clinical course with hypogammaglobulinemia in correlation with rituximab therapy. There was an episode of macrophage activation syndrome following viral gastroenteritis at 6 ½ years of age, treated with corticosteroids, cyclosporine and etoposide.

The child exhibited gut dysmotility from the first few months of life with chronic constipation, marked bowel distension, mild gut protein losses and very slow transit time demonstrated by barium meal and follow-through. Stomach, small and large bowel and rectal biopsies at 15 months of age were non-diagnostic although there was submucosal lymphocytic infiltrate of the distal biopsies, and bowel dysmotility was presumed to be autoimmune enteropathy.

At 8 months of age he developed impressive leukocytosis (WCC $76.9 \times 10^9/L$ and neutrophil $63.1 \times 10^9/L$, with leukoerythroblastic blood film) and mild hepatosplenomegaly that were noted during an E.Coli urinary tract infection. Bone marrow biopsy ruled out leukemia (JMML). Leukocytosis resolved and hepatosplenomegaly improved once the UTI resolved. Impressive leukocytosis was observed in response to infections (sometimes minor viral infections) on several other occasions, with white cell counts ranging from 50 to $70 \times 10^9/L$ with neutrophilia and left-shift, which sometimes plummeted to neutropenic levels some days later.

Autoimmune hemolytic anemia developed from 11 months of age, with relapsing course and recurrent episodes, refractory to intravenous gammaglobulin and mycophenolate but responsive to corticosteroids and rituximab. Intermittent mild-

moderate autoimmune thrombocytopenia with detectable anti-platelet autoantibodies was present from 11 months of age. There was persistent splenomegaly from a year of age; the splenic size fluctuated and was massive on several occasions. Splenomegaly was at its smallest following etoposide therapy for macrophage activation.

Lymphadenopathy was not a prominent feature.

He manifested progressive neurological decline from 3½ - 4 years of age, with symptoms predating the E.coli meningitis. He was increasingly reluctant to walk and was using a walking-frame by 4 years. There was progressive spasticity of all limbs, and he lost the ability to walk and speak accompanied by the onset of seizures by 5 years. Swallowing became unsafe and a gastrostomy was inserted to facilitate feeding. Neuro-imaging showed progressive leukodystrophy of the brain with sparing of the spinal cord. Extensive testing for an etiology found no viral or metabolic cause. Brain biopsy revealed no features of viral infection, vasculitis or malignancy but there was diffused T-lymphocytic infiltration with gliosis and no demyelination or neuronal loss. These findings were suggestive of an autoimmune inflammatory process, which was refractory to all immune modulatory treatments tried, including high-dose corticosteroids and intravenous immunoglobulin, rituximab, cyclophosphamide and rapamycin. He progressed into a vegetative state and died at 8 years and 4 months from complications related to encephalopathy and respiratory infection.

2.10 Materials and Methods

Human Subjects and *in vivo* chemotaxis studies

Patients and their relatives provided written informed consent to participate in research protocols approved by the National Institute of Allergy and Infectious Diseases (NIAID),

National Institutes of Health (NIH) Institutional Review Board (IRB) (NCT00246857) for P1 and the Human Research Ethics Committee of the Sydney Children's Hospitals Network (ID number 10/CHW/114) for P2. Whole blood samples were obtained from these individuals. Primary dermal fibroblast cultures were established from punch skin biopsies as part of the routine diagnostic workup of P1 and P2. Buffy coat cells, which were by-products of volunteer-donor blood units, were distributed in an anonymized manner that was deemed exempted from informed consent and IRB review.

Assessment of cell migration into cutaneous blister fluid of P1 and healthy volunteers was performed under a protocol (NCT00001257) approved by the NIAID, NIH IRB entitled "Comparison of Inflammatory Responses in Normal Volunteers and Patients with Abnormal Phagocyte Function using the Suction Blister Technique." (Kuhns, D.B., et al. J Clin Invest. 1992 Jun;89(6):1734-40)

For assessment of leukocytes in the oral cavity, P1 and healthy volunteer subjects were consented to a protocol (NCT01568697) approved by the NIH National Institute of Dental and Craniofacial Research (NIDCR) IRB. For inclusion in the healthy volunteer group, subjects reported in good general health and had no significant medical history. Subjects had to test negative for infectious agents hepatitis B, hepatitis C, and HIV by PCR and enzyme-linked immunosorbent assay and had HbA1C levels <6% with no history of diabetes. Pregnancy and lactation were exclusion criteria as were use of tobacco within 1 year, and use of antibiotics, immunosuppressive agents, or probiotics within 3 months. For inclusion healthy volunteers had to be in good oral health, with no visible mucosal lesions, no evidence or symptoms of xerostomia, have minimal history/presence of caries, and be periodontally healthy. Healthy volunteers were

approximately age matched (+/- 5 years) with patients. (Wright D.G., et al. Blood. 1986 Apr;67(4):1023-30)

Mice

Mice were bred and used under animal study protocols approved by the NIAID Animal Care Use Committee. Wild-type B6 (C57BL/6J, 000664), CD45.1 congenic B6 (B6.SJL-*Ptprc^a Pepc^b*/BoyJ, 002014), and Thy1.1 congenic B6 (B6.PL-*Thy1^a*/CyJ, 000406) were purchased from the Jackson Laboratory (Bar Harbor). Mice were genotyped by flow cytometry using the isoform specific antibodies anti-mouse CD45.1 APC (BioLegend, 110714), anti-mouse CD45.2 BV711 (BD, 563685), anti-mouse Thy1.1 Pacific Blue (BioLegend, 202522), and anti-mouse Thy1.2 PE (BD, 553006). Six to 8 week old female mice were used in all experiments. Randomization and blinding were not performed.

Whole Exome Sequencing

Genomic DNA was isolated from PBMC for patients and unaffected family members using the DNeasy Blood and Tissue Kit (Qiagen, 69506). Exome libraries from the genomic DNA were generated using SureSelect Human All Exon 50Mb Kit (Agilent Technologies) according to manufacturer's protocol and samples were sequenced by Illumina HiSeq Sequencing System (Illumina). For individual samples, whole exome sequencing (WES) produced ~50-100X sequence coverage for targeted regions.

WES analyses

All DNA sequences were aligned to the hg19 human genome reference by Burrows-Wheeler Aligner (BWA) using default parameters (Li H. and Durbin R. *Bioinformatics*, 2009 May;25:1754-60). Single nucleotide variant and indel calling were performed either using the Genome Analysis Toolkit (GATK, <http://www.broadinstitute.org/gatk/>) (McKenna A, et al. *Genome Res.* 2010 Jul;20:1297-303) and variants were annotated by SeattleSeq Annotation (<http://snp.gs.washington.edu>) or Real Time Genomics (Hamilton, New Zealand) integrated analysis tool rtgFamily v3.6.2 (Cleary J.G., et al. *J Comput Biol.* 2014 Jun; 21(6):405-19) and annotated using SnpEff v4.1k (Cingolani, P., et al. *Fly (Austin)*. 2012 Jun; 6(2):80-92). In-house custom analysis pipelines were used to filter and prioritize variants for autosomal recessive or de-novo disease-causal variants based on the clinical pedigree for the family. Existing exome sequencing databases such as ExAc (Exome Aggregation Consortium, <http://exac.broadinstitute.org>) and the NHLBI exome variant server (<http://evs.gs.washington.edu/EVS/>) have been used to extract previously reported frequency for any given variants and these were used to filter for novel or rare variants.

All genomic variants are described according to Human Genome Variation Society recommendations (<http://www.hgvs.org/mutnomen/recs.html>), using NCBI Reference Sequences NM_002070.3 (cDNA) and NP_002061.1 (protein) based upon NCBI Build 38. Coding DNA variations are described with the A of the ATG translation initiation codon designated as nucleotide +1. The Illumina whole exome sequencing data has been deposited in dbGaP.

Sanger sequencing

For confirmation of identified *GNAI2* mutations in the patients, independent isolations of genomic DNA from both the original and alternative tissues (fibroblasts) were PCR amplified using forward primer 5' - AGC TAC CTG AAC GAC CTG GA - 3' and reverse primer 5' - GAG CCT TGT AAA ACC TCA GTG G - 3'. Sanger sequencing of purified PCR amplified products was performed by the Genomics Unit of the Rocky Mountain Laboratories Research Technologies Section of the NIAID, using BigDye Terminator Sequencing kit (Life technologies) and sequenced on ABI3730xl genetic analyzer (Applied Biosystems).

Cell Isolation and Culture

Human peripheral blood mononuclear cells (PBMC) were collected from whole blood after Ficoll-Hypaque PLUS density gradient centrifugation (GE Healthcare). Human pan T cells were isolated from PBMC by negative selection using the Human Pan T cell isolation kit (Miltenyi Biotech) according to manufacturers recommendations. Of note, before isolating patient T cells (and T cells from the healthy controls purified in parallel with patient cells), PBMC preps were first depleted of CD15⁺ myeloid cells using Human CD15⁺ microbeads (Miltenyi Biotech) before negative selection using Human Pan T cell isolation kit (to minimize contaminating myeloid cells due to patient myelocytosis). CD4⁺ CD45RA⁺ CD45RO⁻ CCR7⁺ naive and CD4⁺ CD45RO⁺ CD45RA⁻ memory T cells were isolated from PBMC by fluorescence-activated cell sorting (FACS) using a BD FACSAria III cell sorter. T cell purities were greater than 99% after FACS, and greater than 97% after magnetic bead separation. For isolation of murine leukocytes, inguinal and axillary lymph nodes were minced together with spleens, passed through 40µM nylon filter

(Falcon), and erythrocytes lysed with ACK (Quality Biological). Human T cells and mouse leukocytes were cultured in RPMI 1640 medium (Gibco) supplemented with 10% fetal bovine serum (Gibco), 4 mM L-glutamine (Invitrogen), 100 IU/mL penicillin (Invitrogen), 100 mg/mL streptomycin (Invitrogen), 50 mM 2-mercaptoethanol (Sigma), and 100 U/mL recombinant human IL-2 (Aldesleukin, Prometheus). Excepting T cell receptor activation studies, human T cells were activated with anti-human CD2, CD3, and CD28 coated beads (1:1 bead to cell ratio) using T Cell Activation/Expansion Kit (Miltenyi Biotec). Murine leukocytes were activated with plate bound anti-mouse CD3 (5 μ g/mL, BD clone 145-2C11) and soluble anti-mouse CD28 (1 μ g/mL, BD clone 37.51). Human embryonic kidney 293T cells (293T, ATCC, passage number 5 to 15) were either cultured in Iscove's modified Dulbecco's medium (IMDM, Gibco) supplemented with 10% fetal bovine serum, 4 mM L-glutamine, and 50 mM 2-mercaptoethanol (for lentivirus production) or Dulbecco's modified Eagle's medium Glutamax (DMEM-Q, Gibco) supplemented with 10% fetal bovine serum (Atlanta Biologicals), 100 IU/mL penicillin, 100 mg/mL streptomycin, 4 mM L-glutamine, and 50 mM 2-mercaptoethanol (for BRET assays). The retroviral packaging line, Platinum-E (Cell Biolabs, RV-101), was carried in DMEM supplemented with 10% fetal bovine serum, 1 μ g/mL puromycin (Gibco), 10 μ g/mL blasticidin (Invivogen), 100 IU/mL penicillin (Gibco), 100 mg/mL streptomycin (Gibco), 4 mM L-glutamine (Gibco), and 50 mM 2-mercaptoethanol (Sigma). Human Jurkat cells were cultured in RPMI 1640 medium supplemented with 10% fetal bovine serum, 4 mM L-glutamine, 100 IU/mL penicillin, 100 mg/mL streptomycin, and 2-mercaptoethanol (Sigma, rest from Gibco). Primary human dermal fibroblasts were isolated from skin punch biopsies as previously described (Jing H., et al., J Allergy Clin Immunol. 2014 Jun; 133(6):1667-75). In brief, dermal and epidermal layers were

dissociated after overnight incubation of biopsy tissue with Dispase (BD Biosciences). The dermis was minced and cultured in complete DMEM-Dulbecco's Modified Eagle Medium (Gibco) supplemented with 10% FBS, 2 mM L-glutamine, 100 U/mL penicillin, 100 µg/mL streptomycin, and 55 µM β -mercaptoethanol (Sigma-Aldrich, rest from Gibco) to allow fibroblasts to grow out. Fibroblasts lines were grown and passaged in DMEM supplemented with 10% fetal bovine serum, 100 IU/mL penicillin, and 100 mg/mL streptomycin.

Immunoblotting

Five million cells were lysed in whole cell lysis buffer (2% sodium dodecyl sulfate, 2 mM ethylenediaminetetraacetic acid pH 8.0 [both KD Medical], 50 mM Tris-HCl pH7.5 [Quality Biological]), heated to 95°C for 10 minutes, and chilled on ice. Protein concentrations were quantified by BCA (Pierce). Lysates were mixed with LDS Sample Buffer (Life Technologies) supplemented with 5% v/v 2-mercaptoethanol (Sigma), heated to 70°C for 10 minutes, and chilled on ice. 15 to 40 µg of protein were loaded per lane and were separated on NuPAGE Bis-Tris SDS-PAGE gels with MOPS running buffer (Invitrogen), followed by semi-dry transfer onto nitrocellulose membranes (Bio-Rad). After blocking with 5% non-fat dry milk (Bio-Rad) in PBS containing 0.1% Tween 20 (Sigma), membranes were incubated with the anti-human GNAI2 (Sigma Clone 2E4 or Proteintech Group, 11136-1-AP). Signal was detected by incubation with appropriate secondary antibodies (Peroxidase AffiniPure Goat Anti-Mouse IgG (H+L) or Peroxidase AffiniPure Goat Anti-Rabbit IgG (H+L) (both Jackson ImmunoResearch), followed by

application of SuperSignal West Pico Chemiluminescent substrate or SuperSignal West Dura Extended Duration Substrate (both Thermo Scientific) and exposing to film.

Plasmids

Human GNAI2 cDNA was obtained from Origene (clone SC118850). The coding sequence was sequence confirmed to match the NCBI reference sequence NM_002070.3.

pCL20c MSCV-GFP-T2A is a modified version of the lentiviral transfer vector pCL20c MSCV-GFP (Hanawa, H. et al. Blood. 2004 Jun 1;103(11):4062-9). Briefly, a self-cleavage T2A peptide sequence plus additional restrictions sites were added in-frame to the 3' end of the GFP cDNA from pCL20c MSCV-GFP via PCR amplification of pCL20c MSCV-GFP using AccuPrime Pfx SuperMix (Invitrogen) and the following primers: forward primer 5' – CTA GGC GCC GGA ATT ACC GGT GGC CGG CCG CGG GCC ACC ATG GTG AGC AAG GGC GAG GAG – 3' and reverse primer 5' – GGC ATC GAT GCG GCC GCA TGC TCA CCT GCA GGG GCC GGG GTT CTC CTC CAC GTC GCC GCA GGT CAG CAG GCT GCC CCG GCC CTC CTT GTA CAG CTC GTC CAT GCC GAG AGT GAT CC – 3'. The resulting product was separated via agarose gel electrophoresis, gel purified (QIAquick Gel Extraction Kit, Qiagen), and ligated into the EcoRI and NotI (New England Biolabs) digested and gel purified vector backbone of pCL20c MSCV-GFP (digested to remove original GFP and multiple cloning site) using the In-Fusion HD Cloning Kit (Clontech).

MSCV-GFP-T2A is a modified version of the retroviral transfer vector MSCV IRES-Thy1.1 (Addgene #17442). The GFP-T2A cDNA and multiple cloning site of pCL20c MSCV-GFP-T2A were PCR amplified using AccuPrime Pfx SuperMix (Invitrogen) and the following primers: forward primer 5' – CGC CGG AAT TAG ATC ACT CCT TCT CTA GGC GCC GG – 3' and reverse primer 5' - ATC GAA TTC TAC GCG TAC GGC ATC GAT GCG GCC GC – 3'. The resulting product was separated via agarose gel electrophoresis, gel purified (QIAquick Gel Extraction Kit, Qiagen), and ligated into the BglIII and MluI (New England Biolabs) digested and gel purified vector backbone of MSCV-IRES-Thy1.1 (digested to remove IRES and Thy1.1 cDNA) using the In-Fusion HD Cloning Kit (Clontech).

Site directed mutagenesis was used to generate the various GNAI2 point mutants. Briefly, 5' and 3' fragments were PCR amplified using AccuPrime Pfx SuperMix (Invitrogen) from wild-type GNAI2-expressing plasmids using shared start-codon (5' fragment) or stop-codon (3' fragment) primers (specific to each vector) and primers containing the appropriate point mutations. The 5' and 3' fragments containing the specific point mutations were then joined together via short overlapping ends (SOEing) PCR using the appropriate start-codon and stop-codon primers for down stream ligation. The joined product was gel purified and ligated in pCL20c MSCV-GFP-T2A (SbfI digested), MSCV-GFP-T2A (SbfI digested), pQE-30 (BamHI and HindIII digested), or pcDNA3.1(HindIII and NotI digested) using the In-Fusion HD Cloning Kit (Clontech). Vector specific GNAI2 start and stop codon primers were as follows: pCL20c MSCV-GFP-T2A-GNAI2 Start 5' – GAG AAC CCC GGC CCC ATG GGC TGC ACC GTG AGC GCC GAG G – 3' and pCL20c MSCV-GFP-T2A-GNAI2 Stop 5' – CCG CAT GCT CAC CTG CAG GTC AGA AGA GGC CGC AGT CCT TCA GG – 3' (used for MSCV-GFP-

T2A also); pQE-30 GNAI2 Start 5' – TCA CCA TCA CGG ATC CAT GGG CTG CAC CGT GAG CGC – 3' and pQE-30 GNAI2 Stop 5' – TCA GCT AAT TAA GCT TTC AGA AGA GGC CGC AGT CC – 3'; pcDNA3.1+ GNAI2 start 5' – AGG GAG ACC CAA GCT TGC CAC CAT GGG CTG CAC CGT GAG CGC and pcDNA3.1+ GNAI2 stop 5' – TTT TGC TCT GCG GCC GCT AGA AGA GGC CGC AGT CCT TCA GG – 3'.

Mutation specific primers used were as follows: T182A forward primer 5'- GCT ACG GAC CCG CGT AAA GGC CAC GGG GAT CGT GG - 3', and reverse primer 5'- GTC TCC ACG ATC CCC GTG GCC TTT ACG CGG GTC CG - 3'; T182I forward primer 5' – CCC GCG TAA AGA TCA CGG GGA TCG TGG AGA CAC AC – 3' and reverse primer 5' – TCC ACG ATC CCC GTG ATC TTT ACG CGG GTC CGT AG – 3'; G184S forward primer 5' – CCC GCG TAA AGA CCA CGA GCA TCG TGG AGA CAC AC – 3' and reverse primer 5' – AGT GTG TCT CCA CGA TGC TCG TGG TCT TTA CGC GG – 3'; Q205L forward primer 5' – TTT GAT GTG GGT GGT TTG CGG TCT GAG CGG AAG AAG TGG – 3' and reverse primer 5' – GAT GTT TGA TGT GGG TGG TTT GCG GTC TGA GCG GAA – 3'.

Firefly luciferase cDNA (used to control for protein overexpression) was obtain from IFNB-pGL3 (Promega), and was clone into pCL20c MSCV-GFP-T2A and MSCV-GFP-T2A using the following primers: iLuc_T2A_F 5' – GAG AAC CCC GGC CCC ATG GAA GAC GCC AAA AAC ATA AAG AAA GG – 3' and iLuc_R 5' – CCG CAT GCT CAC CTG CAG GTT ACA CGG CGA TCT TTC CGC CCT TCT TGG – 3'. The product was gel purified and ligated in pCL20c MSCV-GFP-T2A (SbfI digested) and MSCV-GFP-T2A (SbfI digested) using the In-Fusion HD Cloning Kit (Clontech).

All lentiviral and retroviral vectors were transformed into One Shot Stbl3 chemically competent *E. coli* (Invitrogen). All other vectors were transformed into One Shot Top10 chemically competent *E. coli* (Invitrogen) with the exception of the plasmid used for protein purification (pQE-30) which were transformed into XL-1 Blue Supercompetent *E. coli* (Stratagene). Following chemical transformation and selection with appropriate antibiotics, DNA was purified using the PureLink HiPure Filter Plasmid Kit (Invitrogen). All plasmid sequences were confirmed by Sanger dideoxy sequencing.

All primers were standard synthesis, unmodified, unsalted oligos from MWG Eurofins.

For generation of the BRET constructs pcDNA3.1+ CXCR4-YFP and pcDNA3.1+ CCR7-YFP, the circularly permuted citrine cDNA (citrine-cp229) was PCR amplified from pFB-Neo-CAMYEL (a kind gift from Iain Fraser) (Jiang, L.I., et al. J Biol Chem. 2007 Apr 6;282(14):10576-84) using the following primers to add the flexible linker (GPPVAT) to the 5' end of the cDNA: GPPVAT_Citrine229cp_F 5' – GGC CCT CCC GTG GCC ACC ATG ATC ACT CTC GGC ATG GAC G – 3' and pcDNA3-NotI-Citrine229cp_R 5' – TTT TGC TCT GCG GCC GCC TAC CCG GCG GCG GTC ACG AAC TCC – 3'. CXCR4 (Open Biosystems, IMAGE: 3846345, GenBank: BC020968) and CCR7 (cDNA Resource Center, #CCR0700000, GenBank: AY587876.1) cDNAs were PCR amplified using the following primers: pcDNA_CXCR4_F 5' – AGG GAG ACC CAA GCT TGC CAC CAT GGA GGG GAT CAG TAT ATA CAC – 3', GPPVAT_CXCR4_R 5' – TGA TCA TGG TGG CCA CGG GAG GGC CGC TGG AGT GAA AAC TTG AAG AC, pcDNA_CCR7_F 5' – AGG GAG ACC CAA GCT TGC CAC CAT GGA CCT GGG GAA ACC AAT G – 3', GPPVAT_CCR7_R 5' – CCA CCA CCA CCT TCT CCC CAG GCC CTC CCG TGG CCA CCA TGA TCA – 3'. All PCR products were gel purified and the citrine-cp229 cDNA amplicon was joined to each of the chemokine receptor amplicons

via SOEing PCR (primers: 'pcDNA_CXCR4_F' or 'pcDNA_CCR7_F' and 'pcDNA3-NotI-Citrine229cp_R') using AccuPrime Pfx SuperMix (Invitrogen). The joined product was gel purified and ligated into pcDNA3.1+ (HindIII and NotI digested) using the In-Fusion HD Cloning Kit (Clontech).

Untagged pcDNA3.1+ CXCR4 (#CXCR400000, GenBank: AY242129) and pcDNA3.1+ CCR7 (#CCR0700000, GenBank: AY587876.1) were purchased from cDNA Resource Center.

To generate pcDNA3.1+ GNAI2-91Rluc BRET constructs, *Renilla* Luciferase cDNA was PCR amplified from pFB-Neo-CAMYEL using the following primers to add flexible linkers (SGGGS) to the 5' and 3' end of the cDNA: 91Gi2_SGGGS_hRluc_F 5' – AAG CCA TGG GCA ACC TGT CTG GTG GTG GTG GTT CTA TGG CTT CCA AGG TGT ACG ACC C – 3' and 92Gi2_SGGGS_hRluc_R 5' – TCG GCA AAG TCG ATC TGA GAA CCA CCA CCA CCA GAC TGC TCG TTC TTC AGC ACT CTC TCC – 3'. The product was gel purified and inserted between residues 91 and 92 of the Gαi2 coding sequence (via PstI digestion) in pQE-30 GNAI2 (and analogous point mutation containing vectors). The resulting plasmids were used to PCR amplify GNAI2-91Rluc cDNAs (wild-type and point mutants) using the primers 'pcDNA3.1+ GNAI2 start' and 'pcDNA3.1+ GNAI2 stop' (sequences above). The products were gel purified and ligated into pcDNA3.1+ (HindIII and NotI digested) using the In-Fusion HD Cloning Kit (Clontech).

pcDNA3.1/Zeo GFP10-Epac-Rluc3, the BRET2-cAMP biosensor, was described previously³ and was a kind gift for Dr. Michel Bouvier (Université de Montréal).

GTP-binding and GTPase Activity Assays

Protein expression and purification: plasmids encoding 6xHis-tagged WT or mutant (T182A, T182I, G184S, Q205L) G α i2 or RGS16 (all in pQE-30 backbone) were transformed in *E. coli* strain Rosetta Gami (λ DE3). The cells were grown with shaking in LB medium at 37°C until they reached OD₆₀₀ =1, then were cooled to 25°C and induced with 0.5mM IPTG (Sigma). After 8h of further growth the cells were harvested, lysed in OneShot cell disrupter (Constant Systems) and the proteins were purified from lysate supernatant using Ni-NTA affinity resin (Qiagen). Purification was performed according to manufacturer's protocol using Tris-HCl buffer (pH 7.5) containing 150mM NaCl, 0.2mM DTT buffer for washing steps and the same buffer supplemented with 0.3M imidazole for elution.

GTP Binding and Hydrolysis Assays: recombinant human G α i2 (WT, T182A, T182I, G184S, Q205L) and RGS16 were brought into the 20mM Tris•HCl buffer (pH 7.5) containing 150mM NaCl, 0.2mM DTT and 5mM MgCl₂ by 10000-fold buffer exchange into 1xHKB (50 mM Hepes, 65 mM KCl, and 10 mM NaHCO₃) on Amicon 10K ultracentrifugation concentrators. 1 μ M His₆-G α i2 was mixed with 2 μ M RGS16, and 0.66 μ M BODIPY-FL-GTP or 0.66 μ M BODIPY-FL-GTP γ S (both from Invitrogen) was added to the mixture after 5min incubation. The kinetics of *in vitro* G α i2 protein activation was measured by the VICTOR3 multiwell reader (Perkin Elmer) as described elsewhere (Egger-Adam, D. and Katanaev, V.L. Dev Dyn. 2010 Jan;239(1):168-83) (Koval, A., et al. Anal Biochem. 2010 Feb; 397(2):202-7).

Nucleotide binding data were fit with one phase exponential equation $F = a - b e^{-kt}$, where F is a specific increase of fluorescence, to obtain the k_1 . GTP binding and hydrolysis curves were fit with the equation $F = (C_0 k_1 / (k_2 - k_1)) (e^{-k_1 t} - e^{-k_2 t})$ for the intermediate

product in two sequential reactions (Lin, C., et al. Mol Cell. 2014 Feb 20;53(4):663-71). Both fits were performed using Prism 5 software (GraphPad).

Cell treatments

For analysis of T cell activation, purified primary pan T cells, CD4⁺ CD45RA⁺ CD45RO⁻ CCR7⁺ naive T cells or CD4⁺ CD45RO⁺ CD45RA⁻ memory T cells (see cell isolations above) were stained with the CellTrace CFSE Cell Proliferation Kit (Molecular Probes) according to manufacturers recommendations. Cells were then washed in complete medium and resuspended at 1x10⁶ cells/mL in complete RPMI-1640 supplemented with 100 IU/mL of recombinant human IL-2. Cells were then stimulated with 1µg/mL soluble anti-human CD3 (OKT3, Janssen-Cilag) with or without 1µg/mL soluble anti-human CD28 (BioLegend, clone CD28.2) or anti-human CD2, CD3, and CD28 coated beads (1:1 bead to cell ratio) using T Cell Activation/Expansion Kit (Miltenyi Biotec). Cells were analyzed at 20 hours and 96 hours after stimulation by flow cytometry. For inhibitor studies, CFSE stained cells were then pre-incubated at 37°C for 6 hours in the presence of 10⁻¹⁰ to 10⁻⁸ M piclamilast (Sigma), 1uM to 5uM AS605240 (Sigma), or appropriate doses of the vehicle control, DMSO (Sigma).

For intracellular cytokine staining, unactivated purified pan T cells were stimulated at 37°C for 1 hr with 100 ng/mL of PMA (Sigma-Aldrich) and 1 mg/mL of ionomycin (Sigma-Aldrich) before GolgiStop (BD Biosciences) was added and stimulation continued for a total of 8 hrs. Cells were then fixed and permeabilized with Intracellular Fixation & Permeabilization Buffer Set (eBioscience), before staining for flow cytometric analysis.

For TCR induced phospho-flow staining, primary T cells 12 to 24 days post-activation were resuspended at 4×10^6 cells/mL in serum free RPMI supplemented with 100 IU/mL of recombinant human IL-2 and incubated for 6 hours at 37°C. Cells were then stimulated with 10 µg/mL anti-CD3 (OKT3, Janssen-Cilag) pre-crosslinked with protein A (200 ng/mL final concentration, Sigma). Cells were maintained at 37°C throughout stimulation (variable time). To stop stimulation, 10X the cell volume of ice-cold PBS (Lonza) containing paraformaldehyde (Sigma) was added to a final concentration to create a final concentration of 1.6% paraformaldehyde. After 20 minutes cells were pelleted and permeabilized with Intracellular Fixation & Permeabilization Buffer Set (eBioscience), before staining for flow cytometric analysis.

Calcium Flux Assays

For chemokine induced calcium fluxes, non-transduced (patient studies) or transduced (phenocopy studies) primary T cells 12 to 24 days post-activation were used. For TCR induced calcium fluxes unactivated *ex vivo* primary T cells or primary T cells 7 to 28 days post-activation (both for patient studies) or 21-28 days post-activation (transduced phenocopy studies) were used. $0.5-1.0 \times 10^6$ cells were loaded with 2 µg/mL Indo-1 AM (Molecular Probes, I1223) in complete RPMI 1640 for 30 minutes at 37°C. Cells were then washed with and stained in ice cold Ringer's solution (155 mM NaCl, 4.5 mM KCl, 2 mM CaCl₂, 1 mM MgCl₂, 10 mM D-glucose, 5mM HEPES pH 7.5) for 30 minutes at 4°C. For chemokine induced calcium fluxes, cells were stained with anti-human CD184 PE-Cy7 or PE (both BD Pharmingen, 560669 or 555974, respectively), anti-human CCR7 APC (R&D Systems, FAB197A), anti-human CD8 APC-eFluor 780 (eBioscience, 47-

0088-42), and anti-human CD4 APC (BioLegend, 300537). For TCR induced calcium fluxes, cells were stained with anti-human CD8 APC-eFluor 780 (eBioscience, 47-0088-42) and anti-human CD4 APC (BioLegend, 300537). Cells were washed and resuspended in ice cold Ringer's solution containing 0.5µg/mL propidium iodide (Sigma, P4170). Samples were warmed to 37°C for 7 minutes prior to collecting baseline calcium levels for 15 (chemokine studies) or 30 seconds (TCR studies). Cells were then stimulated at a final concentration of 500 ng/mL CXCL12 (PeproTech), 1 µg/mL CCL21 (PeproTech), or 10 µg/mL anti-CD3 (OKT3, Janssen-Cilag) pre-crosslinked with protein A (200 ng/mL final concentration, Sigma). Samples were maintained at 37°C during collection and intracellular calcium was measured as the ratio of Indo-1 AM violet emission (395nm) to Indo-1 AM blue emission (500nm) using a BD LSRII flow cytometer. FlowJo software package version 9.8.3 or 10.0.8 (TreeStar) was used to analyze single, live (propidium iodide low), CD4+ or CD8+ T cells using the kinetics platform to assess the changes in intracellular calcium over time and perform area under curve (AUC) measurements. For quantification of phenocopy studies, AUC for transduced (GFP⁺) was normalized to non-transduced (GFP⁻) from the same culture as an internal control. Chemokine receptor stains did not effect response (data not shown).

***In vitro* Chemotaxis Assay**

For chemokine *in vitro* chemotaxis assays, non-transduced (patient studies) or transduced (phenocopy studies) primary T cells 12 to 24 days post-activation were used. Cells were maintained in complete RPMI 1640 with 100IU/mL of IL-2 throughout. Polycarbonate Transwell inserts containing 5-µm membrane pores were used in 24-well

plates (Corning). A final concentration of 2 to 500 ng/mL recombinant human CXCL12 (Life Technologies) or 40 to 1600 ng/mL CCL21 (PeproTech) was added to the lower compartment in addition to an equivalent number of CountBright Absolute Counting Beads (Molecular Probes) to each well. 1×10^5 cells were added to the upper compartment. After incubating at 37°C in humidified 5% CO₂ for 2 hr the insert was removed and the contents of the lower chamber were collected final concentration of 1.6% for 15 min. The contents of each well were collected and stained with anti-human CD8 APC-eFluor 780 (eBioscience, 47-0088-42) and anti-human CD4 APC (BioLegend, 300537), and run in sample buffer containing propidium iodide (Sigma). The number of viable (propidium iodide negative) CD4⁺ and CD8⁺ cells was normalized relative to the number CountBright Absolute Counting Beads collected and expressed as % of the total number of cells collected from a well lacking a transwell insert.

***In vivo* Chemotaxis Assay**

Assessment of cell migration into cutaneous blister fluid of P1 and healthy volunteers: Following 1-1.5 hrs of gentle suction the neat blister fluid (hemolymph-like liquid forming the blister) was removed with a hypodermic syringe and the epidermis is removed. The wound is bathed in 70% autologous serum (heat-treated at 56°C for 30 minutes, and filtered) for 16 hrs then the exudate is collected for analysis. For fully detailed method see: Kuhns D.B., et al. J Clin Invest. 1992 Jun;89(6):1734-40.

For assessment of leukocytes in the oral cavity, patient and healthy volunteers performed a timed (10 second) oral rinsing procedure with 10 ml of sterile saline (0.9% Sodium Chloride, B. Braun Medical Inc.) and rinse solution was spin down for 10 min at

1200 rpm. The pellet was stained with anti-human CD3 FITC (eBioscience, 11-0036-42), anti-human CD19 FITC (eBioscience, 11-0199-42), anti-human CD20 FITC (eBioscience, 11-0209-73), anti-human CD15 PerCP-Cy5.5 (eBioscience, 46-0159-42), anti-human CD64 BV450 (BD, 562872), anti-human CD11b BV605 BD, 562721), anti-human CD62L BV650 (BD, 563808), anti-human HLA-DR BV711 (BD, 563696), anti-human CD14 BV786 (BD, 563698), anti-human Singlec-8 (BioLegend, 347104), anti-human CD117 PE-Cy7 (eBioscience, 25-1178-42), anti-human CD18 APC (BD, 551060), anti-human CD45 Alexa Fluor 700 (BioLegend, 304024), anti-human CD16 APC-Cy7 (BD, 561726), and Live/Dead Fixable Aqua Dead Cell Stain Kit (Molecular Probes, L34966) according to standard flow cytometry protocol detailed below. Cells were analyzed on a BD LSRFortessa. (Fine, N., et al. J Dent Res. 2016 Jul;95(8):931-8).

BRET Assays

Materials: Recombinant chemokines were from PeproTech, Inc. (Rocky Hill, NJ). Coelenterazine 400A for BRET2 experiments was from Biotium (Hayward, CA) and Coelenterazine h for BRET1 experiments was obtained from Nanolight technologies. Forskolin, pertussis toxin (PTX) and poly-D-lysine were from Sigma (St. Louis, MO), and the anti-CXCR4 12G5 and anti-CCR7 mAb directly coupled to phycoerythrin was from R&D Systems (Minneapolis, MN). Polyethylenimine (PEI) was obtained from Polysciences (CAT). Dulbecco's modified Eagle's medium Glutamax (DMEM-Q), 1% penicillin-streptomycin and Phosphate saline buffer (PBS) were from Life Technologies.

BSA fraction V, fatty acid free was from EMD Millipore and 96-well white microplates with clear bottom were from Corning.

Cell culture and Transfection: 293T cells (passage number 5 to 15, ATCC, Manassas, VA) were maintained in DMEM-Q, 1% penicillin-streptomycin, and 10% fetal bovine serum (Atlanta Biologicals). Transient transfection was performed in six-well plates using the polyethylenimine (PEI) method as described previously (Percherancier, Y., et al. J Biol Chem. 2005 Mar 18;280(11):9895-903). The total amount of transfected DNA was kept constant at 2 μ g/well for six-well by adding empty vector pcDNA3.1+. Transient high-throughput in-plate transfections were performed in 96-well plates also using the PEI method with some modifications. Briefly, cells were trypsinized, counted and mixed with the DNA- PEI (1:4 cDNA/PEI) complex then directly plated in 0.01% poly-D-lysine coated 96-well plates at a density of 100,000 cells/well. The total amount of transfected DNA was kept constant at 200ng/well for 96 well plates by adding empty vector pcDNA3.1+.

Flow Cytometry: 293T cells transfected in six-well plates with unfused and YFP fused CXCR4 and CCR7 were detached in ice cold PBS. Cells were labeled with monoclonal phycoerythrin-conjugated antibodies anti-CXCR4 12G5 and anti-CCR7 (BD Biosciences) for 30 minutes at 4°C in BRET buffer (PBS containing 0.5mM MgCl₂ and 0.1% BSA). Cells were then washed three times in ice cold PBS. Cell surface expression was quantified by flow cytometry using the Accuri C6 flow cytometer (BD Biosciences).

BRET Measurements: cells expressing BRET fusions were seeded in 0.01% poly-D-Lysine coated 96-well, white microplates with clear bottom 24 hours prior to BRET measurements at a density of 100,000 cells/well. On the day of the experiment, media was replaced with BRET buffer while cells remained attached to the plate. Coelenterazine

h, or coelenterazine 400A was added at the final concentration of 5 μ M followed by 5 or 10 min incubation at room temperature (RT), respectively. In BRET1 experiments, fluorescence and luminescence reading were collected by allowing the sequential integration of the signals detected in the 480 \pm 20 nm and 530 \pm 20 nm windows for luciferase (Rluc) and YFP light emissions, respectively. In BRET2 experiments readings were collected by allowing the sequential integration of the signals detected between Rluc3 and GFP10 of the signals detected in the 365 to 435 nm (Rluc3) and 505 to 525 nm (GFP10) windows. Luminescence and fluorescence readings were collected using the Synergy NEO plate reader from Biotek (Winooski, USA) and Gen5 software. BRET ratios were calculated as described previously (Leduc, M., et al. *J Pharmacol Exp Ther.* 2009 Oct;331(1):297-307) (Berchiche, Y.A., et al. *Mol Pharmacol.* 2011 Mar;79(3):488-98).

Receptor-GNAI2 Interaction: we assessed the interaction between CXCR4-YFP or CCR7-YFP and GNAI2-Rluc wild type or mutants in the absence and presence of chemokines using a BRET1 proximity assay. 293T cells were transfected with the high-throughput in plate transfection method and BRET1 readings were performed 24 hours after transfection. First, we determined the assay conditions by determining the optimal donor (Rluc) quantity and then performed acceptor (YFP) titrations experiments with optimal donor quantity to determine BRET_{max} ratios for each -YFP and -Rluc fusion pair as described previously (Berchiche, Y.A., et al. *J Biol Chem.* 2007 Feb 23;282(8):5111-5) (Kalatskaya, I., et al. *Mol Pharmacol.* 2009 May;75(5):1240-7) (Bonnetterre, J., et al. *Methods in enzymology.* 2016 Jan; 570:131-53). For dose-response experiments, cells expressing the -YFP and -Rluc fusion proteins at BRET_{max} ratios, were stimulated for 5 min at 37°C with increasing concentrations of the indicated ligand before the addition of

the substrate. The values were corrected to net BRET by subtracting the background BRET1 signal detected when the –Rluc construct was expressed alone.

Adenylyl cyclase activity: cAMP levels were measured by using the Rluc3-EPAC-GFP10, a BRET2 cAMP sensor, a gift from Dr Michel Bouvier (Université de Montréal) as described previously (Leduc, M., et al. *J Pharmacol Exp Ther.* 2009 Oct;331(1):297-307). Briefly, 293T cells co-transfected with 1.0 µg CXCR4 or 1.0 µg CCR7 and 0.06 µg Rluc3-EPAC-GFP10 reporter in six-well plates were seeded in poly-D-Lysine coated 96-well, white microplates with clear bottom 24 hours after transfection. Forty-eight hours after transfection, coelenterazine 400A was added to the cells followed by a 10 min incubation at RT. Cells were then stimulated with chemokines in the presence of 5 µM of forskolin at RT for 5 min.

Lentiviral and Retroviral Transductions

Specific lentiviral transfer vectors (all in pCL20c MSCV-GFP-T2A) were generated as detailed above. VSV-G–pseudotyped lentivirus particles were generated by transient co-transfection of the specific transfer vector together with the packaging plasmids pCMV delta R8.2 (HIV-1 GAG/POL, Tat, and Rev expressing plasmid, Addgene #12263) and pCMV VSV-G (VSV-G envelope expressing plasmid, Addgene #8454) (Stewart, S.A., et al. *RNA.* 2003 Apr;9(4):493-501) into 293T cells using calcium phosphate precipitation. Briefly, 13 million 293T cells were seeded in poly-L-lysine (Sigma) coated Cell Culture Treated TripleFlasks (Nunc). When cells reached 95% confluency, 250 µg of specific transfer vector, 125 µg pCMV delta R8.2, and 42 µg of pCMV VSV-G were precipitated with calcium phosphate and added to the cells. DNA precipitate was

washed out 12 hours after transfection and cell supernatants were collected daily for 3 days (stored at 4°C), filtered through 0.22 µm pore-size filter (GE), concentrated by centrifugation at 18,000 g for 3 hours at 4°C, resuspended in Opti-MEM I reduced serum media (Gibco), and stored at -80°C until use.

All lentivirus preparations were titered on 293T to determine the concentration of infectious units. 1×10^5 293Ts were resuspended in complete IMDM containing 8 µg/mL polybrene (Sigma) and 10 µL of diluted lentivirus to a final volume of 1 mL. The suspension was added to a 24-well plate (Corning) and spin infected at 1350 x g for 30 minutes at 35°C. 48 hours later, cells monolayers were washed twice with PBS, trypsinized (Gibco), transferred to 14 mL round bottom FACS tubes (Falcon), washed with PBS, and resuspended in PBS containing 0.5µg/mL propidium iodide. Single cell suspensions were then analyzed on a BD FACSCanto II to determine the percentage of GFP+ cells amongst the propidium iodide low (live) population. Lentivirus dilutions transducing between 2 and 15% of target cells was used to determine concentration of each preparation.

Specific retroviral transfer vectors (all in MSCV-GFP-T2A) were generated as detailed above. Retrovirus particles pseudotyped with ecotropic envelope protein were generated via transient co-transfection of the specific retroviral transfer vector together with pCL-Eco (Ecotropic envelope expressing plasmid, Addgene #12371) into Platinum-E cells via Lipofectamine 2000 (Invitrogen, cat no). 6×10^6 Platinum-E cells were plated on poly-L-lysine coated 10cm dish (Corning) in complete DMEM (without antibiotics). 24 hours later, cells were transfected with 24 µg of transfer vector and 6 µg of pCL-Eco.

Flow Cytometric Analyses

For assessments of activation, T cells were stained with the following antibodies: anti-human CD69 BV421 (BD Biosciences, 562884), anti-human CD25 PE (BD Biosciences, 555432), anti-human CD4 APC-Cy7 (BioLegend, 300518), anti-human CD8 PE-Texas Red (Life Technologies, MHCD0817), CellTrace CFSE Cell Proliferation Kit (Molecular Probes), and Zombie Aqua™ Fixable Viability Kit (BioLegend).

For intracellular cytokine staining, T cells were stained with the following antibodies: anti-human IL-4 FITC (BD, 554484), anti-human IL-13 APC (R&D Systems, IC2131A), anti-human IL-2 PE (BD, 559334), anti-human TNF α PE-Cy7 (BD, 560678), anti-human IFN γ FITC (BD, 552887), anti-human IL-22 APC (eBioscience, 17-7222), anti-human IL-17 PE (BD, 560486), anti-human IL-10 PE-CF594 (BD, 562400).

For intracellular phospho-flow staining, T cells were stained with the following antibodies: anti-human CD4 PE-Cy7 (BioLegend, 300512), anti-human LAT (pY171) Alexa Fluor 647 (BD Biosciences, 558518), anti-human ZAP70 (pY319)/Syk (Y352) PE-Cy7 (BD Biosciences, 561458), anti-human PLC γ 1 Alexa Fluor 488 (BD Biosciences, 558566), anti-human PLC γ 1 PE (BD Biosciences, 558575), anti-human Btk (pY551)/Itk (pY511) PE (BD Biosciences, 558129), anti-human Btk (pY223)/Itk (pY180) Alexa Fluor 488 (BD Biosciences, 564847), anti-human SLP-76 (pY128) PE (BD Biosciences, 558437), anti-human phospho-S6 ribosomal protein (Ser235/236) Pacific Blue (Cell Signaling Technologies, 8520), anti-human phospho-S6 ribosomal protein (Ser240/244) Alexa Fluor 488 (Cell Signaling Technologies, 5018), anti-human phospho-Akt (Thr308) Alexa Fluor 647 (Cell Signaling Technologies, 3375), anti-human phospho-Akt (Ser473) PE (Cell Signaling Technologies, 5315), anti-human ERK1/2 (pT202/pY204) PE-Cy7 (BD,

560116), anti-human PLC γ 1 (pY783) Alexa Fluor 647 Clone (BD, 557883), and Zombie Aqua™ Fixable Viability Kit (BioLegend, 423102).

Samples were acquired on a BD LSRII or BD LSRFortessa instrument using FACSDiva software. Analyses were performed using the FlowJo software version 9 and higher (Tree Star).

2.11 Contributions

Yu Zhang, Joshua J. McElwee, Cas Simons, and John Christodoulou analyzed WES and discovered the *GNAI2* mutations. Ian T. Lamborn, Heardley M. Murdock, Hyoungjun Ham, and Sangeeta Bade assessed *GNAI2* RNA and protein expression. Evan Masutani performed molecular modeling, and Ian T. Lamborn performed immunophenotyping. BRET experiments were performed by Yamina A. Berchiche with help from Ian T. Lamborn (construct design and cloning). *In vitro* biochemistry was performed by Alexey Koval (GTP binding and hydrolysis) and Kirk M. Druey (RGS binding). Debra A. Long Priel and Douglas B. Kuhns performed neutrophil chemotaxis studies. Uimook Choi and Ian T. Lamborn designed lentivirus approach and prepared lentivirus. Ian T. Lamborn performed T cell chemotaxis, calcium fluxes, and activation studies. Judith N. Mandl and Ian T. Lamborn performed murine *in vivo* chemotaxis studies. Kol A. Zarembler (blister study) or Niki M. Moutsopoulos and Nicolas Raul Dutzan Munoz (oral migration) performed human *in vivo* chemotaxis experiments. Robert Brink performed CRISPR knock-in experiments. Huie Jing and Ian T. Lamborn performed cAMP measurements. Peter J. Mustillo cared for the patients and collected and analyzed clinical data with assistance from Juliana Teo, Melanie Wong, and Corinne S. Happel. Tom Dimaggio, Helen F. Matthews and Angela Wang coordinated clinical

study protocol and sample collection. Helen C. Su planned and supervised the experimental work and data analyses. Ronald N. Germain, Harry L. Malech, Thomas P. Sakmar, Vladimir L. Katanaev, Christopher C. Goodnow, and Michael J. Lenardo provided advice and assisted in supervising experimental work. Helen C. Su and Ian T. Lamborn prepared the manuscript. All authors discussed and revised the manuscript.

CHAPTER 3 - Recurrent rhinovirus infections in a child with inherited MDA5 deficiency

3.1 Abstract

MDA5 is a cytosolic sensor of double-stranded RNA (ds)RNA including viral byproducts and intermediates characteristically produced by most viruses. However, the role of human MDA5 in the natural infectious environment during childhood is unknown. We studied a child with life-threatening and recurrent respiratory tract infections, caused by multiple viruses including rhinovirus, influenza virus, and respiratory syncytial virus (RSV). We identified a homozygous missense mutation in *IFIH1* that encodes MDA5. The MDA5 mutant protein was expressed, but did not recognize the synthetic MDA5 agonist and dsRNA mimic polyinosinic-polycytidylic acid. When overexpressed, the mutant protein failed to activate *IFN* β ISRE, and NF- κ B promoters, indicating its loss-of-function. In respiratory epithelial cells, wild-type but not mutant MDA5 restricted human rhinovirus infection while increasing IFN-regulated gene expression. Rhinovirus replication could be inhibited by transducing wild-type but not mutant MDA5. By contrast, wild-type MDA5 did not restrict influenza virus and RSV replication. Moreover, nasal epithelial cells from the patient showed increased replication of rhinovirus but not influenza or RSV, further suggesting that these infections in our patient were secondary complications of rhinovirus infection. Thus, MDA5-deficiency is a novel inborn error of innate immunity that results in impaired dsRNA-sensing, reduced IFN induction, and susceptibility to the common cold virus.

3.2 Introduction

Acute respiratory infections are the leading cause of acute illness worldwide [165]. Of these, upper respiratory infections are estimated at 18.8 billion per year, and

lower respiratory infections at 150 million per year. Most upper respiratory infections or common colds are caused by viruses, with human rhinoviruses (HRV) comprising over 100 serotypes identified in up to half of cases [166, 167]. Although common colds are usually mild and self-limited, they can be complicated by sinus or middle ear infections and croup [168]. They can also spread to cause lower respiratory infections such as bronchiolitis and pneumonia, or worsen asthma or chronic obstructive pulmonary disease (COPD). Among lower respiratory infections, influenza virus (flu) is identified in ~4-22% of cases, respiratory syncytial virus (RSV) in ~30-75%, and HRV in ~15-50% [168-171]. Of all commonly circulating respiratory viruses, flu leads in causing disability and death in hospitalized adults, whereas RSV, followed by HRV, does so in hospitalized infants and children [172]. Flu, RSV, and HRV are the three leading causes of disease burden in the elderly, further underscoring the pathogenic consequences of these viruses [172].

Host immunity to many viruses, including those targeting the respiratory tract, can be initiated in mice by the RIG-I-like helicase receptors (RLR) melanoma differentiation-associated protein 5 (MDA5) and retinoic acid-inducible gene 1 (RIG-I). MDA5 and RIG-I, which are encoded by the *IFIH1* and *DDX58* genes, function as intracellular cytoplasmic sensors of double-stranded (ds)RNA viral replicative intermediates or byproducts. Both sensors signal through the adaptor mitochondrial antiviral-signaling protein (MAVS, also known as IPS-1, Cardif, and VISA) to activate production of IFN and IFN-regulated gene transcription. This can inhibit virus replication and modulate cellular immune responses. MDA5 has a major role in recognizing and limiting picornavirus replication in mice and in vitro in human cells [76, 173-180]. Together with RIG-I, MDA5 can also recognize and limit replication of other positive

single-stranded RNA viruses of the coronavirus, calcivirus, and flavivirus families [79-84], dsRNA viruses of the orthoreovirus family [83], negative single-stranded (ss)RNA viruses of the paramyxovirus and orthomyxovirus families [76, 85-89], and even a DNA virus of the poxvirus family [181, 182]. However, those studies were conducted in vivo in Mda5-deficient mice and in vitro using mouse and human cells. By contrast, the role of MDA5 deficiency in the course of human natural infections is not yet known.

3.3 Results

Genetic analysis

Because the patient was from an isolated small people group of Burma (Myanmar), we hypothesized an autosomal recessive inheritance with a probable founder effect. Whole exome sequencing (WES) was performed on the patient and her healthy immediate relatives, which revealed 1.8% homozygosity in the patient, 2.7% in the mother, and 2.0% in the father. These values were within the upper range of normal of previously exome-sequenced in our non-consanguineous immunodeficiency cohort (data not shown) and were consistent with the lack of known consanguinity in this family. The patient carried a homozygous missense mutation in *IFIH1* NM_022168.3: c.1093A>G, p.K365E, which was confirmed by Sanger dideoxy sequencing (**Fig. 3.2b**, and **Table 3.1** and **3.2**). This variant (rs117608083) was extremely rare with an average allele frequency in ExAC of 0.06%, where it was found in East and South Asian populations although no homozygotes were observed. The patient's missense mutation occurred at a location that was conserved across species (PhastCons, 1) and under evolutionary constraint (GERP, 3.96). Substitution of glutamate for lysine resulted in loss of physicochemical conservation (Grantham score, 56) and was predicted to have

deleterious effects on protein structure and function (PolyPhen2, 0.998). The patient also carried several other rare homozygous missense mutations, but of these the *IFIH1* mutation was computationally predicted to be most deleterious (CADD score, 25) with its normal gene product being highly expressed in immune cells and lung (**Table 3.2**), so we focused our attention on this variant.

Consequences of the MDA5 mutation

The MDA5 protein encoded by *IFIH1* consists of N-terminal tandem caspase activation recruitment domains (CARD) and a C-terminal domain (CTD), which surround a central tripartite helicase core [183]. MDA5 forms a “C”-shaped ring encircling dsRNA, such that its monomers stack together along the dsRNA stem to form long filaments necessary for recognition of viral RNA. Lysine at 365 is located in the Hel1 domain of the helicase core (**Fig. 3.2b**), where it interacts with the 2'-hydroxyl group of ribose in the target RNA backbone [183]. Substitution with glutamic acid introduces a negative charge that is predicted to abolish the protein-nucleic acid interaction and hence MDA5 oligomerization (**Fig. 3.2c**). Consistent with our prediction, either before or after induction by IFN- α treatment, the endogenous MDA5 protein in homozygous mutant patient cells was expressed as well as in cells from normal healthy controls or heterozygous or homozygous wild-type family members (**Fig. 3.2d**, and data not shown). Levels of endogenous RIG-I or MAVS proteins were unaffected (**Fig. 3.2d**). However, when overexpressed in cells that lack endogenous protein, mutant MDA5 failed to affinity co-precipitate with a synthetic MDA5 ligand, poly(I:C) (**Fig. 3.2e**) [76, 173].

These data suggested that K365E, although normally expressed in patient cells, could not assemble to activate downstream signals. We therefore overexpressed wild-type or mutant MDA5 to test whether they could drive expression of luciferase from

several promoters. Cells transfected with wild-type MDA5 increased *IFNB1* promoter activity after stimulation with intracellular poly(I:C) (**Fig. 3.3a,b**). By contrast, those transfected with the K365E mutant showed minimal activity above non-transfected cells, which did not increase upon stimulation. K365E also failed to drive luciferase activity from IFN-stimulated response element (ISRE)- and NF- κ B-driven promoters (**Fig. 3.3c,d**). Co-transfections of the mutant with wild-type MDA5 showed no dominant negative effect (**Fig. 3.3e,f**). Although biallelic loss-of-function mutations in *IFIH1* have not been previously identified in humans, mono-allelic gain-of-function mutations have been reported in humans with Aicardi-Goutières syndrome [184, 185], Singleton-Merton syndrome [186], and systemic lupus erythematosus with IgA deficiency [187]. Our patient had neurodevelopmental delay but lacked the cerebral calcifications or white matter abnormalities characteristic of Aicardi-Goutières syndrome or congenital infection (data not shown). Moreover, her K365E mutation did not increase luciferase activity, either at baseline or after stimulation, in contrast to the known gain-of-function MDA5 mutants R337G or R779H (**Fig. 3.2a,c,d**) [184]. Additionally, our patient's cells did not express a type I IFN transcriptional signature characteristic of gain-of-function *IFIH1* mutations (data not shown). Thus, we conclude that the K365E missense mutation was loss-of-function.

Virus replication in respiratory epithelial cells

The patient's infection history suggested that MDA5 might function as a general sensor of viruses infecting the respiratory tract in humans, especially of HRV. Alternatively, MDA5 deficiency might underlie only a few viral diseases, perhaps even only one, causing respiratory lesions that could favor other viral diseases. To test innate immune responses in respiratory epithelium, we infected a transformed respiratory

epithelial cell line A549, in which genes of the RLR pathway were silenced by transient transfection of siRNA. Silencing of MDA5, RIG-I, or MAVS expression increased both HRV transcripts and production of infectious virus (**Fig. 3.4a-f**). HRV induced low levels of IFN-regulated transcripts, including MDA5 itself, which were decreased upon MDA5 silencing, consistent with further impairment in virus recognition and antiviral responses (**Fig. 3.5a,b**). Increased HRV replication was also observed by 72 hours in primary respiratory nasal epithelial cells from the patient as compared to her parents (**Fig. 3.6a** and data not shown). Importantly, transduction with wild-type but not mutant K365E MDA5 improved control of HRV replication (**Fig. 3.6b**). Thus, the patient's recurrent or persistent HRV infections supported an important role for MDA5 in their control in humans.

Although RIG-I is thought to function as the major sensor for the orthomyxoviruses and paramyxoviruses especially in mice, a few studies have suggested an additional role for MDA5 in responding to flu A/B and RSV [83, 86, 89, 188, 189]. We investigated these possibilities since our patient had been hospitalized for severe flu (flu B in 2011, flu A H3N2 in 2011 and 2014) and RSV infections. We silenced MDA5, RIG-I, or MAVS expression by transfecting siRNA in the respiratory epithelial cell line A549, which were then infected with a pathogenic flu A strain (H3N2) isolated in 2011. Consistent with the literature using other flu strains, silencing of either RIG-I or MAVS expression increased flu transcripts (**Fig. 3.7a,b**). However, silencing of MDA5 did not increase flu replication, nor did it increase pro-inflammatory cytokine production in contrast to silencing of RIG-I (**Fig 3.7c-f**). Infection of primary nasal epithelial cells from the patient did not show any increased flu replication as compared to her parents (**Fig. 3.8a**). Production of infectious flu (H1N1) virus was also unaltered in SV40-

transformed fibroblasts in which CRISPR/Cas genome editing had been used to generate single-cell clones either hemizygous for the patient's mutant *IFIH1* allele or completely lacking both *IFIH1* alleles (**Fig. 3.8b**, and data not shown). These cells did not exhibit increased cytotoxicity or decreased IFN- α production (**Fig. 3.8c,d**). Finally, using a recombinant RSV that expresses enhanced GFP as a marker of virus replication, we observed that silencing MDA5 did not increase RSV transcripts, although it did decrease IFN-regulated transcripts, which were more rapidly induced to higher levels than during HRV infection (**Fig. 3.9a-d**). Unlike HRV, RSV transcripts or infectivity and spread were not increased in primary respiratory nasal epithelial cells from the patient (**Fig. 3.9e,f**). RSV replication was also unaltered in gene-edited fibroblasts either hemizygous for the patient's mutant *IFIH1* allele or completely lacking both *IFIH1* alleles (data not shown). Together, these results show that under the same conditions where MDA5 deficiency results in increased HRV replication, flu and RSV replication remain unaffected. Hence, MDA5 has a non-redundant role in innate immune responses against respiratory infections caused by HRV.

3.4 Discussion

Studies in single patients can establish causality between genotype and phenotype in humans, provided that the mutant genotype is only found in the affected patient, the specific variant impairs corresponding protein function, and cellular phenotype can be recapitulated or rescued at the molecular level [27, 190]. By these criteria, we have shown that human MDA5 protects against respiratory infections caused by HRV. HRV accounts for a substantial disease burden of acute lower respiratory infections requiring hospitalization, especially in infants and children in whom it

surpasses that of flu [172]. Additionally, HRV is primarily responsible for half of upper respiratory infections, but has not been adequately studied as it is often dismissed as innocuous [165, 166]. This has impeded clinical recognition of additional patients with genetic susceptibility to the common cold. Whether MDA5 also physiologically protects against other respiratory viruses that we did not test such as human coronaviruses and adenovirus, or against systemic RNA viruses that our patient has not been exposed to such as poliovirus and Hepatitis A virus, is not yet known. Interestingly, our patient has not had hand-foot-mouth disease, nor has she had detectable non-respiratory enteroviruses associated with acute viral gastroenteritis, possibly due to protective effects of intravenous immunoglobulin treatments that variably contain neutralizing antibodies to enteroviruses [191, 192]. However, we speculate that the type 1 diabetes mellitus that she developed at two years of age might have been precipitated by persistent infection with pancreatropic enteroviruses which have been detected in pancreatic autopsy specimens from recent-onset disease [193, 194]. Moreover, it is also possible that she was congenitally infected with untested viruses that could cause systemic effects when MDA5 is lacking.

Our patient clearly demonstrates that MDA5 has an important physiological and non-redundant role in the human respiratory tract, where it senses and initiates innate immune responses to HRV. Importantly, by carrying out in vitro infection experiments in MDA5-silenced respiratory epithelial cells – and also in the patient’s own MDA5-deficient nasal epithelial cells – we have established that the MDA5 genotype is responsible for the increased HRV replication and HRV clinical phenotype in our patient. By contrast, the lack of in vitro phenotypes for flu and RSV in the same cell types suggests that the MDA5 genotype is not responsible for these infections in our patient. These results also

indicate that, surprisingly, other viruses such as flu and RSV, which have dsRNA intermediates that can be recognized by MDA5, are recognized and controlled by other means when MDA5 is deficient. Although it is possible that defective responses to these viruses might occur in other MDA5-deficient cell types, our results clearly show that this does not occur at the initial site of infection in the lung within respiratory epithelial cells. Additionally, in our patient, the decreased incidence of infections with age coincided with maturation of antibody responses. This ability of antibodies to compensate for defective innate immunity is similarly observed in other deficiencies of innate immunity. For example, in IRF7 deficiency associated with isolated flu susceptibility, subsequent flu infection is prevented by annual seasonal flu vaccination [190].

Of note, our patient had several other unexplained clinical features including neurodevelopmental delay that could be explained by her other genetic findings, including copy number variation in the *TM4SF20* gene (Supplemental Clinical Description) or alternatively de novo or rare autosomal recessive variants that were identified in genes highly expressed in the brain (Supplemental Table 2). Nevertheless, those clinical features and genetic findings do not diminish or negate our discovery that MDA5 is required for dsRNA-sensing, reduced IFN induction, and control of HRV infections in humans.

HRV is generally considered relatively non-pathogenic when additional factors such as respiratory co-infection or underlying respiratory disease are absent. Thus, unlike other primary immunodeficiencies characterized by susceptibility to highly pathogenic microbes, the lack of strong purifying selection against homozygous genotypes is not unexpected for MDA5. As shown by our knockdown experiments, MDA5 function appears to be partially redundant with RIG-I function for controlling HRV

replication, where other sensors can contribute to protection when MDA5 function is lacking. Alternatively, other genetic variants in our patient might contribute to her susceptibility to flu or RSV. However, this explanation seems less likely since replication of flu or RSV in her nasal epithelial cells was comparable to that in cells from healthy controls. Given these considerations, in our patient's particular case, it instead seems likely that her severe persistent HRV infections in infancy, which contributed to her chronic lung disease, in turn led to secondary complications including susceptibility to other viruses such as flu and RSV and bacterial superinfections. Thus, in some individuals, a selective genetic susceptibility to HRV can under certain circumstances contribute more broadly to the pathogenesis of severe respiratory infections during childhood.

3.5 Tables

Table 3.1 Summary of WES Variants found after each filtering stage.

DNA variants	Patient
Total variants from WES (SNP/indels)	79315
Nonsynonymous variants	11076
Novel or Rare variants	2984
Homozygous variants	18
Candidate variants (deleterious, expressed, etc)	1

Table 3.2 Non-synonymous rare genetic variants found in the patient by WES.

Table S2. Non-synonymous rare genetic variants found in the patient by WES

Genetic model	Chr	Position	Reference Base	Patient	Function	rsID	AminoAcids	Protein Position	PolyPhen	ConsScore GERP	Grantham Score	Score PhastCons	Score CADD	GeneList	GenomesESP (MAF < 0.001)	GenomesExAC (MAF < 0.001)	Expression in target tissue (Immune system and respiratory tract)
Homozygous recessive	2	16314647	T	C	missense	117608083	LYS,GLU	365/1026	0.998	5.96	56	1	25	IFH1	T=13006	C=74/T=121532	Yes
	7	43601466	A	C	missense	371612774	MET,LEU	1588/1607	0.002	5.93	15	1	14.55	HECW1	G=1/A=12435	G=1/A=122135	No
	6	51944763	C	T	missense	143979330	ALA,THR	109/4075	0.241	4.43	58	0.628	13.07	PKHD1	C=13006	T=113/C=122811	No
	2	174085985	C	G	missense	-	ASN,LYS	365/456	0.985	4.12	94	1	12	ZAK,MLK7-AS1	C=13006	G=3/T=7/C=122356	Ubiquitously expressed
	12	5916518	G	C	missense	374607322	ILE,MET	304/1004	0.999	-6.65	10	0.878	11.75	ANO2	G=11852	C=7/G=24409	No
	15	28986430	G	T	splice-donor	12438322	none	NA	unknown	0.853	NA	0.308	10.01	WHAMMP2	unknown	unknown	No
	20	57429627	C	A	missense	61749698	PRO,THR	374/627	0.002	-4.27	38	0	9.302	GNAS	C=8082	unknown	No
	19	55327960	C	T	missense	605219	SER,LEU	2/445	0.99	0.388	145	0.069	9.183	KIR3DL1	C=8768	unknown	Yes
	3	195925177	C	T	missense	74579410	GLY,ARG	307/310	0	-0.586	125	0.23	5.693	ZDHHC19	T=10/C=12382	unknown	No
	19	55107313	T	C	missense	36029771	TYR,HIS	291/440	0	-1.24	83	0	0.004	LILRA1	T=13004	unknown	Yes
	5	23527469	C	A	missense	112501567	ARG,SER	758/895	0	2.65	110	0.052	0.001	PRDM9	C=12776	unknown	No
	8	103573036	CG	C/C	frameshift	59109401	none	NA	unknown	-2.81	unknown	0.898	unknown	ODF1	unknown	unknown	No
	11	48285985	CT	C/C	frameshift	80271293	none	NA	unknown	2.51	unknown	0.999	unknown	OR4X1	unknown	unknown	No
	12	11420333	AG	A/A	frameshift	3842295	none	NA	unknown	0.182	unknown	0.002	unknown	PRB3	unknown	unknown	No
	20	47775474	A	AC/AC	splice-donor	11480966	none	NA	unknown	-0.339	unknown	0.001	unknown	STAU1	unknown	unknown	Ubiquitously expressed
Compound heterozygous recessive	19	5693431	C	Y	missense	375486513	VAL,ILE	797/896	0.66	4.75	29	0.878	15.5	LONP1	T=1/C=13005	T=8/C=121650	Ubiquitously expressed
	19	5711966	G	R	missense	80050321	ALA,VAL	165/896	0.24	-1.77	64	0.005	7.319		A=3/G=13003	A=68/G=119994	
De-novo	2	48725837	C	Y	missense	0	ALA,VAL	633/781	0.712	0.001	64	2.55	11.41	PPP1R21	C=13006	unknown	Yes
	4	110415981	C	Y	missense	186652926	PRO,LEU	451/1234	0.007	0	98	2.53	2.259	SEC24B	C=12308	T=1/C=122257	Yes
	17	77043676	T	W	missense	0	SER,THR	118/282	0.157	0.219	58	5.33	4.266	C1QTNF1	T=13000	unknown	No

3.6 Figures

Figure 3.1 Infection history in a human with recurrent respiratory tract infections.

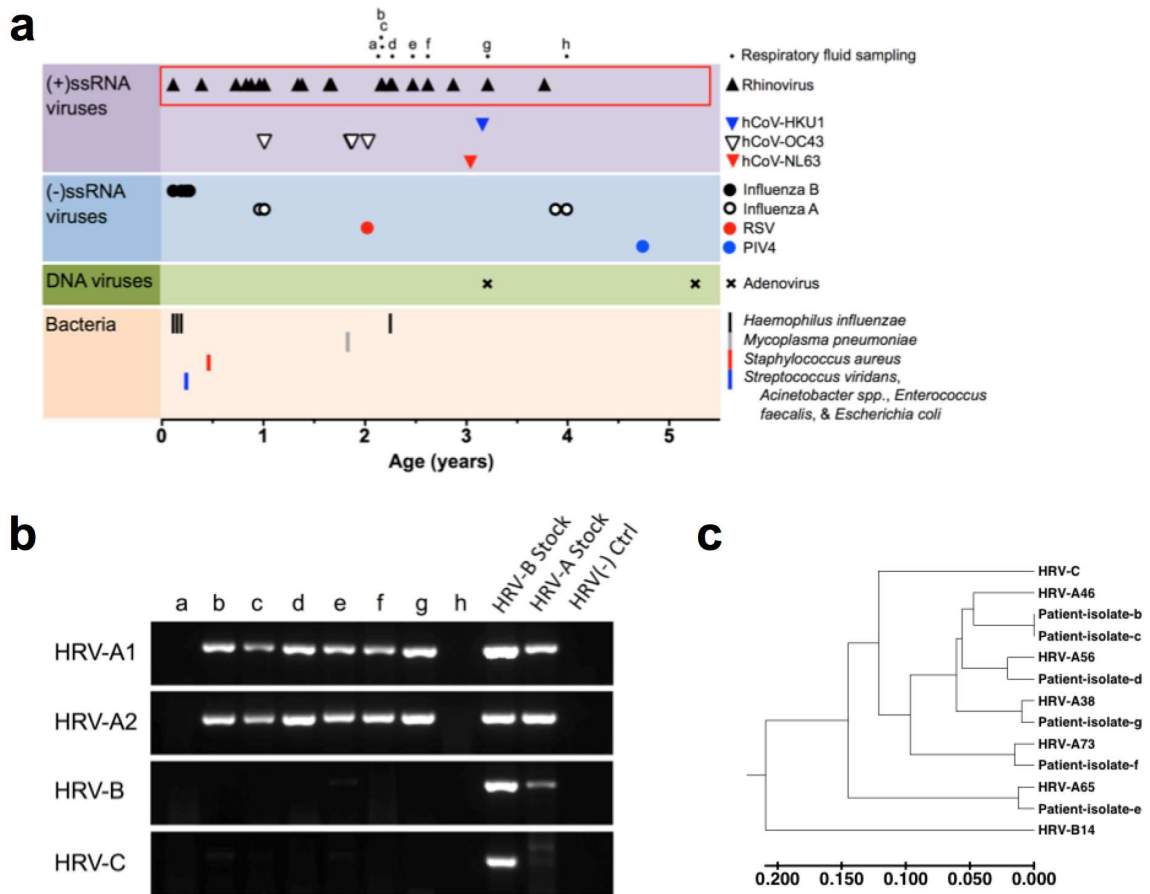


Figure 3.1 Infection history in a human with recurrent respiratory tract infections. **(a)** Timeline of pathogens recovered from the respiratory tract. These were classified as positive single-stranded RNA virus, negative single-stranded RNA virus, double-stranded DNA virus, bacteria as indicated in the adjacent symbol key. **(b)** RT-PCR molecular typing of RNA isolated from nasopharyngeal samples, using primer sets that preferentially amplify the indicated HRV species. Patient's samples "a" to "h," as indicated on **(a)**, were collected between 2 and 4 years of age. Sample "a" was negative for respiratory pathogens and "h" positive for flu A. Purified HRV -B14 and -A16 virus stocks, and a sample from a different subject having respiratory symptoms but negative for HRV/enterovirus, were also tested. **(c)** Phylogenetic tree based on nucleotide sequences of 5'UTR of HRV isolates showing evolutionary relationship of the patient's samples to closest serotypes and representative HRV species. Sample "b" has 91% homology to HRV-A46, and sample "g" has 98% homology to HRV-A38.

Figure 3.2 Autosomal recessive, homozygous *IFIH1* mutation in the proband.

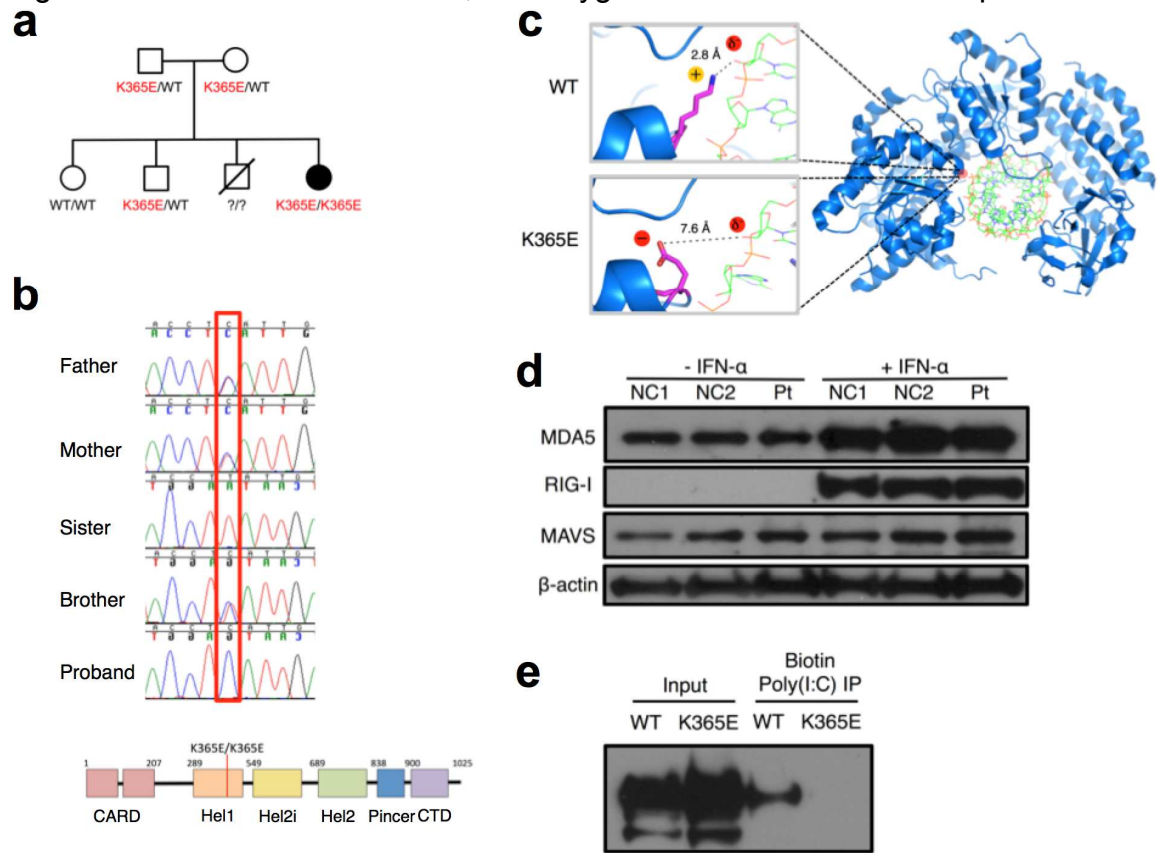


Figure 3.2 Autosomal recessive, homozygous *IFIH1* mutation in the proband. **(a)** Pedigree indicating genotypes. **(b)** Confirmatory Sanger sequencing. Schematic below showing mutation location relative to MDA5 protein domains. **(c)** Ribbon diagram of the MDA5 structure with close-up showing lysine 365 interaction with ribose in RNA, and effects of glutamic acid substitution on distances (Å) between charged groups (yellow sphere, positive; red spheres, negative). **(d)** Immunoblot of MDA5, RIG-I, and MAVS proteins, relative to β -actin, in cycling T cells, either untreated or treated for 20 hours with IFN- α . NC, healthy normal control. Pt, patient. **(e)** Immunoblotting of overexpressed MDA5 (wild-type (WT) or K365E) after affinity precipitation with biotinylated-poly(I:C). **(d)** and **(e)** are representative of four repeats.

Figure 3.3 Loss-of-function *IFIH1* mutation.

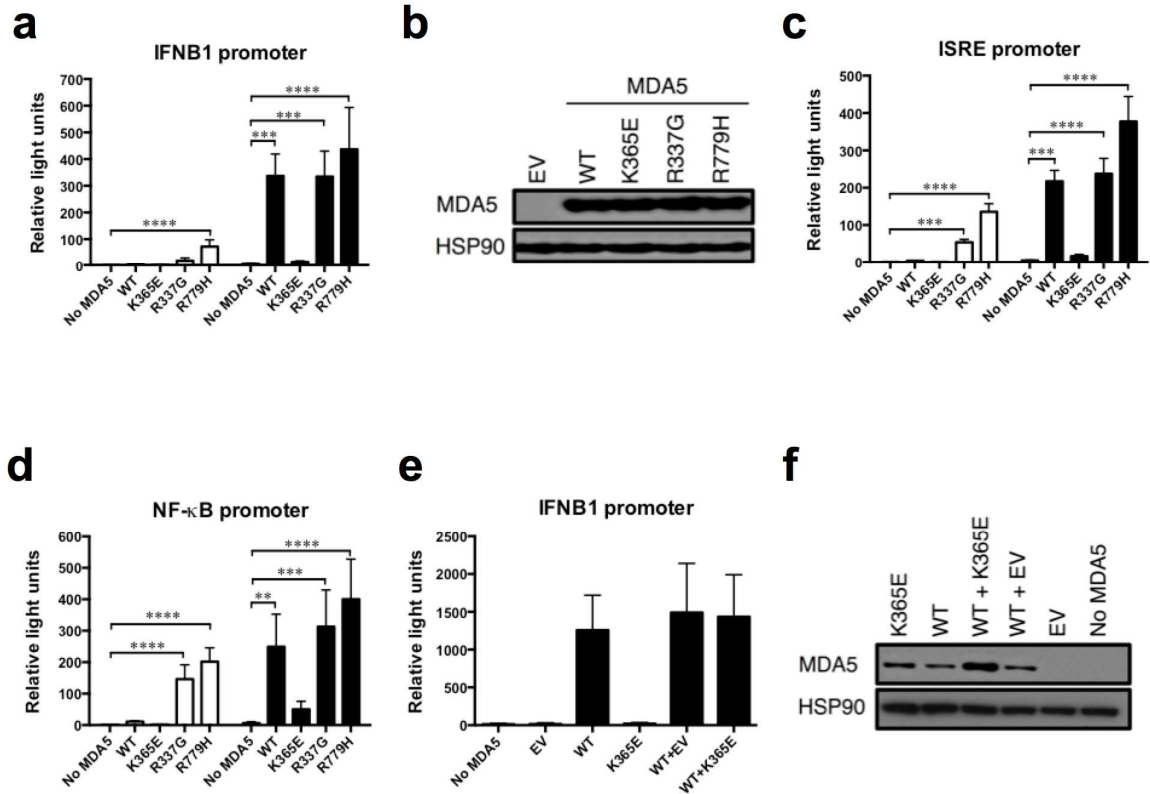


Figure 3.3 Loss-of-function *IFIH1* mutation. (a,c,d) Relative increase in normalized luciferase activity driven by the *IFN* β 1 promoter (a), ISRE (c), or NF- κ B (d) reporter constructs. Cells were co-transfected with WT or mutant MDA5, and with (solid) or without (open) transfected poly(I:C) as indicated. R337G and R779H are gain-of-function mutants. (b) Immunoblotting for MDA5 proteins after transient transfection of 20 ng wild-type (WT) or mutant K365E MDA5, both under CMV promoters. (e) Similar to (a) except that cells were co-transfected with 20 ng WT MDA5 (under CMV promoter), and either K365E MDA5 or empty vector (EV) (under MSCV promoter). (f) Immunoblotting for MDA5 proteins in lysates from (e). Data show means \pm SD from four experiments in (a) and (e), three in (c), and five in (d). Data in (b) and (f) are examples from experiments shown in (a), (c), and (d), and (e), respectively. 293T cells lack endogenous MDA5 expression (data not shown). Equivalent lysates from \sim 30,000 cells were run across lanes. ** $p < 0.01$, *** $p < 0.001$, **** $p < 0.0001$, by one-way ANOVA.

Figure 3.4 Loss of MDA5 function results in increased replication of HRV in respiratory epithelial cells.

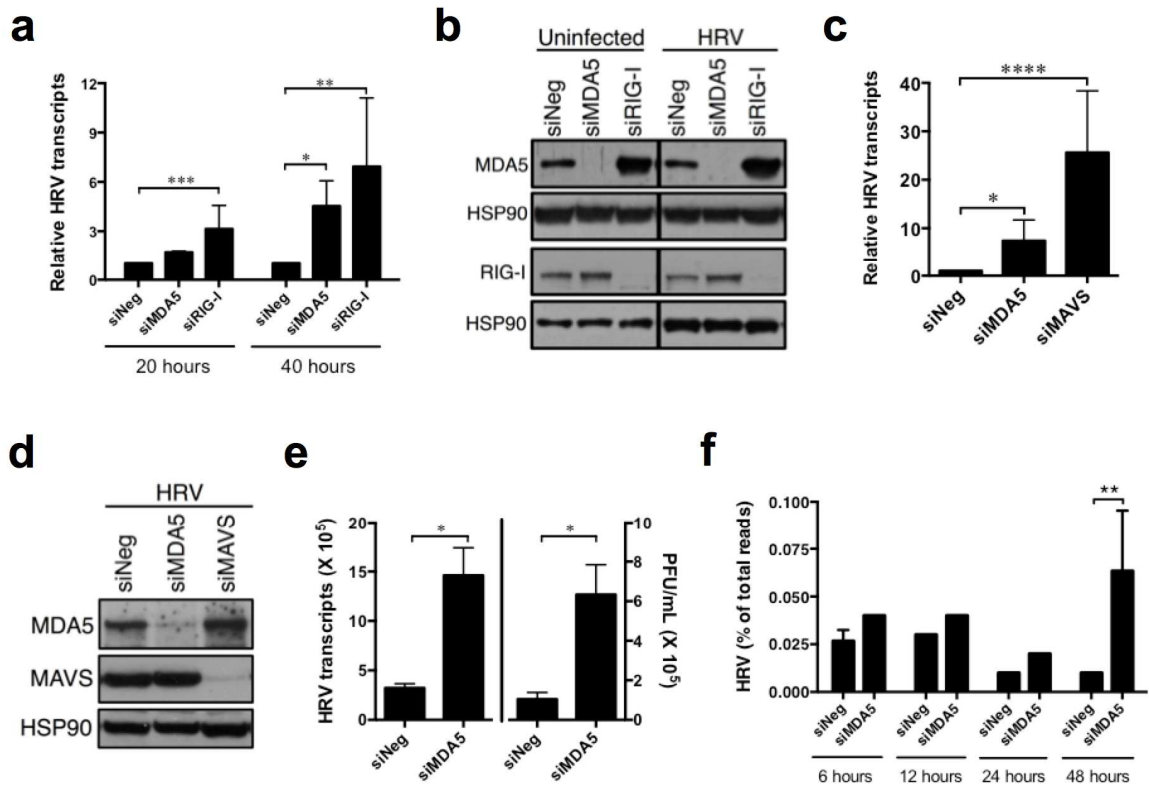


Figure 3.4 Loss of MDA5 function results in increased replication of HRV in respiratory epithelial cells. **(a)** HRV transcripts, normalized to non-specific siRNA negative (siNeg) control. HRV-infected (MOI: 1) A549 cells were previously transfected with the indicated siRNA. **(b)** Immunoblotting showing efficiencies of MDA5 and RIG-I knockdown in **(a)**. Transfected cells were left uninfected or infected with HRV for 48 hours. 120 μ g of lysates were run per lane. **(c)** Similar to **(a)**, at 48 hours after infection and two rounds of transient transfection with the indicated siRNA. **(d)** Immunoblotting showing efficiencies of MAVS and MDA5 knockdown in **(c)**. **(e)** HRV transcripts and HRV simultaneously quantitated by infectious plaque assay, at 60 hours after infection. **(f)** Number of HRV reads in RNA-seq data during HRV infection. A549 cells were previously transfected with MDA5 or non-specific negative control siRNA (siNeg). Average of triplicate expression ratios from triplicate infections were shown for each time point. Data show means \pm SD from five experiments in **(a)**; eight in **(c)**; four in **(e)**. Representative experiments are shown in **(b)** and **(d)**. * $p < 0.05$, ** $p < 0.01$, *** $p < 0.001$, **** $p < 0.0001$, by Kruskal-Wallis test in **(a)** and **(c)**; Mann-Whitney U test in **(e)**; and Kolmogorov-Smirnov test in **(f)**; other comparisons in **(a)** and **(f)** were non-significant.

Figure 3.5 MDA5 effects on IFN during HRV infection of respiratory epithelial cells.

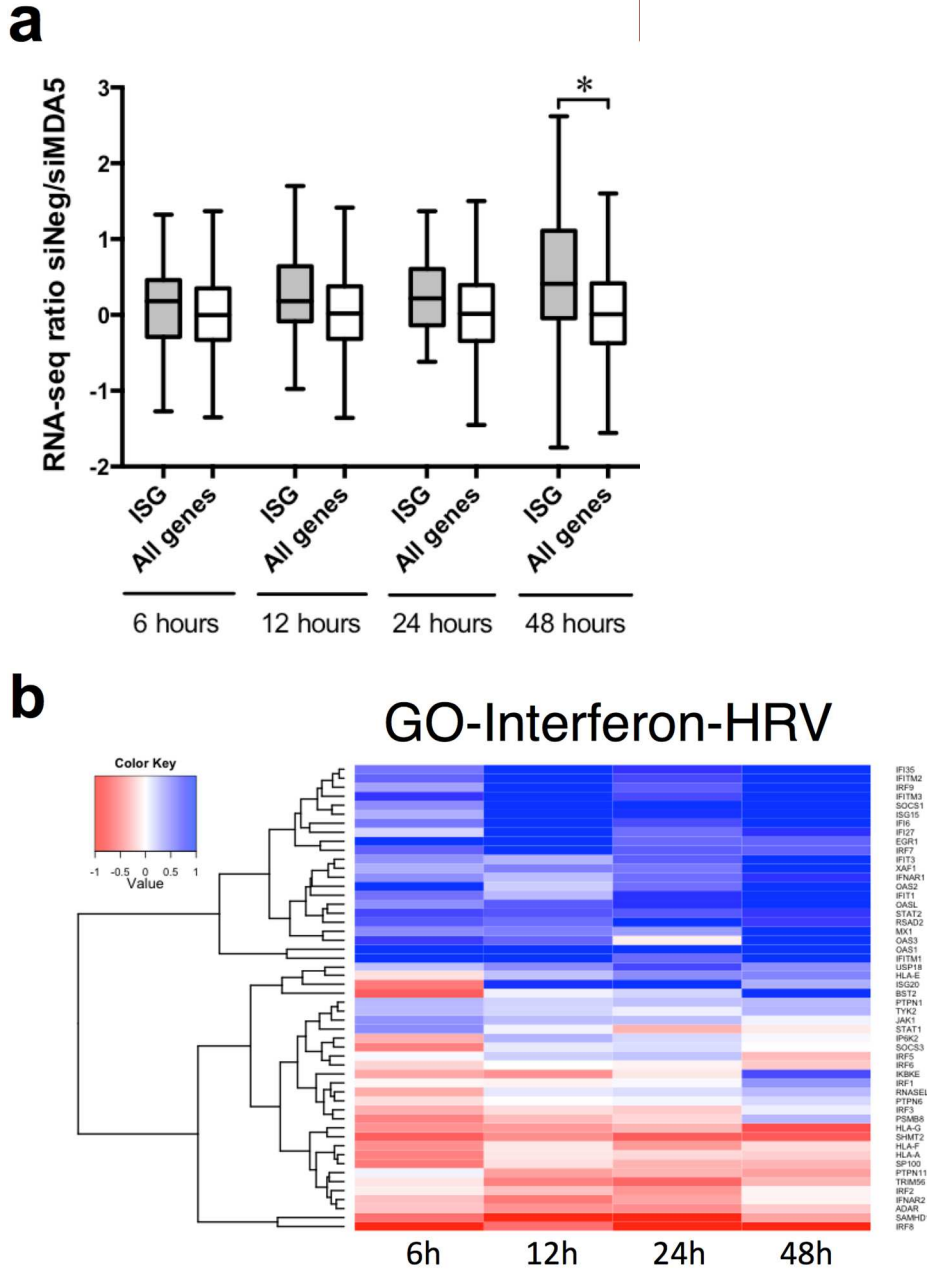


Figure 3.5 MDA5 effects on IFN during HRV infection of respiratory epithelial cells. **(a)** “Response to type I interferon” genes (GO term GO0034340) versus all genes. **(b)** Heatmap representation of RNA-seq data showing HRV-induced IFN-regulated gene transcripts (RPKM) over the course of infection. Data in **(a)** show box-and-whisker plots from triplicate infections. A549 cells were previously transfected with MDA5 or non-specific negative control siRNA (siNeg) and correspond to Fig. 4F. Average of triplicate expression ratios from triplicate infections were shown for each time point. * $p < 0.05$, by Kolmogorov-Smirnov test in **(a)** and **(b)**; other comparisons were non-significant.

Figure 3.6 Loss of MDA5 function results in increased replication of HRV in respiratory epithelial cells.

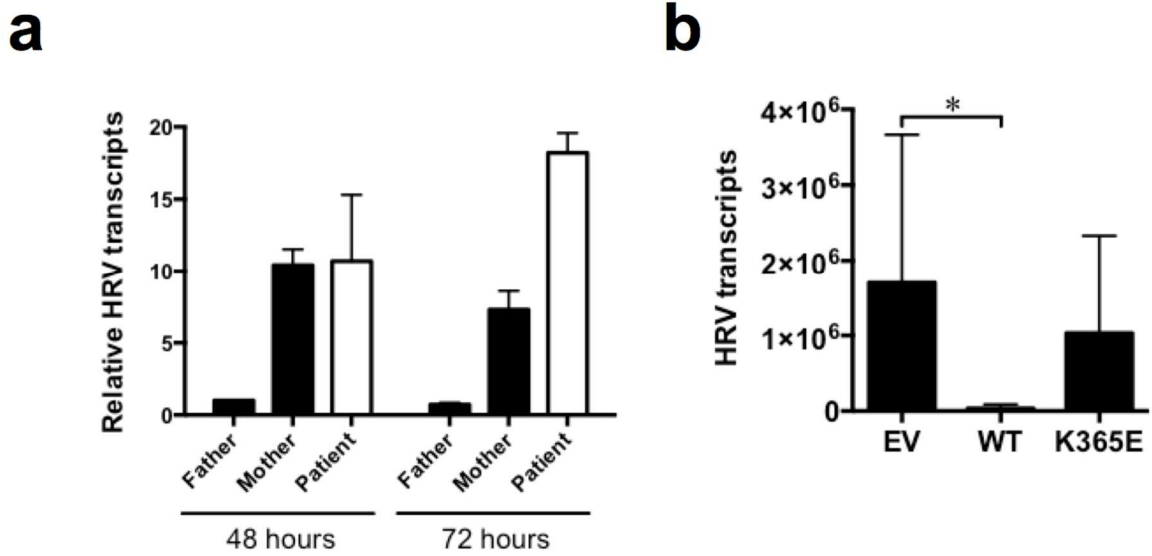


Figure 3.6 Loss of MDA5 function results in increased replication of HRV in respiratory epithelial cells. (a) HRV transcripts, normalized to non-specific siRNA negative (siNeg) control. Primary nasal epithelial cells from the patient and parents were infected with HRV (MOI: 1). (b) HRV transcripts in A549 cells previously transduced with empty vector (EV), wild-type (WT) or K365E MDA5, at 72 hours after infection. Data show means \pm SD from three experiments in (a), and five in (b). * $p < 0.05$, by Kruskal-Wallis test in (b); other comparisons in (b) were non-significant.

Figure 3.7 Loss of MDA5 function does not affect replication of flu or production of pro-inflammatory cytokines in respiratory epithelial cells.

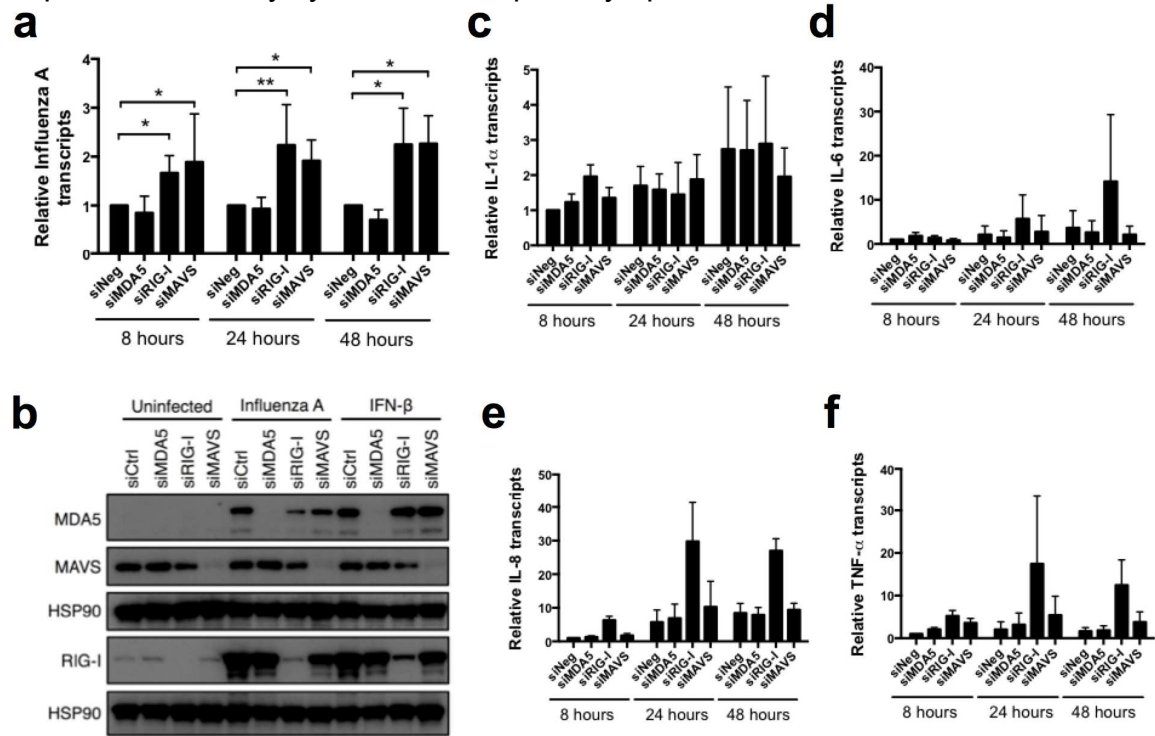


Figure 3.7 Loss of MDA5 function does not affect replication of flu or production of pro-inflammatory cytokines in respiratory epithelial cells. **(a)** Flu (MOI: 0.1) transcripts, normalized to siNeg control. Flu-infected A549 cells were previously transfected with the indicated siRNA. **(b)** Immunoblotting showing efficiencies of MDA5, RIG-I, and MAVS protein expression, relative to HSP90 loading control, after transient transfection with the indicated siRNA into A549 cells. Transfected cells were left uninfected or infected with flu strain A/Victoria/361/2011 (MOI: 0.5) for 24 hours or treated with IFN- α (10 IU/mL) for 24 hours. 20 μ g of lysates were run per lane. Shown is a representative experiment corresponding to **(a)**. **(c-f)** Pro-inflammatory gene transcripts quantitated by qRT-PCR from **(a)**. Levels of IL-1 α **(c)**, IL-6 **(d)**, IL-8 **(e)**, TNF- α **(f)** were normalized to β -actin and are shown relative to normalized levels at 8 hours after infection. Data show means \pm SD from six to seven experiments in **(A)** and three independent experiments in **(a)** to **(f)**. * $p < 0.05$, ** $p < 0.01$, by Kruskal-Wallis test in **(a)**; all other comparisons were non-significant.

Figure 3.8 Loss of MDA5 function does not affect flu replication, or flu-induced IFN production or cytotoxicity, in respiratory epithelial cells or fibroblasts.

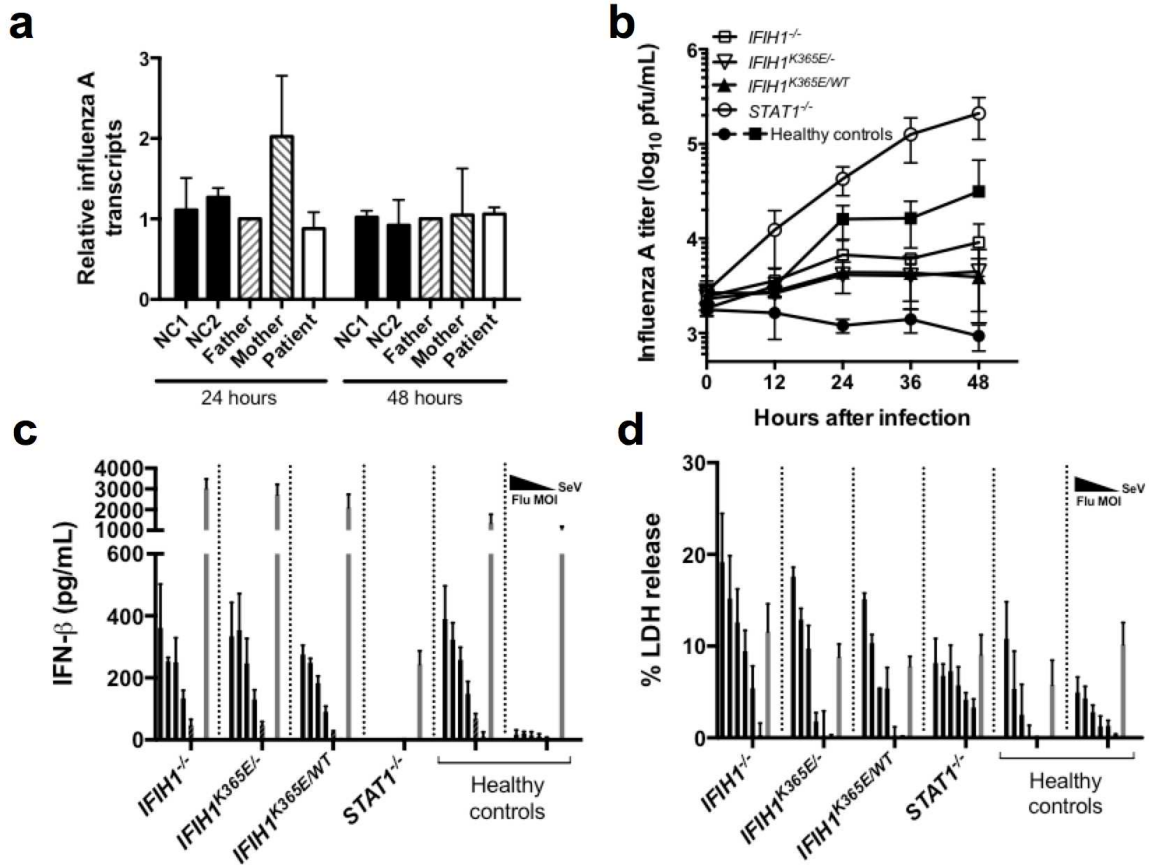


Figure 3.8 Loss of MDA5 function does not affect flu replication, or flu-induced IFN production or cytotoxicity, in respiratory epithelial cells or fibroblasts. (a) Flu transcripts, normalized to siNeg control. Primary nasal epithelial cells from the patient, parents, and two normal healthy controls were infected with flu (MOI: 0.02). (b) Flu virus quantitated by infectious plaque assay, after infection (MOI: 1) of SV40-transformed fibroblasts having the indicated genotypes. (c) IFN- β released into supernatants as measured by ELISA after infection with flu strain A/Puerto Rico/8/1934 (MOI: 0.37 – 54). Sendai Virus (SeV) was included as positive control of interferon induction. Genotypes of SV40-transformed fibroblasts are as indicated. (d) LDH released into samples from (c). Data show means \pm SD from four experiments in (a), three independent experiments in (b) that are representative of 11 experiments with varying MOIs (0.1 to 30) and three different flu strains (A/Netherlands/602/2009, A/California/4/2009, and A/Puerto Rico/8/1934), and three independent experiments in (c) and (d) that are representative of 6 and 7 experiments, respectively, in which the MOI were varied.

Figure 3.9 Loss of MDA5 function does not affect RSV replication while affecting RSV-induced IFN-regulated transcripts.

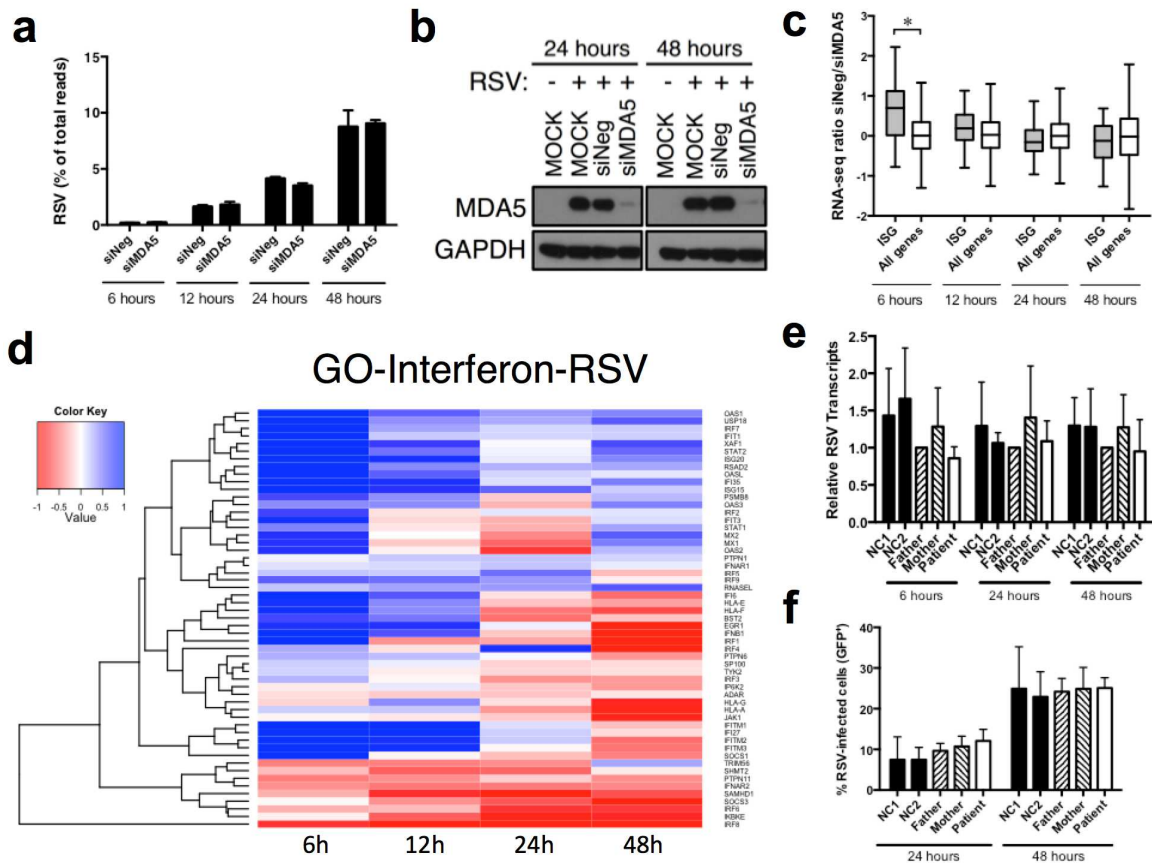


Figure 3.9 Loss of MDA5 function does not affect RSV replication while affecting RSV-induced IFN-regulated transcripts. **(a)** Number of RSV reads in RNA-seq data during RSV infection. RSV-infected (MOI: 1) A549 cells were previously transfected with MDA5 or non-specific negative control siRNA (siNeg). **(b)** Immunoblotting showing efficiencies of MDA5 protein expression after transient transfection of A549 cells with the indicated siRNA, or without transfection (MOCK). Cells were either left uninfected or infected with RSV, as indicated. 20 μ g of lysates were run per lane. Shown is a representative experiment corresponding to **(a)**. **(c)** “Response to type I interferon” genes (GO term GO0034340) versus all genes, from **(a)**. **(d)** Heatmap representation of RNA-seq data showing the expression change between MDA5 siRNA and non-specific siRNA control of IFN-regulated gene over the course of RSV infection. Average of triplicate expression ratios from triplicate infections were shown for each time point in **(a)**, **(c)**, and **(d)**. **(e)** RSV transcripts in primary nasal epithelial cells from the patient (open bar), parents (hatched bars), and two normal healthy controls (solid bars), normalized to father, after RSV-GFP infection (MOI: 0.2). **(f)** % GFP⁺ of gated live RSV-infected cells from **(e)**. Data show means \pm SD from four experiments in **(e)** and **(f)**. * $p < 0.05$, by Kruskal-Wallis test in **(c)** and **(d)**; other comparisons were non-significant.

3.7 Supplementary Notes

Supplementary Note 3.1 Patient clinical course.

At birth, she was found to have intrauterine growth retardation. Infection screening during routine prenatal care had indicated past maternal infection with HSV-1, Toxoplasma, and CMV. At 40 days old, she had an upper respiratory infection that was PCR-positive for both HRV/enterovirus and flu B. She developed respiratory failure, which required mechanical ventilation including extra-corporeal membrane oxygenation. Tracheal aspirates grew out *Haemophilus influenzae*, *Streptococcus viridans*, *Acinetobacter* spp., enterococcus, *Escherichia coli*, and other coliform bacteria. Subsequently, she had more than 15 hospital admissions for respiratory distress precipitated by viral respiratory infections. Multiplex PCR revealed two episodes of flu A; three prolonged intervals of HRV/enterovirus shedding, for over more than half of her lifetime; four episodes of coronaviruses (OC43, NL63, HKU1); and one each of RSV, adenovirus, and human parainfluenza virus type 4. She continues to require supplemental oxygen, and had ground glass opacities but no bronchiectasis on chest CT. She has been hospitalized on multiple occasions for coliform urinary tract infection and acute gastroenteritis with dehydration but without detectable viral pathogens. She had an abscess near her G tube insertion site that grew out *Klebsiella pneumoniae* and *Enterobacter cloacae*. Although she initially had low serum immunoglobulin levels and decreased lymphocyte counts (affecting T, NK, and B cell subsets), these all normalized between 3 to 4 years old. Replacement immunoglobulins were discontinued and she has responded with functional antibodies to tetanus, diphtheria, and *Haemophilus influenzae* vaccines. She has no history of opportunistic or chronic systemic virus infection including EBV or CMV despite serological evidence of past exposure. Additionally, when 2 years

old, she developed new-onset type 1 diabetes mellitus with detectable GAD65 autoantibodies. She has short stature, low weight, hypotonia, weakness, and delays in motor and language development. Brain MRI showed low periventricular white matter volume with ventriculomegaly, and structural abnormalities of hippocampus, olfactory bulbs, septum pellucidum, and corpus callosum. High-resolution chromosomal microarray analysis identified a 4kb deletion on chromosome 2 that included the *TM4SF20* gene. This copy number variant has been associated with language delay, white matter hyperintensities, and varied developmental abnormalities in South Asian populations [195]. Several regions of absence of heterozygosity (AOH) totaling 45 MB on 5 separate chromosomes were also identified.

3.8 Materials and Methods

Patients

Whole blood, serum, skin biopsies, and nasal airway epithelial scrapings were obtained from the patient, her relatives, or paid healthy volunteers. These individuals gave written informed consent to participate in research protocols approved by Institutional Review Boards (IRB) at NIAID and National Jewish Health, which are registered in ClinicalTrials.gov under NCT00246857, NCT00128973, and NCT00895271. Buffy coat cells, which were by-products of volunteer-donor blood units, were distributed in an anonymized manner and thus were exempted from need for informed consent and IRB review.

Rhinovirus Molecular Typing

TRizol LS reagent (Ambion) was used to extract total RNA from 350 μ L of nasopharyngeal washes/aspirates obtained from patients or anonymized controls, or from laboratory virus preparations. 20 μ L of RNA was reverse-transcribed using a high-capacity cDNA reverse transcription kit with RNase inhibitor (Applied Biosystems). PCR was performed as described previously [196], except that 32 cycles of a single round of PCR amplification were performed in a 25 μ L volume using 2 μ L cDNA template and 0.5 μ M of forward and reverse primers. The previously published primers, which were relatively species-specific, were used for amplification of the 5'UTR of Rhinovirus (5'UTRn-A1, 5'UTRn-A2, 5'UTRn-B1, 5'UTRn-Cc, 5'UTR-rev). The PCR-amplified products were resolved by electrophoresis on 2% agarose gel. PCR-amplified products were also purified by QIAquick Gel Extraction Kit (Qiagen) and cloned using TOPO TA Cloning Kit for Sequencing (Invitrogen). Plasmid DNA were isolated from transformed TOP10 *E. coli* colonies using the R.E.A.L. Prep 96 Plasmid Kit (Qiagen). For each PCR product, 96 cloned inserts were Sanger dideoxy sequenced using plasmid-specific M13 Forward and Reverse primers. Sequences were analyzed using Sequencher 5.1 software, and BLAST searches of GenBank sequences were performed to identify the virus serotype. The phylogenetic analysis was performed using the UPGMA method of MEGA 7 software, and all positions containing gaps and missing data were eliminated. The phylogenetic trees were drawn to scale, with branch lengths in the same units as those of the evolutionary distances used to infer the phylogenetic tree. The evolutionary distances were computed using the Maximum Composite Likelihood method and are in the units of the number of base substitutions per site. The NCBI HRV reference sequences included in the tree are HRV-A89 (NC_001617.1), HRV-B14 (NC_001490.1), and HRV-C (NC_009996.1).

Genomic Analyses

Genomic DNA from the patient and family members were isolated from PBMC using the DNeasy kit (Qiagen). Whole exome sequencing, using SureSelect Human All Exon 50 Mb Kit (Agilent Technologies) coupled with massively parallel sequencing by Illumina HiSeq Sequencing System, was performed using 3 µg of genomic DNA collected from patient, both parents, and unaffected sister. Sequenced DNA reads were mapped to the hg19 human genome reference by Burrows-Wheeler Aligner (BWA) with default parameters. Single nucleotide variant and indel calling were performed using the Genome Analysis Toolkit (GATK, <http://www.broadinstitute.org/gatk/>). All SNVs/indels were annotated by SeattleSeq Annotation (<http://snp.gs.washington.edu>) and an in-house custom analysis pipeline was used to filter and prioritize for nonsynonymous and novel/rare variants (MAF < 0.001) under autosomal recessive or de-novo genetic models. UCSC gene sorter Microarray data (GNF Expression Atlas 2 Data from U133A and GNF1H chips) and Illumina Human BodyMap RNA-seq data were used to prioritize variants for functional validation. For confirmation of *IFIH1* mutations and genotyping of the brother, genomic DNA was PCR-amplified using forward primer 5'- CAA TGA CAC AAA TGC CAT CA-3' and reverse primer 5'- CAG GGA GTG GAA AAA CCA GA-3'. Sanger dideoxy sequencing of purified PCR-amplified products was performed by the Genomics Unit of the Rocky Mountain Laboratories Research Technologies Section of the NIAID. The WES data will be deposited under dbGaP accession number X.

Molecular Modeling

Molecular dynamics simulations were carried out using the Assisted Model Building with Energy Refinement (AMBER14) simulation package [197] with GPU acceleration [198].

The FF99SB all-atom potential [199] was used along with parameters for ATP [200] and Zn^{2+} [201]. Starting with the crystal structure of MDA5 (PDB ID: 4GL2) [183], ANP was changed to ATP and lysine at position 365 was mutated to glutamic acid in PyMol (The PyMol Molecular Graphics System, Version 1.7.2.1, Schrödinger, LLC). The system was protonated in tleap, solvated with TIP3P explicit water in a periodic truncated octahedron extending 10Å beyond the MDA5 complex, neutralized with Na^+ , and brought to approximately 150 mM of sodium chloride by randomly exchanging solvent molecules with Na^+ or Cl^- . The system was then subjected to energy minimization with diminishing harmonic restraints, followed by heating from 100K to 303K over 30 ps at constant volume with a Berendsen thermostat. Production runs were generated by switching the heated system to a constant pressure and temperature ensemble and allowing the system to equilibrate over 120 ps. All simulations were run in triplicate using the SHAKE algorithm.

Primary T cells

Peripheral blood mononuclear cells (PBMC) were isolated by density centrifugation through Ficoll-Hypaque™ PLUS (GE Healthcare Life Sciences). Pan T cells were isolated by negative selection using Pan T Cell Isolation Kit (Miltenyi Biotec) to ≥98 % purity. Pan T cells were stimulated with anti-CD2/CD3/CD28 coated beads from the T Cell Activation/Expansion Kit (Miltenyi Biotec), at a bead to cell ratio of 1:1. T cells were cultured in RPMI medium supplemented with 10% fetal bovine serum (FBS, Gibco), 100 U/mL recombinant human IL-2 (Aldesleukin, Prometheus), 2 mM L-glutamine, 100 U/mL penicillin, 100 µg/mL streptomycin, and 55 µM β -mercaptoethanol (Sigma-Aldrich, rest from Gibco). Where indicated, previously activated cycling T cells were treated with 100

IU/mL recombinant human IFN- α (Intron A, Merck) for 20 hours to induce MDA5 expression.

Primary and SV40-Transformed Fibroblasts

Fibroblasts were isolated from skin punch biopsies as previously described.[202] In brief, dermal and epidermal layers were dissociated after overnight incubation of biopsy tissue with Dispase (BD Biosciences). The dermis was minced and cultured in complete DMEM-Dulbecco's Modified Eagle Medium (Gibco) supplemented with 10% FBS, 2 mM L-glutamine, 100 U/mL penicillin, 100 μ g/mL streptomycin, and 55 μ M β -mercaptoethanol (Sigma-Aldrich, rest from Gibco) to allow fibroblasts to grow out. Fibroblasts isolated from a healthy normal donor or the patient's mother were used for *IFIH1* genome editing. Cells from the patient's mother were used to generate wild-type/null, mutant (c.1093A>G, p.K365E)/null, and null/null genotypes. U6gRNA-Cas9-2A-GFP plasmids (HS0000455078, Sigma-Aldrich) were transfected into the fibroblasts using the P3 Primary Cell 96-well Nucleofector kit with Nucleofector Program 96-DT-130 (Lonza). Three days after transfection, cells highly expressing GFP were single-cell sorted into 96-well plates using a BD FACSAria Fusion cell sorter and cultured until confluent. Cells from the patient's mother, or from a healthy normal donor, that had not undergone genome editing were also single-cell sorted and cultured in parallel for use as controls. Genotypes for each genome-edited clone were screened by agarose gel electrophoresis of PCR amplified products using forward primer 5'-AAA GGG GAA ATA CGG AAT TGG-3' and reverse primer 5'-GAG TCA ATG ACA CAA ATG CCA TC-3', followed by confirmation by Sanger dideoxy sequencing. Three to five clones each of *IFIH1* genotypes wild-type/null, mutant/null, wild-type/mutant, and null/null were selected and expanded for experiments.

To generate SV40-transformed fibroblast lines, 3×10^6 primary dermal fibroblasts were electroporated in 400 μL of complete DMEM with 3 μg of pLAS plasmid [203] in a 0.4 cm cuvette using the Gene Pulser® II electroporation system (1 pulse; 250 V, 1400 μF , resistance = ∞ ; Bio-Rad). Cells were divided into three 75cm² flasks and monitored 1 to 2 weeks for outgrowth of rapidly growing colonies. Cultures were then passaged > 4 times to ensure elimination of primary fibroblasts. STAT1-deficient SV40-transformed fibroblasts were described previously [204].

Primary Nasal Epithelial Cells

Nasal airway epithelial cells were collected from the lower surface of the inferior nasal turbinate using a sterile cytology brush (*Cytosoft*, Medical Packaging Corporation) as previously described.[205, 206] Cells were placed in Ham's F-12 medium (Gibco) supplemented with 10% dimethyl sulfoxide (Sigma-Aldrich), 30% heat inactivated FBS (Gibco), and 0.1% Y-27632 Rho kinase inhibitor (ApexBio). The collection medium was also supplemented with 1.25 $\mu\text{g}/\text{mL}$ amphotericin B (Sigma-Aldrich), 2 $\mu\text{g}/\text{mL}$ fluconazole (Gallipot), and 50 $\mu\text{g}/\text{mL}$ gentamicin (Gibco). Cells were stored cryopreserved until needed for culture, using adapted methods that combined use of an irradiated fibroblast feeder layer and Rho kinase inhibition.[207] The major modification was the use of irradiated 3T3 fibroblasts (ATCC) as the feeder cell layer. Nasal airway epithelial cells were cultured in T75 flasks to approximately 80% confluence and harvested using the multistep trypsinization procedure described [207]. Harvested cells were cryopreserved using the medium described above but without antibiotic supplementation. Cells of the same passage number and no greater than passage three were used for experiments.

Other Cell Lines

The human embryonic kidney 293T cell line (ATCC) was cultured in DMEM medium (Gibco) supplemented with 10% FBS (Gibco or Hyclone), 2 mM glutamine, 100 U/mL penicillin, 100 µg/mL streptomycin, and 55 µM β-mercaptoethanol (Sigma-Aldrich, rest from Gibco) for all experiments, or Iscove's Modified Dulbecco's Medium (IMDM, Gibco) supplemented with 10% FBS (Gibco or Hyclone) and 55 µM β-mercaptoethanol (Sigma-Aldrich) for lentivirus production. The monkey kidney cell line Vero E6 (ATCC) was cultured in DMEM supplemented with 10% FBS, 2 mM glutamine, 100 U/mL penicillin, 100 µg/mL streptomycin, and 55 µM β-mercaptoethanol. The lung epithelial carcinoma cell line A549 (ATCC) was cultured in F-12K medium (Gibco) supplemented with 10% FBS, 2 mM glutamine, 100 U/mL penicillin, 100 µg/mL streptomycin, and 55 µM β-mercaptoethanol. The H1-HeLa cell line (gift from Wai-Ming Lee) was cultured in MEM suspension medium with Earle's salts and no calcium (Gibco, #11380-037), supplemented with 10% FBS (Hyclone), 1x MEM non-essential amino acids, 2 mM L-glutamine, 100 U/mL penicillin, 100 µg/mL streptomycin, 0.1% Pluronic F-68, and 55 µM β-mercaptoethanol (Sigma-Aldrich, rest from Gibco). H1-Hela cells were maintained in suspension by growing at 37°C on an incubator shaker set at 230 rpm. The Madin-Darby Canine Kidney (MDCK, ATCC) cell line was cultured in DMEM medium (Gibco) supplemented with 10% FBS (Gibco).

Immunoblotting

Five million cells were lysed in 2% SDS or LDS sample loading buffer (Pierce), with 5% 2-mercaptoethanol (Sigma-Aldrich), and heated to 95°C for 10 minutes. Proteins contained within the supernatants were quantified by BCA (Pierce). Unless otherwise

indicated, 40 µg of protein were loaded per lane and were separated on NuPAGE Bis-Tris SDS-PAGE gels with MOPS running buffer (Invitrogen), followed by semi-dry transfer onto nitrocellulose membranes (Bio-Rad). After blocking with 5% non-fat dry milk (Bio-Rad) in PBS containing 0.1% Tween 20 (Sigma-Aldrich), membranes were incubated with the antibodies directed against MDA5 (clone #D74E4), RIG-I (clone #D14G6), MAVS (clone #3993, all from Cell Signaling Technologies), β -actin (clone #AC-15, Sigma-Aldrich), and HSP90 (clone 68, BD Biosciences). Signal was detected by incubation with appropriate HRP-conjugated secondary antibodies (Jackson ImmunoResearch or Southern Biotech), followed by application of SuperSignal West Pico Chemiluminescent substrate or SuperSignal West Dura Extended Duration Substrate (Pierce) and exposing to film.

Plasmids and Molecular Cloning

Firefly luciferase plasmid driven by the human IFN- β promoter (IFNB-pGL3, Promega)[208] and the constitutively expressed *Renilla* luciferase reporter plasmid (pRL-TK, Promega) were kind gifts from Yong He. The firefly luciferase plasmids driven by the interferon-stimulated response element (pGL4.33-*luc2P*/ISRE/Hygro, Promega) and the NF- κ B response element luciferase (pGL4.32-*luc2P*/NF- κ B-RE/Hygro, Promega) were modified to express GFP instead of the hygromycin resistance cassette. Briefly, pGL4.33-*luc2P*/ISRE/Hygro and pGL4.32-*luc2P*/NF- κ B-RE/Hygro plasmids were digested with BamHI and NotI (New England Biolabs) and gel-purified (QIAquick Gel Extraction Kit, Qiagen) to remove the hygromycin resistance cDNA. The coding sequence of EGFP was PCR-amplified from pcDNA3-EGFP (Addgene #13031) using AccuPrime Pfx SuperMix (Invitrogen) and subcloned into the linearized vector

backbones using the In-Fusion HD Cloning Kit (Clontech), to generate pGL4.33-*luc2P/ISRE/EGFP* and pGL4.32-*luc2P/NF- κ B-RE/EGFP*.

pCL20c MSCV-GFP-T2A is a modified version of the lentiviral transfer vector pCL20c MSCV-GFP [209]. Briefly, a self-cleavage T2A peptide sequence plus additional restriction sites were added in-frame to the 3' end of the GFP cDNA from pCL20c MSCV-GFP. This was accomplished by PCR amplification of pCL20c MSCV-GFP using AccuPrime Pfx SuperMix (Invitrogen) with forward primer 5'-CTA GGC GCC GGA ATT ACC GGT GGC CGG CCG CGG GCC ACC ATG GTG AGC AAG GGC GAG GAG-3' and reverse primer 5'-GGC ATC GAT GCG GCC GCA TGC TCA CCT GCA GGG GCC GGG GTT CTC CTC CAC GTC GCC GCA GGT CAG CAG GCT GCC CCG GCC CTC CTT GTA CAG CTC GTC CAT GCC GAG AGT GAT CC-3'. The PCR-amplified product was resolved by agarose gel electrophoresis, gel-purified (QIAquick Gel Extraction Kit, Qiagen), and ligated using the In-Fusion HD Cloning Kit (Clontech) into the EcoRI- and NotI- (New England Biolabs) digested and gel-purified vector backbone of pCL20c MSCV-GFP (digested and purified to remove the original GFP and multiple cloning site).

The lentiviral transfer vector pLenti-III-UbC/mCherry was generated by replacing the puromycin resistance cDNA in pLenti-III-UbC with mCherry cDNA from pLenti-PGK-mCherry (both from Applied Biological Materials). The mCherry cDNA was PCR-amplified with primers that appended 15bp that are homologous with the pLenti vector. pLenti-III-UbC/Puro was linearized by restriction digest with BsiWI. Homologous recombination of the linearized vector and mCherry cDNA was performed by mixing the vector, cDNA and Cold Fusion Cloning Kit master mix (System Biosciences) as per manufacturer's protocol.

Human *IFIH1* sequence-verified cDNA was purchased from Open Biosystems (Clone ID: 40008600) and subcloned into pcDNA3.1 (Invitrogen), pCL20 MSCV GFP T2A (immediately 3' to T2A sequence), and pLenti-III-UbC/mCherry (under the ubiquitin C promoter) mammalian expression plasmids using the In-Fusion HD Cloning Kit (Clontech). Site-directed mutagenesis was used to generate constructs encoding the MDA5 mutants K365E, R337G, and R779H. In brief, wild-type MDA5-expressing plasmids were PCR-amplified using AccuPrime Pfx SuperMix (Invitrogen) and primers containing appropriate point mutations. Primers used were as follows: K365E forward primer 5'-GTT ATA GTT CTT GTC AAT GAG GTA CTG CTA G-3', and reverse primer 5'-GCT GTT CAA CTA GCA GTA CCT CAT TGA CAA G-3'; R337G forward primer 5'-TAC AGG GAG TGG AAA AAC CGG AGT GGC TGT TTA CA-3', and reverse primer 5'-GGC AAT GTA AAC AGC CAC TCC GGT TTT TCC ACT CC-3'; R779H forward primer 5'-GAA GTC ATT AGT AAA TTT CAC ACT GGA AAA ATA AA-3', and reverse primer 5'-GCA GAT TTA TTT TTC CAG TGT GAA ATT TAC TAA TG-3'. This was followed by Dpn1 digestion (New England Biolabs) and transformation into TOP10 competent cells (Invitrogen). Plasmid DNA was purified using the PureLink HiPure Filter Plasmid Kit (Invitrogen). The introduced mutations were confirmed by Sanger dideoxy sequencing.

Affinity Precipitations

Five hundred thousand 293T cells were seeded per well in tissue culture-treated 6 well plates (Corning). 12-16 hours later, cells were transfected with 4 µg of pCL20c MSCV GFP-T2A-WT MDA5, pCL20c MSCV GFP-T2A-K365E MDA5, or pmaxGFP (Lonza), complexed with Lipofectamine 2000 (Invitrogen) according to the manufacturer's recommendations. 48 hours later, cells were lysed in 0.05% Nonidet P-40 (Calbiochem), 20 mM HEPES, 1.5 mM magnesium chloride (both from Quality Biological), 150 mM

sodium chloride, 0.038% of β -mercaptoethanol (both from Sigma-Aldrich), and 1x cOmplete™ EDTA-free protease inhibitor cocktail (Roche). After incubating on ice for 20 minutes, cell lysates were mechanically disrupted by passing through a 25-gauge needle ten times. Lysates were centrifuged at 13,200 x g for 15 minutes at 4°C, before collecting supernatants. Proteins contained within the supernatants were quantified by BCA (Pierce). To 2 mg of protein, β , γ -methyleneadenosine 5'-triphosphate (ADPCP) (Sigma-Aldrich) was added to a final concentration of 2 mM before adding 1 μ g of biotin-labeled high molecular weight (HMW) polyinosinic:polycytidylic acid poly(I:C) (InvivoGen). After incubating at 37°C for 10 minutes, the mixture was added to M-270 hydrophilic streptavidin Dynabeads (Invitrogen) that had been pre-blocked for 20 minutes at 4°C with 600 μ g to 1 mg of lysate from pmaxGFP (Lonza) transfected control 293T cells. After incubation at 4°C for 3 minutes, the beads were washed 3X with lysis buffer containing 2 mM ADPCP. MDA5 protein was eluted by incubating at 95°C for 5 minutes in 2X SDS buffer protein gel loading solution (Quality Biological) supplemented with 0.3 M sodium chloride and 5% v/v 2-mercaptoethanol. Proteins were separated by SDS-PAGE and immunoblotting for MDA5 was performed as described above.

Luciferase Reporter Gene Assays

Fifty- to 100- thousand 293T cells were seeded per well in 24-well tissue culture plates. After culture for 18-24 hours to ~70-80% confluency, Lipofectamine 2000 (Invitrogen) was used for co-transfections of cells with pcDNA 3.1 mammalian expression plasmids expressing wild-type MDA5 and/or mutants (20 ng or 100 ng), a firefly luciferase reporter plasmid (200 ng) driven by human IFN- β promoter, and a constitutively expressed *Renilla* luciferase reporter plasmid (20 ng). For some experiments, firefly luciferase reporter plasmids driven by the interferon-stimulated response element (ISRE) or NF- κ B

response element were instead used. In dominant interference experiments, 20 ng pcDNA3.1 plasmid expressing wild-type MDA5, 100 ng pCL20 MSCV plasmid expressing GFP-T2A-K365E MDA5, and/or 100 ng pCL20 MSCV plasmid expressing GFP-T2A (empty vector) were transfected, along with luciferase reporter plasmids. Six hours later, cells were stimulated with a mixture of 1.2 µg high molecular weight poly(I:C) (InvivoGen) complexed with 1.5 µL Lipofectamine 2000 in 100 µL Opti-MEM® I reduced serum medium (Gibco), added to cells for an additional 18 to 24 hours before lysis. The Dual Luciferase Reporter assay (Promega) was used on a Fluostar Omega plate reader (BMG Labtech) to measure luciferase activities contained in cell lysates. Firefly luciferase activity was normalized to *Renilla* luciferase activity. Fold-increase in the normalized activity in MDA5-transfected cells is reported relative to normalized activity in untransfected cells.

HRV Stocks

Virus stocks were prepared from HRV-B14 seed stocks (a gift from Wai-Ming Lee) as previously described [210]. In brief, H1-HeLa cells were maintained in suspension at 37°C using an incubator shaker set at 230 rpm. Cells were cultured in MEM suspension medium with Earle's salts and no calcium (sMEM, Gibco, #11380-037), supplemented with 10% FBS (Hyclone), 1x MEM non-essential amino acids, 2 mM L-glutamine, 100 U/mL penicillin, 100 µg/mL streptomycin, and 0.1% Pluronic F-68 (rest from Gibco). Cells were incubated with high-titer HRV-B14 at a MOI of 15, in DPBS containing calcium and magnesium (Lonza) for 1 hour at room temperature. After adsorption, infected H1-HeLa cells were cultured in complete medium for 8 more hours at 35°C, with shaking at 120 rpm. Cell pellets were subjected to three freeze-thaw cycles in 10 mM HEPES pH 7.2 (Quality Biological), and 0.5% Nonidet P-40 (Calbiochem) added before

lysates were clarified by high-speed centrifugation. After incubating clarified lysates with 400 µg RNase A (Invitrogen) for 30 minutes at 35°C, 0.9% *N*-laurylsarcosine (Sigma-Aldrich) and 28.5 µM 2-mercaptoethanol (Sigma-Aldrich) were added. Virions were concentrated and partially purified by ultracentrifuging for 2 hours at 40,000 rpm, 16°C, over a 30% (w/v) sucrose cushion (Sigma-Aldrich) containing 16.7 mM Tris acetate pH 7.5 (Sigma-Aldrich) and 0.833 M sodium chloride (Quality Biological). The virus pellet was resuspended in DPBS containing calcium and magnesium, with 0.01 % bovine albumin fraction V (Sigma-Aldrich). Virus aliquots were stored at – 80°C until use.

HRV Plaque Assay □

Plaque assays quantitating infectious HRV were performed as previously described, with modifications [211]. In brief, HRV-B14 virus stock or cell supernatants were serially diluted in DPBS containing calcium, magnesium, and 0.1% bovine albumin fraction V (Sigma-Aldrich). 200 µL diluted samples were added in duplicate to confluent monolayers of H1-HeLa cells in 6-well plates. After virus adsorption for 1 hour at room temperature, the cells were overlaid with 0.8% Noble agar (Sigma-Aldrich) in 1x P6 medium (1x sMEM (Gibco), 26.2 mM sodium bicarbonate, 40.6 mM magnesium chloride hexahydrate, and 0.1% bovine albumin fraction V (rest from Sigma-Aldrich)). Nutritive medium was then overlaid to obtain final concentrations of 1x P6 medium, 2 mM L-glutamine (Gibco), 1.2 mM pyruvic acid (Sigma-Aldrich), 2 mM oxaloacetic acid (Sigma-Aldrich), and 0.1% glucose (Corning). After incubation at 35°C for 2 to 3 days, monolayers were fixed with 10% buffered formalin (Sigma-Aldrich) for 15 minutes at room temperature, overlaid agar removed, and plaques visualized by staining with 0.1% crystal violet (Sigma-Aldrich) in 20% ethanol for 1 hour. Plaques were counted and calculated as plaque forming units (PFU)/mL of original virus stock or cell supernatant.

HRV Infections

For in vitro infections, A549 cells, seeded at 100,000 per well in 12-well tissue culture plates one day prior, were transfected when ~50-70% confluent with Stealth siRNA to MDA5 (HSS127414), RIG-I (HSS119008), and non-silencing negative control (Cat# 12935300, all from ThermoFisher Scientific) at 40 nM in triplicate wells using siLentFect transfection reagent (Bio-Rad). For silencing of MAVS in parallel with controls, cells underwent a second round of Stealth siRNA (HSS127415) transfection 3 days after the first round. After transfection, cells were cultured for 48 to 72 more hours at 37°C prior to infection. HRV-B14 virus stock, diluted in DPBS containing calcium and magnesium (Lonza), and 0.1% bovine albumin fraction V (Sigma-Aldrich), was added at a MOI of 1. Virus was adsorbed for 1 hour at room temperature followed by 1 hour at 35°C. After washing 5 times with DPBS containing calcium and magnesium to remove unbound virus, infected cells were cultured in Ham's F-12K (Kaighn's) medium (Gibco), supplemented with 5% FBS (Hyclone), for 24 to 72 hours at 35°C. Cell supernatants were collected to measure virion release by plaque assay and total RNA isolated from cells to measure virus transcripts by qRT-PCR, as described below. In some experiments, A549 cells were transfected with a silencer siRNA to MDA5 (S34498) and Silencer® Select Negative Control (Cat# 4390843, ThermoFisher Scientific) before HRV infection.

In other experiments, nasal epithelial cells were digested from feeder cells and seeded in 12-well plates at 100,000 cells per well in 1 mL epithelial culture medium (Promocell, cat# C21060) with 10 µM Y-27632 (ApexBio) and incubated at 37°C 5% CO₂. The cells were seeded into plates that had been previously coated with 300 µl rat tail collagen (BD BioSciences, cat# 354236) at 30 µg/ml in PBS for 45 min at room temperature, washed

twice with PBS, and air dried for 20 minutes. The next day, the cells were washed once with DPBS and then infected with HRV-B14 at a MOI of 1 in DPBS with 0.25% bovine serum albumin (BSA, Sigma-Aldrich). Virus was adsorbed for 40 minutes at room temperature and then 90 minutes at 35°C. After washing 3 times with DPBS, the cells were cultured in epithelial culture medium with 10 µM Y-27632, for 48 or 72 hours at 35°C. Total RNA isolated from cells were used to measure virus transcripts by qRT-PCR, as described below.

Pan-HRV qRT-PCR:

After washing off non-adherent cells twice with PBS, total RNA was isolated using TRIzol extraction (Invitrogen). 2 µg total RNA was reverse transcribed using High-Capacity cDNA Reverse Transcription Kit with RNase Inhibitor (Applied Biosystems). Diluted cDNA was analyzed by quantitative real-time PCR using TaqMan Universal PCR Master Mix on a 7500 Real Time PCR System (Applied Biosystems), as previously described [212]. The forward primer D110 was 5'-CTA GCC TGC GTG G-3', reverse primer RVQ1 was 5'-AAA CAC GGA CAC CCA AAG TAG T-3', and probe RVQ2 was 5'-6FAM-TCC TCC GGC CCC TGA-MGB-NFQ-3'. Viral copy numbers were calculated based upon a standard curve generated from HRV-B14 virion RNA and were shown relative to siRNA negative control. For infection of nasal epithelial cells, viral copy numbers were shown relative to values from father's cells.

Lentivirus Particle Production

Specific lentiviral transfer vectors (all in pLenti-III-UbC/mCherry) were constructed as described above. VSV-G–pseudotyped lentivirus particles were generated by transient co-transfection into 293T cells of the specific transfer vector together with the packaging

plasmids pCMV delta R8.2 (HIV-1 GAG/POL, Tat, and Rev expressing plasmid, Addgene #12263) and pCMV VSV-G (VSV-G envelope expressing plasmid, Addgene #8454) [213] using calcium phosphate precipitation [214]. Briefly, 13 million 293T cells were seeded in poly-L-lysine (Sigma-Aldrich) coated Cell Culture Treated TripleFlasks (Nunc). When cells reached 95% confluency, 250 µg of specific transfer vector, 125 µg pCMV delta R8.2, and 42 µg of pCMV VSV-G were precipitated with calcium phosphate, mixed with 100 mL of complete IMDM, and added to the cells. DNA precipitates were washed out 12 hours after transfection and cell supernatants were collected daily for 3 days (stored at 4°C), filtered through 0.22 µm pore-size filter (GE), concentrated by centrifugation at 18,000 x g for 3 hours at 4°C, and resuspended in Opti-MEM I reduced serum media (Gibco). Lentivirus preparations were stored at -80°C until use.

All lentivirus preparations were titered on 293T cells to determine the concentration of infectious units. 100,000 293T cells were resuspended in complete IMDM containing 8 µg/mL polybrene (Sigma-Aldrich) and 10 µL of diluted lentivirus to a final volume of 1 mL. The suspension was added to a 24-well plate (Corning) and spin-infected at 1350 x g for 30 minutes at 35°C. 48 hours later, cell monolayers were washed twice with PBS, trypsinized (Gibco), transferred to 14 mL round bottom FACS tubes (Falcon), washed with PBS, and resuspended in PBS containing 0.5 µg/mL propidium iodide (Sigma-Aldrich). Single cell suspensions were analyzed on a BD FACSCanto II to determine the percentages of GFP⁺ cells among the propidium iodide low (live) populations. Lentivirus dilutions transducing between 2 and 15% of target cells were used to determine concentration of each preparation.

Wild-type *IFIH1* (Genbank accession BC111750), or K365E *IFIH1* cDNA were subcloned

under the human ubiquitin C promoter. VSV-G–pseudotyped lentivirus particles were generated by transient co-transfection into 293T cells of the specific transfer vector with the packaging plasmids pCMV delta R8.2 (HIV-1 GAG/POL, Tat, and Rev expressing plasmid) and pVSV-G (VSV-G envelope expressing plasmid).[213] Cell supernatants were collected daily for 3 days, filtered through 0.22 µm pore-size filter, concentrated by centrifugation at 18,000 x g for 3 hours at 4°C, resuspended in Opti-MEM® I reduced serum media (Gibco), and stored at -70°C until use.

Assessment of *in vitro* Antiviral Function of K365E MDA5

A549 cells, seeded at 50,000 per well in 24-well tissue culture plates 20 hours prior, were transduced with lentivirus stocks for 48 hours to similar transduction efficiencies. Briefly, the cell culture medium was replaced with lentivirus particles diluted in F-12K medium (Gibco) containing 8 µg/mL polybrene (Sigma-Aldrich) and spin-infected at 1350 x g for 30 minutes at 35°C. Transduced cells were infected with HRV-B14 at MOI of 1 for 72 hours, as described above. Transduction efficiencies were assessed by flow cytometry, after gating on dead negative (Zombie Aqua, BioLegend) transduced (mCherry⁺) cells. HRV-B14-infected cultures were washed with DPBS containing calcium and magnesium (Lonza), and pan-HRV qRT-PCR was performed as described above.

Flu Stocks

A/Victoria/361/2011 (H3N2), A/California/4/2009 (H1N1), and A/Puerto Rico/8/1934 (H1N1) were propagated in embryonated chicken eggs from virus stocks as previously described.[215] A/Netherlands/602/2009 was propagated in cell culture on MDCK cells

as previously described [215]. All virus stocks were titered by infectious plaque assay on Madin-Darby Canine Kidney (MDCK) cells (ATCC) as previously described [215].

Flu Replication

For infection of A549 cells, cells were seeded at 100,000 per well in 12-well tissue culture plates one day prior to transfecting when ~50-70% confluent with Stealth siRNA targeting MDA5 (HSS127414), RIG-I (HSS119008), MAVS (HSS127415), and non-silencing negative control (Cat# 12935300, all from ThermoFisher Scientific) at 40 nM in triplicate wells using siLentFect transfection reagent (Bio-Rad). After transfection, cells were cultured for 72 additional hours at 37°C prior to infection. Alternatively, primary nasal epithelial cells were digested from feeder cells and seeded in 24-well plates at 100,000 cells per well in 0.5 mL epithelial culture medium (Promocell, cat# C21060) with 10 µM Y-27632 (ApexBio) and incubated at 37°C in 5% CO₂. The cells were seeded on plates previously coated with 150 µl rat tail collagen (BD BioSciences, cat# 354236) at 30 µg/ml in PBS for 45 min at room temperature, washed twice with PBS, and air dried for 20 minutes. 36 hours later, the cells were washed twice with PBS before infection. Transfected A549 cells were infected with A/Victoria/361/2011 (H3N2) at MOI of 0.1 (diluted in PBS containing 0.3% BSA (Sigma-Aldrich) to a final volume of 300 µL/12-well) for 1 hour at room temperature, washed twice with PBS to remove unadsorbed virus, and the medium was replaced with F-12K supplemented with 0.1% BSA, 0.1% FBS (Hyclone), 2 mM glutamine, 55 µM 2-mercaptoethanol, and 1 µg/mL TPCK-trypsin (Sigma-Aldrich). Primary nasal epithelial cells were infected with A/Victoria/361/2011 (H3N2) at MOI: 0.02 (diluted in complete epithelial culture medium without Y-27632 to a final volume of 150 µL/24-well) for 1 hour at room temperature, washed twice with PBS

to remove unadsorbed virus, and medium was replaced with complete epithelial culture medium plus 1 µg/mL TPCK-trypsin (Sigma-Aldrich) and without Y-27632. Following infection, all cultures were returned to 37°C in 5% humidified CO₂.

SV40-transformed fibroblasts were seeded at 50,000 cells/well in 48 well tissue cultures plates in complete DMEM. 16-24 hours later, cells were infected with A/Netherlands/602/2009 (H1N1) or A/Puerto Rico/8/1934 (H1N1) at the indicated MOI for 60 minutes at 37°C in Hanks's Balanced Salt Solution with Calcium and Magnesium (HBSS) supplemented with 0.3% bovine serum albumin (BSA, Sigma-Aldrich). Cells were washed twice with PBS and cultured at 37°C in DMEM supplemented with 0.1% FBS (Hyclone) and 0.3% BSA, 2 mM glutamine (Gibco), and 55 µM 2-mercaptoethanol (Sigma-Aldrich) in the presence of 1 µg/mL TPCK-trypsin (Sigma-Aldrich). Cell supernatants were collected at indicated time points after infection and stored at -80°C. Once all samples were collected, supernatants were thawed and flu titers were determined by infectious plaque assay on MDCK cells as previously described.[215] Briefly, MDCK cells were plated in 12-well plates and grown to 100% confluency. Cells were washed twice with PBS, and serial dilutions of flu infection supernatants diluted in PBS were absorbed onto MDCK cells for 1 hour at room temperature. Cells were then overlaid with agar medium of MEM, 28 mM sodium bicarbonate, 2 mM L-glutamine, 100 U/mL penicillin, 100 µg/mL streptomycin (all from Gibco), 0.4% BSA, 1 µg/mL TPCK-trypsin (both from Sigma-Aldrich), and 1% Oxoid Agar (Thermo Scientific). After 36 to 60 hours, plaques were counted by direct visualization or by fixation and crystal violet counterstain as described above in HRV plaque assay, and then calculated as PFU/ml of flu infection supernatant.

qRT-PCR for Flu-induced Pro-inflammatory Cytokines

A549 cells in which MDA5, RIG-I, MAVS, or negative control were silenced by transfecting in siRNA were infected with flu strain A/Victoria/361/2011 (H3N2) as described above. Total RNA were isolated from Flu-infected A549 cells using TRIzol extraction (Invitrogen). 2 µg total RNA per sample was reverse transcribed using High-Capacity cDNA Reverse Transcription Kit with RNase Inhibitor (ABI). All quantitative RT-PCR were performed by the SYBR green method on a 7500 Real Time PCR System (ABI). Primer sequences are as follows: human TNF- α forward primer: 5'-CTG CTG CAC TTT GGA GTG AT-3'; human TNF- α reverse primer: 5'-AGA TGA TCT GAC TGC CTG GG -3'; human IL-1 α forward primer: 5'-ACT GCC CAA GAT GAA GAC CA-3'; human IL-1 α reverse primer: 5'-CCG TGA GTT TCC CAG AAG AA-3'; human IL-6 forward primer: 5'-AGT GAG GAA CAA GCC AGA GC-3'; human IL-6 reverse primer: 5'-GTC AGG GGT GGT TAT TGC AT-3'; human IL-8 forward primer: 5'-TCC TGA TTT CTG CAG CTC TGT-3'; human IL-8 reverse primer: 5'-AAA TTT GGG GTG GAA AGG TT-3'; human β -actin forward primer: 5'-GCA CAG AGC CTC GCC TT-3'; human β -actin reverse primer: 5'-GTT GTC GAC GAC GAG CG-3'. The expression of mRNA for pro-inflammatory cytokine genes of interest was normalized to the expression of β -actin and then normalized to the control groups at 8 hours post-infection.

Flu Induction of IFN- α ELISA and Cytotoxicity

SV40-transformed fibroblasts were infected with flu (A/Puerto Rico/8/1934 (H1N1)) at the indicated MOI for 60 minutes at 37°C in Hanks's Balanced Salt Solution with Calcium and Magnesium (HBSS) supplemented with 0.3% BSA. Cells were washed twice with PBS and cultured at 37°C in DMEM supplemented with 10% FBS. Cell supernatants were collected at the indicated time points after infection. Sendai Virus (SeV) infections were performed in parallel as positive controls, in which cells were infected with 5

hemagglutination units of SeV Cantell strain in DMEM supplemented with 10% FBS and left in the well until the time of collection. For quantitation of IFN- α , supernatants were diluted twofold and were assayed for Human IFN- β using the VeriKine Human Interferon Beta ELISA Kit (PBL Assay Science). For quantitation of flu-induced cytotoxicity, supernatants were diluted 2.5-fold and were assayed for LDH release using the Cytotoxicity Detection Kit Plus (Roche) to measure enzymatic activity. Colorimetric absorbance was measured according to kit manufacturers' recommendations, using a VICTOR X4 Multi-label Plate Reader (Perkin-Elmer).

RSV Infections

Recombinant wild-type RSV strain A2 in which enhanced GFP was inserted between the P and M genes was propagated, sucrose-purified, and titered by plaque assay on Vero cells as previously described [216]. The virus stock was sequenced and virus was recovered without any adventitious mutations as confirmed by Sanger dideoxy sequencing. A549 cells were seeded and transfected with siRNA to MDA5, RIG-I, MAVS, or a non-silencing negative control as described above for HRV infections. Alternatively, primary nasal epithelial cells were digested from feeder cells and seeded in 12-well plates at 150,000 cells per well in 1 mL epithelial culture medium (Promocell, cat# C21060) with 10 μ M Y-27632 (ApexBio) and incubated at 37°C in 5% CO₂. The cells were seeded on plates previously coated with 300 μ l rat tail collagen (BD BioSciences, cat# 354236) at 30 μ g/ml in PBS for 45 min at room temperature, washed twice with PBS, and air dried for 20 minutes. 36 hours later, the cells were washed once with PBS. Transfected A549 cells or primary nasal epithelial cells were infected with RSV-GFP at an MOI of 1 or 0.2, respectively (diluted in appropriate complete medium, 300 μ L per 12-well) for 1 hour at room temperature, washed twice with PBS to remove

unadsorbed virus, medium was replaced (complete F-12K for A549; epithelial culture media without Y-27632 for nasal epithelial cells), and cultures returned to 37°C in 5% humidified CO₂.

RSV-GFP qRT-PCR

At 6, 24, or 48 hours at RSV-GFP infection, infected cell cultures were washed twice with PBS to remove non-adherent cells, total RNA was isolated using TRIzol extraction (Invitrogen) according to manufacturer's instructions. 0.5 to 2.0 µg total RNA was reverse transcribed using High-Capacity cDNA Reverse Transcription Kit with RNase Inhibitor (Applied Biosystems). Diluted cDNA (1:5 to 1:10 in H₂O) was analyzed for RSV N gene transcripts by quantitative real-time PCR using TaqMan Universal PCR Master Mix on a 7500 Real Time PCR System (Applied Biosystems) per manufacturer's instructions. The N gene forward primer sequence was 5'-TGG CAT GTT ATT AAT CAC AGA AGA TGC T -3', N gene reverse primer sequence was 5'-TTC TCT TCC TAA CCT AGA CAT CGC ATA -3', and the N gene probe sequence was 5'-6FAM-AAC CCA GTG AAT TTA TG -MGB-NFQ-3'. Viral copy numbers were calculated based upon a standard curve generated from RSV-GFP virion RNA and were shown relative to the RSV transcript levels in the father's cells.

RSV-GFP Flow Cytometry

At 24 and 48 hours after RSV-GFP infection, whole well contents were collected for flow cytometric analysis. First, cell supernatants followed by sequential PBS washes were collected in 5 mL FACS tubes (Falcon). Next, single-cell suspensions were collected after treating with 0.25% trypsin/EDTA (Gibco) for 10 minutes and combining with cell supernatants and washes. Contents were washed 1 time with PBS and stained with

LIVE/DEAD Fixable Near-IR Dead Cell Stain (Molecular Probes) or Zombie NIR Fixable Viability Kit (Biolegend) for 20 minutes at room temperature, fixed in BD Cytotfix/Cytoperm solution (BD Biosciences) or 1% paraformaldehyde (Electron Microscopy Sciences) in PBS for 20 minutes, washed and resuspended in PBS containing 1% FCS or 1% BSA and 0.09% sodium azide. The stained and fixed cells were acquired on a BD FACS Canto II or BD LSR II flow cytometers without compensation controls given the negligible spectral overlap between fluorophores. FlowJo 9.8.3 or 10.0.8 (TreeStar) software used to enumerate singlet live cells expressing GFP. The values of % GFP⁺ cells treated with siRNA to MDA5 are shown relative to the values for negative control siRNA.

RNA-Seq

A549 cells that had been transfected 48 hours earlier with siRNA to MDA5 or non-specific negative control siRNA, were uninfected or infected for 6, 12, 24, and 48 hours with HRV-B14 or RSV, as described above. For each time point, infections were performed in triplicate. Total cellular RNA were isolated using RNeasy Mini Kit (Qiagen). Multiplexed RNA libraries were prepared using the Truseq RNA sample prep kit (Illumina). Briefly, poly(A)-containing mRNA were captured with oligodT beads, fragmented, reverse-transcribed, and the cDNA ligated to Illumina adapters containing indexing barcodes. Libraries were quantified using KAPA Library Quant Kits (KAPA Biosystems), before running on a HiSeq 2000 Sequencing System (Illumina) to produce 50 bp single end reads. Sequencing reads were aligned with ELAND to the human reference genome version hg19. Count data of the annotated transcripts from individual samples were normalized for sequence depth. Analyses of differentially expressed genes were performed using the Statistical R package DESeq

(<http://bioconductor.org/packages/2.12/bioc/html/DESeq.html>). Sequencing reads were also aligned with Bowtie2 to the HRV-B14 or RSV reference genomes to count the read number corresponding to the virus transcripts. The RNA-seq coverage across the virus transcripts were checked for normal distribution and count data of the virus transcripts were also normalized for overall sequence depth. Fold changes were calculated by comparing the RPKM expression values (Reads Per Kilobase per Million mapped reads) under siNeg vs. siMDA5 conditions. Logarithm₂-transformed expression fold changes were analyzed for distribution (box-and-whisker diagrams) and hierarchical clustering (heat map of expression values) using R. “Response to type I interferon” genes were selected based on the GO term definition (GO term GO0034340). The comparisons for the fold change distributions of different gene sets were performed using two sample Kolmogorov-Smirnov tests (KS tests). RNA-seq data will be deposited into the Gene Expression Omnibus (GEO) repository under accession number X.

Statistical Analyses

One-way ANOVA with Dunnett’s multiple comparisons, Kruskal-Wallis test with Dunn’s multiple comparisons, and Mann-Whitney U testing were performed using Prism software (GraphPad). Two sample Kolmogorov-Smirnov testing were performed using the Statistical R package.

3.9 Contributions

Yu Zhang, Joshua J. McElwee, and Jason D. Hughes analyzed WES, and Yu Zhang and Joshua J. McElwee discovered the *IFIH1* mutation. Ian T. Lamborn and Heardley M. Murdock assessed MDA5 expression, Evan Masutani performed molecular modeling, and Heardley M. Murdock performed immunoprecipitations. Huie Jing, Ian T. Lamborn,

and Sangeeta Bade performed luciferase reporter assays. Huie Jing and Ian T. Lamborn performed HRV experiments. Shirin Munir developed methods for A549 siRNA transfections. Ian T. Lamborn, Shirin Munir, and Linda G. Brock performed RSV experiments. Ian T. Lamborn, Scott B. Drutman, Michael J. Ciancanelli, Celia P. Santos, and Huie Jing performed flu experiments. Yu Zhang evaluated transcriptomes and performed rhinovirus molecular typing for phylogenetic analysis. Heardley M. Murdock, Sangeeta Bade, and Emmanuel Y. Fordjour assisted with immunoblotting. Ian T. Lamborn, Huie Jing, and Michael J. Ciancanelli generated CRISPR fibroblast lines, and Dave P. Nichols generated nasal epithelial cell lines. Jordan K. Abbott and Erwin W. Gelfand cared for the patient, and collected and analyzed clinical data with assistance from Helen C. Su and Corinne S. Happel. Helen F. Matthews coordinated clinical study protocol and sample collection. Helen C. Su planned and supervised the experimental work and data analyses. Jean-Laurent Casanova, Michael J. Ciancanelli, Kanta Subbarao, and Peter L. Collins provided advice and assisted in supervising experimental work. Helen C. Su and Ian T. Lamborn prepared the manuscript. All authors discussed and revised the manuscript.

CHAPTER 4 – Discussion and Future Experiments

The field of primary immunodeficiency research has matured and evolved immensely since its infancy in the 1960s.[2, 5] From the first molecular diagnosis of a PID in ADA deficiency in 1972, there are now over 300 different causal genes implicated in the pathogenesis of primary immunodeficiencies, and that number is growing faster than ever.[4, 15, 16] Here we implicate two additional genes in the pathogenesis of two previously unidentified immunodeficiencies.

4.1 Dominant-activating mutations in $G\alpha i2$ cause MAGIS Syndrome - Discussion and Future experiments

In **Chapter 2** we present the identification of *de novo* mutations in *GNAI2*, the gene encoding the heterotrimeric G protein $G\alpha i2$, in two individuals who presented with life-threatening multi-system autoimmunity and immunodeficiency to mucocutaneous bacterial and viral infections. Notably these patients presented with elevated circulating neutrophils and monocytes, likely attributable to impaired chemokine mediated leukocyte extravasation resulting in an accumulation of these cells in the blood. We termed this disease 'MAGIS syndrome' (Myelocytosis, Autoimmunity, G $\alpha i2$ gain-of-function Immunodeficiency and Short stature).

Both patients exhibited apparently *de novo* mutations of the same amino acid (threonine 182) in $G\alpha i2$. Mutational studies of $G\alpha$ subunits have identified a number of missense mutations that result in differing degrees and types of activation.[135, 217, 218] It will be interesting to see if future sequencing efforts in healthy and diseased individuals uncover *de novo* or inherited less-activating mutations such as G184S $G\alpha i2$ or more activating mutations such as R179C/H or Q205L $G\alpha i2$ and how presentation

among these individuals compares to the patients described here. Although we will not be able to tell until the an accurate incidence of this syndrome can be ascertained and compared to estimates of the spontaneous mutation rate for this genomic region in humans, there is mounting evidence of *in utero* selection against activating mutations in Gαi2. First, a G184S Gαi2 knock-in mouse has been shown to breed heterozygous and homozygous mutant pups at rates significantly below the expected Mendelian frequencies.[108] Additionally, our own efforts to generate knock-in mice bearing the T182I Gαi2 allele are suggestive of significant embryonic lethality (**Chapter 2, Supplementary Table 2.3**) in heterozygous animals. If, in time, it is determined that *in utero* selection against activating *de novo* mutations of Gαi2 occurs in humans, it will be important to see if co-inherited variations promote the survival patients who are born as these may shed light on potential targets for therapeutic intervention.

The clinical presentation of these patients and the deleterious effects of their mutations on leukocyte chemotaxis strongly argue that MAGIS syndrome is, at least in part, a disease of leukocyte migration. Interestingly MAGIS syndrome, along with WHIM syndrome, which is due to dominant-activating mutations in the chemokine GPCR CXCR4, are the only two currently identified defects of leukocyte migration due to mutations in a GPCR or their associated G-proteins, the foundation of chemokine signaling.[219] With the upward trajectory sequencing efforts and advances in medical care for immunodeficient patients, individuals with mutations other chemokine receptors or heterotrimeric G-proteins will likely be identified.

Our findings indicate a partial defect in chemotaxis, but it is clinically significant. It mimics aspects of other defects of chemotaxis (i.e. accumulation of circulating white blood cells, deficient antibody production, chronic viral skin infections, recurrent

sinopulmonary infections, etc.); however, as demonstrated by our *in vivo* assessment of leukocytes into the skin and oral cavity as well as the clinical findings of lymphocytic infiltration into the brain of P2, not so severe that leukocytes cannot enter solid tissues entirely.[109, 116] Chemokine receptors rely on G α i2 to differing degrees in a cell-type specific manner.[220, 221] It will be interesting to dissect which chemokine receptor signaling pathways are affected in which cells types in MAGIS syndrome, and see how that break down influences disease pathogenesis.

The complete etiology of the life-threatening autoimmune phenotype in these individuals is still largely unknown. Other defects of chemotaxis often present with autoimmune cytopenias, autoimmune arthritis, vasculitis, and more, the etiology of which is poorly understood and most often attributed to generalized immune dysregulation as a result of impaired immune cell localization/interaction in lymphoid tissues or to sites of inflammation.[110, 222, 223]. While our studies cannot rule out that similar processes are contributing to autoimmunity in MAGIS syndrome, the TCR hyper-responsiveness seen in MAGIS syndrome T cells provides an additional possibility. A fundamental determinant for the appropriate initiation of the immune response is the requirement for two signals for T cell activation: the TCR signal and costimulation.[224, 225] The diminished requirement for T cell costimulation by MAGIS syndrome T cells *in vitro* represents an impairment of this fundamental protective mechanism, and a phenotype important to consider in further studies of the autoimmune etiology of MAGIS syndrome.

Exactly how increased G α i2 activity (on effectors) or decreased G α i2 activity (in response to chemokine receptor/GPCR signaling) effects T cell activation will necessitate further study. The interaction between GPCR signaling and receptor tyrosine kinase (RTK) or non-receptor tyrosine kinase signaling (nRTK) signaling has

long been observed, but precise mechanisms have remained obscure.[226-228] I have demonstrated augmented TCR-mediated Ca^{2+} fluxes in patient cells and that stable expression of patient derived $G\alpha i2$ in normal cells is sufficient to recapitulate this alteration in TCR signaling. Notably, the changes in TCR mediate Ca^{2+} flux in healthy control cells occurred after prolonged expression (>21 days). This suggests the mutant proteins' effects are not simply a result of the acute presence of mutant protein within the cell, but a result of cellular changes due to the presence of the mutant protein over multiple cellular divisions. Transcriptional and proteomic analysis of cells acutely expressing GOF $G\alpha i2$ versus cells after prolonged expression will be important for understanding how GOF $G\alpha i2$ is altering these cells over time.

One example of the cross-talk between GPCR signaling and RTK signaling, is the affect of either $G\alpha i2$ deficiency or expression of constitutively activated Q205L $G\alpha i2$ on insulin receptor sensitivity and glucose uptake in mice.[55, 56] An important role for glucose receptor upregulation and glucose uptake in T cells occurs as a consequence of T cell costimulation whereby the cells shift their metabolism from fatty acid oxidation to glycolytic metabolism, a process necessary for sustaining rapid cell growth and proliferation.[152, 229] Additionally we have observed increased phosphorylation of ribosomal protein S6 in cell expressing activated $G\alpha i2$, a known consequence of increased glycolysis and anabolic metabolism from other studies.[148] Studying the expression and responsiveness of glucose receptors in T cells from MAGIS syndrome patients will be an important initial step understanding the T cell hyper-responsive phenotype seen in these patients, and may provide insight into the costimulatory effect of GOF $G\alpha i2$ on T cell activation.

The Signal transducer and activator of transcript (STAT) family proteins are members of the Janus kinase (JAK)-STAT signaling pathway, a nRTK (non-receptor tyrosine kinase) signaling family heavily utilized by cytokine receptors. Once activated, STAT family members initiate a transcriptional program that is essential for T cell activation, differentiation, and effector function in addition to many other processes.[230] Patients with dominant interfering STAT3 mutations fail to generate T helper 17 (Th17) cells properly and suffer from chronic mucocutaneous candidiasis, recurrent staphylococcus skin infections, hyper IgE secretion, and bone and connective tissue abnormalities.[231-233] Patients with germline GOF STAT3 mutations develop life-threatening autoimmunity while identical somatic mutations are potent oncogenes promoting dysregulation of the cell cycle.[141, 234, 235] Interestingly, STAT3 activity can be initiated and augmented by G α i/o family members or their associated G β γ dimers.[236] Although G α i2 is not yet a known driver of STAT3 signaling, the G β γ dimers they regulate are.[237] Furthermore, identifying effectors of GPCR pathways is very cell type dependent due to the cross utilization of G α subunits and variety of combinations of G β γ dimers by GPCRs.[46] If the activating G α i2 mutations observed in MAGIS syndrome are driving STAT3 activity, this could tie the autoimmunity of MAGIS syndrome to the life-threatening autoimmunity of patient's with germline GOF STAT3 mutations. Additionally, P1 exhibited greatly increased Th17 cells and an elevated proportion of IL-17 producing CD8⁺ T cells, a consequence predicted from the known function of STAT3 and frequently observed in the GOF STAT3 patients.[141, 231] It will be important to explore the effects of MAGIS syndrome-derived G α i2 mutations on STAT3 activity in future studies to understand the autoimmune phenotype seen in this disease.

4.2 Human MDA5 Deficiency - Discussion and Future

experiments

In **Chapter 3** we present the identification of homozygous missense mutations in *MDA5*, the gene encoding a cytosolic pattern recognition receptor of dsRNA, in an individual presenting with life-threatening respiratory infections with RNA viruses. Although this patient inherited identical rare mutations from each parent, WES showed her rate of homozygosity was higher than average but still within the normal range, suggesting this inheritance was likely the result of a founder effect on a small and genetically isolated people group in Southeast Asia from which she originates.

As the genetic etiologies of more primary immunodeficiencies are discovered a few patterns have emerged. One pattern is that it appears many essential genes and gene pathways of the immune system have been retained through genetic selection and evolved to resist a narrow range of pathogens encountered in the natural environment.[5] A prominent example is the exploration of Mendelian susceptibility to mycobacterial disease (MSMD), which has uncovered dozens of genetic mutations in the sensing, production, or response to interferon gamma (IFN γ). These patients consistently present with life-threatening susceptibility to weakly virulent mycobacterial species or occasionally other intramacrophagic infections.[238] These studies demonstrated that the major function of IL-12 (the predominant cytokine generating IFN γ producing T helper type 1 or Th1 cells), IFN γ production, and IFN γ function in humans is to confer protection to mycobacterial infection.[239] Similar efforts examining the genetic etiologies of chronic mucocutaneous candidiasis (CMC) and more recently of Epstein-Barr virus (EBV) viremia have corroborated the idea that major pathways of the

immune system have been selected and retained within the human immune system due to constant pathogenic pressure from common microbes and the protection they confer to them.[240, 241]

The observations from efforts to understand the genetic basis of MSMD were surprising because mice carrying mutations in MSMD-associated genes (and thus deficient in Th1 mediated immunity), exhibited susceptibility to a much larger spectrum of pathogens including intracellular bacteria and viruses.[239] We now recognize that many relevant animal models display much broader susceptibilities than the human diseases they model.[5, 8] Before patients deficient in Toll-like receptor 3 (TLR3), a transmembrane sensor of dsRNA, were identified, TLR3 knockout mice exhibited lethal susceptibility to 8 of 16 viruses tested in the laboratory.[242] However, humans deficient in TLR3 display highly specific susceptibility to Herpes simplex encephalitis (HSE) due to Herpes simplex virus 1 (HSV1) and many are known to live completely healthy lives.[243, 244] This discrepancy between animal models and patients is likely due to the myriad of differences between laboratory infections in specific pathogen free environments and human infections *in natura*, not to mention the added complexity of outbred human genetics.

As it pertains to this current study, MDA5 knockout mice or MDA5 deficient cells exhibit susceptibility to a host of RNA viruses in the laboratory setting including coronaviruses, calciviruses, flaviviruses, picornaviruses, orthoreoviruses, paramyxoviruses, orthomyxoviruses, and more. [76, 79-89] The patient we have identified with loss of function mutations in MDA5 has a history of recurrent viral infections including a picornavirus (i.e. rhinovirus), coronaviruses, orthomyxoviruses (i.e. influenza A and B), and paramyxoviruses (i.e. respiratory syncytial virus , human

parainfluenza virus 4). This was somewhat surprising because many of these viruses such as influenza A (IAV) and B (IAB), respiratory syncytial virus (RSV), human parainfluenza virus 4 (HPIV4) are thought to be sensed and controlled through RIG-I mediated recognition with MDA5 being more critical and specific for picornavirus and coronavirus family members. Although in one sense the patient's range of infection was not broader than prior animal studies and *in vitro* experiments might have indicated, it was more inclusive than one might have predicted based on patient presentations from other PRR pathways such as TLR3, MyD88, IRAK4, etc. [243-247]

I investigated the possibility that MDA5 played an unappreciated role in the recognition and/or control of IAV and RSV, two sources of significant medical burden.[248] We did so using WT viruses and the primary targets of these viruses, human respiratory epithelium. Consistent with the observation that defects in specific pathways of immunity predispose affected individuals to a narrow range of infection, I did not find that MDA5 deficiency resulted in a susceptibility to IAV or RSV. I did however find that MDA5 deficiency significantly impaired restriction of human rhinovirus (HRV) infection.

Exactly why the patient's presentation includes such a broad range of severe respiratory infections remains to be answered. One possibility is that chronic/prolonged infection with HRV predisposed the patient to the other infections endured by the patient. Because HRV, also known as the 'common cold,' is generally cleared quickly, the effects of prolonged infectious episodes on the human respiratory system are not well understood. [165, 166] Early in life the patient did exhibit lung pathology consistent with bronchiectasis, a condition known to increase susceptibility to respiratory tract infections.[249] Another possibility is that MDA5 is critical for protection against

paramyxoviruses and orthomyxoviruses in humans *in vivo* in coordinating a dynamic immune response involving multiple cell types. Restriction and clearance of respiratory infections involves intrinsic cellular immunity (modeled in *in vitro* infections of respiratory epithelium), but also coordinated responses from the leukocytes of the innate immune system as well as the adaptive immune system.[250] Signaling through MDA5 initiates transcription of the chemokines that promote leukocyte infiltration as well as proinflammatory cytokines that activate antigen presenting cells for antigen presentation.[251] Additionally MDA5 is expressed in T cells and B cells and recent studies have demonstrated an essential role for RLRs in generating T cell independent antibody responses.[252] Although T independent antibodies are not known to be critical for clearance and protection from RNA viruses, it is an indication that PRR like MDA5 are likely to have additional functions beyond the traditional roles in innate immunity.

BIBLIOGRAPHY

1. Murphy, K., et al., *Janeway's immunobiology*. 2012, New York: Garland Science.
2. Bruton, O.C., *Agammaglobulinemia*. *Pediatrics*, 1952. **9**(6): p. 722-8.
3. Ochs, H.D. and W.H. Hitzig, *History of primary immunodeficiency diseases*. *Curr Opin Allergy Clin Immunol*, 2012. **12**(6): p. 577-87.
4. Picard, C., et al., *Primary Immunodeficiency Diseases: an Update on the Classification from the International Union of Immunological Societies Expert Committee for Primary Immunodeficiency 2015*. *J Clin Immunol*, 2015. **35**(8): p. 696-726.
5. Casanova, J.L. and L. Abel, *Primary immunodeficiencies: a field in its infancy*. *Science*, 2007. **317**(5838): p. 617-9.
6. Casanova, J.L., *Severe infectious diseases of childhood as monogenic inborn errors of immunity*. *Proc Natl Acad Sci U S A*, 2015. **112**(51): p. E7128-37.
7. Casanova, J.L., *Human genetic basis of interindividual variability in the course of infection*. *Proc Natl Acad Sci U S A*, 2015. **112**(51): p. E7118-27.
8. Casanova, J.L. and L. Abel, *The human model: a genetic dissection of immunity to infection in natural conditions*. *Nat Rev Immunol*, 2004. **4**(1): p. 55-66.
9. Bennett, C.L., et al., *The immune dysregulation, polyendocrinopathy, enteropathy, X-linked syndrome (IPEX) is caused by mutations of FOXP3*. *Nat Genet*, 2001. **27**(1): p. 20-1.
10. Finnish-German, A.C., *An autoimmune disease, APECED, caused by mutations in a novel gene featuring two PHD-type zinc-finger domains*. *Nat Genet*, 1997. **17**(4): p. 399-403.
11. Conley, M.E., et al., *Defects in early B-cell development: comparing the consequences of abnormalities in pre-BCR signaling in the human and the mouse*. *Immunol Rev*, 2000. **178**: p. 75-90.
12. Ochs, H.D., Smith C.I.E., Puck, J., ed. *Primary Immunodeficiency Diseases: A Molecular and Genetic Approach*. 3rd ed. 2013, Oxford University Press.
13. Schuetz, C., et al., *Autoimmunity, autoinflammation and lymphoma in combined immunodeficiency (CID)*. *Autoimmun Rev*, 2010. **9**(7): p. 477-82.
14. Roifman, C.M., et al., *Defining combined immunodeficiency*. *J Allergy Clin Immunol*, 2012. **130**(1): p. 177-83.
15. Giblett, E.R., et al., *Adenosine-deaminase deficiency in two patients with severely impaired cellular immunity*. *Lancet*, 1972. **2**(7786): p. 1067-9.
16. *Enzyme defects in immunodeficiency*. *Lancet*, 1972. **2**(7786): p. 1075.
17. Puel, A., et al., *Defective IL7R expression in T(-)B(+)NK(+) severe combined immunodeficiency*. *Nat Genet*, 1998. **20**(4): p. 394-7.
18. Noguchi, M., et al., *Interleukin-2 receptor gamma chain mutation results in X-linked severe combined immunodeficiency in humans*. *Cell*, 1993. **73**(1): p. 147-57.
19. van der Burg, M., et al., *A DNA-PKcs mutation in a radiosensitive T-B- SCID patient inhibits Artemis activation and nonhomologous end-joining*. *J Clin Invest*, 2009. **119**(1): p. 91-8.
20. Arpaia, E., et al., *Defective T cell receptor signaling and CD8+ thymic selection in humans lacking zap-70 kinase*. *Cell*, 1994. **76**(5): p. 947-58.
21. Goldman, F.D., et al., *Defective expression of p56lck in an infant with severe combined immunodeficiency*. *J Clin Invest*, 1998. **102**(2): p. 421-9.

22. Zhang, Q., et al., *Combined immunodeficiency associated with DOCK8 mutations*. N Engl J Med, 2009. **361**(21): p. 2046-55.
23. Geha, R.S., et al., *Primary immunodeficiency diseases: an update from the International Union of Immunological Societies Primary Immunodeficiency Diseases Classification Committee*. J Allergy Clin Immunol, 2007. **120**(4): p. 776-94.
24. International Union of Immunological Societies Expert Committee on Primary, I., et al., *Primary immunodeficiencies: 2009 update*. J Allergy Clin Immunol, 2009. **124**(6): p. 1161-78.
25. MacArthur, D.G., et al., *Guidelines for investigating causality of sequence variants in human disease*. Nature, 2014. **508**(7497): p. 469-76.
26. Conley, M.E. and J.L. Casanova, *Discovery of single-gene inborn errors of immunity by next generation sequencing*. Curr Opin Immunol, 2014. **30**: p. 17-23.
27. Casanova, J.L., et al., *Guidelines for genetic studies in single patients: lessons from primary immunodeficiencies*. J Exp Med, 2014. **211**(11): p. 2137-49.
28. Pennisi, E., *Breakthrough of the year. Human genetic variation*. Science, 2007. **318**(5858): p. 1842-3.
29. Dal, G.M., et al., *Early postzygotic mutations contribute to de novo variation in a healthy monozygotic twin pair*. J Med Genet, 2014. **51**(7): p. 455-9.
30. Francioli, L.C., et al., *Genome-wide patterns and properties of de novo mutations in humans*. Nat Genet, 2015. **47**(7): p. 822-6.
31. Lupski, J.R., *Genetics. Genome mosaicism--one human, multiple genomes*. Science, 2013. **341**(6144): p. 358-9.
32. Butcher, R.W., et al., *The role of cyclic AMP in hormone actions*. Adv Enzyme Regul, 1968. **6**: p. 357-89.
33. Sutherland, E.W. and T.W. Rall, *Formation of adenosine-3,5-phosphate (cyclic adenylate) and its relation to the action of several neurohormones or hormones*. Acta Endocrinol Suppl (Copenh), 1960. **34**(Suppl 50): p. 171-4.
34. Sutherland, E.W., Jr., *Earl W. Sutherland, Jr. - Nobel Lecture: Studies on the Mechanism of Hormone Action*. 1971.
35. Milligan, G. and E. Kostenis, *Heterotrimeric G-proteins: a short history*. Br J Pharmacol, 2006. **147** Suppl 1: p. S46-55.
36. Gill, D.M. and R. Meren, *ADP-ribosylation of membrane proteins catalyzed by cholera toxin: basis of the activation of adenylate cyclase*. Proc Natl Acad Sci U S A, 1978. **75**(7): p. 3050-4.
37. Coffino, P., H.R. Bourne, and G.M. Tomkins, *Somatic genetic analysis of cyclic AMP action: selection of unresponsive mutants*. J Cell Physiol, 1975. **85**(3): p. 603-10.
38. Bourne, H.R., P. Coffino, and G.M. Tomkins, *Somatic genetic analysis of cyclic AMP action: characterization of unresponsive mutants*. J Cell Physiol, 1975. **85**(3): p. 611-20.
39. de Mendoza, A., A. Sebe-Pedros, and I. Ruiz-Trillo, *The evolution of the GPCR signaling system in eukaryotes: modularity, conservation, and the transition to metazoan multicellularity*. Genome Biol Evol, 2014. **6**(3): p. 606-19.
40. Mattoo, S. and J.D. Cherry, *Molecular pathogenesis, epidemiology, and clinical manifestations of respiratory infections due to Bordetella pertussis and other Bordetella subspecies*. Clin Microbiol Rev, 2005. **18**(2): p. 326-82.
41. Bharati, K. and N.K. Ganguly, *Cholera toxin: a paradigm of a multifunctional protein*. Indian J Med Res, 2011. **133**: p. 179-87.

42. Higashijima, T., et al., *Mastoparan, a peptide toxin from wasp venom, mimics receptors by activating GTP-binding regulatory proteins (G proteins)*. J Biol Chem, 1988. **263**(14): p. 6491-4.
43. Lee, S.H., J.H. Baek, and K.A. Yoon, *Differential Properties of Venom Peptides and Proteins in Solitary vs. Social Hunting Wasps*. Toxins (Basel), 2016. **8**(2): p. 32.
44. Kimple, A.J., et al., *Regulators of G-protein signaling and their Galpha substrates: promises and challenges in their use as drug discovery targets*. Pharmacol Rev, 2011. **63**(3): p. 728-49.
45. Oldham, W.M. and H.E. Hamm, *Structural basis of function in heterotrimeric G proteins*. Q Rev Biophys, 2006. **39**(2): p. 117-66.
46. Oldham, W.M. and H.E. Hamm, *Heterotrimeric G protein activation by G-protein-coupled receptors*. Nat Rev Mol Cell Biol, 2008. **9**(1): p. 60-71.
47. Offermanns, S. and M.I. Simon, *Genetic analysis of mammalian G-protein signalling*. Oncogene, 1998. **17**(11 Reviews): p. 1375-81.
48. Beals, C.R., C.B. Wilson, and R.M. Perlmutter, *A small multigene family encodes Gi signal-transduction proteins*. Proc Natl Acad Sci U S A, 1987. **84**(22): p. 7886-90.
49. Kim, S.Y., et al., *Identification of cDNA encoding an additional alpha subunit of a human GTP-binding protein: expression of three alpha i subtypes in human tissues and cell lines*. Proc Natl Acad Sci U S A, 1988. **85**(12): p. 4153-7.
50. Kuwano, Y., et al., *Galphai2 and Galphai3 Differentially Regulate Arrest from Flow and Chemotaxis in Mouse Neutrophils*. J Immunol, 2016. **196**(9): p. 3828-33.
51. Zarbock, A., et al., *Galphai2 is required for chemokine-induced neutrophil arrest*. Blood, 2007. **110**(10): p. 3773-9.
52. Pero, R.S., et al., *Galphai2-mediated signaling events in the endothelium are involved in controlling leukocyte extravasation*. Proc Natl Acad Sci U S A, 2007. **104**(11): p. 4371-6.
53. Dalwadi, H., et al., *B cell developmental requirement for the G alpha i2 gene*. J Immunol, 2003. **170**(4): p. 1707-15.
54. Rudolph, U., et al., *Ulcerative colitis and adenocarcinoma of the colon in G alpha i2-deficient mice*. Nat Genet, 1995. **10**(2): p. 143-50.
55. Chen, J.F., et al., *Conditional, tissue-specific expression of Q205L G alpha i2 in vivo mimics insulin action*. J Mol Med (Berl), 1997. **75**(4): p. 283-9.
56. Moxham, C.M. and C.C. Malbon, *Insulin action impaired by deficiency of the G-protein subunit G ialpha2*. Nature, 1996. **379**(6568): p. 840-4.
57. Zuberi, Z., et al., *Absence of the inhibitory G-protein Galphai2 predisposes to ventricular cardiac arrhythmia*. Circ Arrhythm Electrophysiol, 2010. **3**(4): p. 391-400.
58. Beutler, B., *Innate immunity: an overview*. Mol Immunol, 2004. **40**(12): p. 845-59.
59. Medzhitov, R., *Pattern recognition theory and the launch of modern innate immunity*. J Immunol, 2013. **191**(9): p. 4473-4.
60. Westphal, O., et al., *Bacterial lipopolysaccharide and its lipid A component: some historical and some current aspects*. Biochem Soc Trans, 1981. **9**(3): p. 191-5.
61. Nikaido, H., *Studies on the biosynthesis of cell wall polysaccharide in mutant strains of Salmonella. II*. Proc Natl Acad Sci U S A, 1962. **48**: p. 1542-8.
62. Osborn, M.J., *Studies on the Gram-Negative Cell Wall. I. Evidence for the Role of 2-Keto-3-Deoxyoctonate in the Lipopolysaccharide of Salmonella Typhimurium*. Proc Natl Acad Sci U S A, 1963. **50**: p. 499-506.

63. Nikaido, H., Y. Naide, and P.H. Makela, *Biosynthesis of O-antigenic polysaccharides in Salmonella*. Ann N Y Acad Sci, 1966. **133**(2): p. 299-314.
64. Crotty, S., *A brief history of T cell help to B cells*. Nat Rev Immunol, 2015. **15**(3): p. 185-9.
65. Lavini, C., *The Thymus from Antiquity to the Present Day: the History of a Mysterious Gland*, in *Thymus Gland Pathology: Clinical, Diagnostic, and Therapeutic Features*, C. Lavini, et al., Editors. 2008, Springer Milan: Milano. p. 1-12.
66. Hodgkin, P.D., W.R. Heath, and A.G. Baxter, *The clonal selection theory: 50 years since the revolution*. Nat Immunol, 2007. **8**(10): p. 1019-26.
67. Masopust, D., et al., *A brief history of CD8 T cells*. Eur J Immunol, 2007. **37** Suppl 1: p. S103-10.
68. Janeway, C.A., Jr., *Approaching the asymptote? Evolution and revolution in immunology*. Cold Spring Harb Symp Quant Biol, 1989. **54** Pt 1: p. 1-13.
69. Medzhitov, R., P. Preston-Hurlburt, and C.A. Janeway, Jr., *A human homologue of the Drosophila Toll protein signals activation of adaptive immunity*. Nature, 1997. **388**(6640): p. 394-7.
70. Lemaitre, B., et al., *The dorsoventral regulatory gene cassette spatzle/Toll/cactus controls the potent antifungal response in Drosophila adults*. Cell, 1996. **86**(6): p. 973-83.
71. Poltorak, A., et al., *Defective LPS signaling in C3H/HeJ and C57BL/10ScCr mice: mutations in Tlr4 gene*. Science, 1998. **282**(5396): p. 2085-8.
72. Poltorak, A., et al., *Genetic and physical mapping of the Lps locus: identification of the toll-4 receptor as a candidate gene in the critical region*. Blood Cells Mol Dis, 1998. **24**(3): p. 340-55.
73. O'Neill, L.A., D. Golenbock, and A.G. Bowie, *The history of Toll-like receptors - redefining innate immunity*. Nat Rev Immunol, 2013. **13**(6): p. 453-60.
74. Yoneyama, M., et al., *The RNA helicase RIG-I has an essential function in double-stranded RNA-induced innate antiviral responses*. Nat Immunol, 2004. **5**(7): p. 730-7.
75. Andrejeva, J., et al., *The V proteins of paramyxoviruses bind the IFN-inducible RNA helicase, mda-5, and inhibit its activation of the IFN-beta promoter*. Proc Natl Acad Sci U S A, 2004. **101**(49): p. 17264-9.
76. Kato, H., et al., *Differential roles of MDA5 and RIG-I helicases in the recognition of RNA viruses*. Nature, 2006. **441**(7089): p. 101-5.
77. Hornung, V., et al., *5'-Triphosphate RNA is the ligand for RIG-I*. Science, 2006. **314**(5801): p. 994-7.
78. Goubau, D., et al., *Antiviral immunity via RIG-I-mediated recognition of RNA bearing 5'-diphosphates*. Nature, 2014. **514**(7522): p. 372-5.
79. Li, J., Y. Liu, and X. Zhang, *Murine coronavirus induces type I interferon in oligodendrocytes through recognition by RIG-I and MDA5*. J Virol, 2010. **84**(13): p. 6472-82.
80. Roth-Cross, J.K., S.J. Bender, and S.R. Weiss, *Murine coronavirus mouse hepatitis virus is recognized by MDA5 and induces type I interferon in brain macrophages/microglia*. J Virol, 2008. **82**(20): p. 9829-38.
81. Zust, R., et al., *Ribose 2'-O-methylation provides a molecular signature for the distinction of self and non-self mRNA dependent on the RNA sensor Mda5*. Nat Immunol, 2011. **12**(2): p. 137-43.
82. McCartney, S.A., et al., *MDA-5 recognition of a murine norovirus*. PLoS Pathog, 2008. **4**(7): p. e1000108.

83. Loo, Y.M., et al., *Distinct RIG-I and MDA5 signaling by RNA viruses in innate immunity*. J Virol, 2008. **82**(1): p. 335-45.
84. Errett, J.S., et al., *The essential, nonredundant roles of RIG-I and MDA5 in detecting and controlling West Nile virus infection*. J Virol, 2013. **87**(21): p. 11416-25.
85. Gitlin, L., et al., *Melanoma differentiation-associated gene 5 (MDA5) is involved in the innate immune response to Paramyxoviridae infection in vivo*. PLoS Pathog, 2010. **6**(1): p. e1000734.
86. Kim, W.K., et al., *Deficiency of melanoma differentiation-associated protein 5 results in exacerbated chronic postviral lung inflammation*. Am J Respir Crit Care Med, 2014. **189**(4): p. 437-48.
87. Banos-Lara Mdel, R., A. Ghosh, and A. Guerrero-Plata, *Critical role of MDA5 in the interferon response induced by human metapneumovirus infection in dendritic cells and in vivo*. J Virol, 2013. **87**(2): p. 1242-51.
88. Shingai, M., et al., *Differential type I IFN-inducing abilities of wild-type versus vaccine strains of measles virus*. J Immunol, 2007. **179**(9): p. 6123-33.
89. Grandvaux, N., et al., *Sustained activation of interferon regulatory factor 3 during infection by paramyxoviruses requires MDA5*. J Innate Immun, 2014. **6**(5): p. 650-62.
90. Yoneyama, M., et al., *Shared and unique functions of the DExD/H-box helicases RIG-I, MDA5, and LGP2 in antiviral innate immunity*. J Immunol, 2005. **175**(5): p. 2851-8.
91. Yoneyama, M., et al., *Viral RNA detection by RIG-I-like receptors*. Curr Opin Immunol, 2015. **32**: p. 48-53.
92. Gralinski, L.E. and R.S. Baric, *Molecular pathology of emerging coronavirus infections*. J Pathol, 2015. **235**(2): p. 185-95.
93. Berry, M., J. Gamielidien, and B.C. Fielding, *Identification of new respiratory viruses in the new millennium*. Viruses, 2015. **7**(3): p. 996-1019.
94. Bjarnadottir, T.K., et al., *Comprehensive repertoire and phylogenetic analysis of the G protein-coupled receptors in human and mouse*. Genomics, 2006. **88**(3): p. 263-73.
95. Malbon, C.C., *G proteins in development*. Nat Rev Mol Cell Biol, 2005. **6**(9): p. 689-701.
96. Lania, A.G., G. Mantovani, and A. Spada, *Mechanisms of disease: Mutations of G proteins and G-protein-coupled receptors in endocrine diseases*. Nat Clin Pract Endocrinol Metab, 2006. **2**(12): p. 681-93.
97. Krishnan, A. and H.B. Schioth, *The role of G protein-coupled receptors in the early evolution of neurotransmission and the nervous system*. J Exp Biol, 2015. **218**(Pt 4): p. 562-71.
98. Vassart, G. and S. Costagliola, *G protein-coupled receptors: mutations and endocrine diseases*. Nat Rev Endocrinol, 2011. **7**(6): p. 362-72.
99. Oh, D.Y. and W.S. Lagakos, *The role of G-protein-coupled receptors in mediating the effect of fatty acids on inflammation and insulin sensitivity*. Curr Opin Clin Nutr Metab Care, 2011. **14**(4): p. 322-7.
100. Kamp, M.E., Y. Liu, and A. Kortholt, *Function and Regulation of Heterotrimeric G Proteins during Chemotaxis*. Int J Mol Sci, 2016. **17**(1).
101. Bansal, G., K.M. Druey, and Z. Xie, *R4 RGS proteins: regulation of G-protein signaling and beyond*. Pharmacol Ther, 2007. **116**(3): p. 473-95.
102. Willars, G.B., *Mammalian RGS proteins: multifunctional regulators of cellular signalling*. Semin Cell Dev Biol, 2006. **17**(3): p. 363-76.

103. Thompson, B.D., et al., *Inhibition of G alpha i2 activation by G alpha i3 in CXCR3-mediated signaling*. J Biol Chem, 2007. **282**(13): p. 9547-55.
104. Jiang, M., et al., *Mouse gene knockout and knockin strategies in application to alpha subunits of Gi/Go family of G proteins*. Methods Enzymol, 2002. **344**: p. 277-98.
105. Li, P., et al., *Toll-like receptor-induced inflammatory cytokines are suppressed by gain of function or overexpression of Galpha(i2) protein*. Inflammation, 2012. **35**(5): p. 1611-7.
106. Fan, H., et al., *Heterotrimeric Galpha(i) proteins are regulated by lipopolysaccharide and are anti-inflammatory in endotoxemia and polymicrobial sepsis*. Biochim Biophys Acta, 2011. **1813**(3): p. 466-72.
107. DiBello, P.R., et al., *Selective uncoupling of RGS action by a single point mutation in the G protein alpha-subunit*. J Biol Chem, 1998. **273**(10): p. 5780-4.
108. Huang, X., et al., *Pleiotropic phenotype of a genomic knock-in of an RGS-insensitive G184S Gnai2 allele*. Mol Cell Biol, 2006. **26**(18): p. 6870-9.
109. Jin, T., X. Xu, and D. Hereld, *Chemotaxis, chemokine receptors and human disease*. Cytokine, 2008. **44**(1): p. 1-8.
110. Su, H.C., H. Jing, and Q. Zhang, *DOCK8 deficiency*. Ann N Y Acad Sci, 2011. **1246**: p. 26-33.
111. Notarangelo, L.D. and R. Badolato, *Leukocyte trafficking in primary immunodeficiencies*. J Leukoc Biol, 2009. **85**(3): p. 335-43.
112. Crowley, C.A., et al., *An inherited abnormality of neutrophil adhesion. Its genetic transmission and its association with a missing protein*. N Engl J Med, 1980. **302**(21): p. 1163-8.
113. Luhn, K., et al., *The gene defective in leukocyte adhesion deficiency II encodes a putative GDP-fucose transporter*. Nat Genet, 2001. **28**(1): p. 69-72.
114. Lubke, T., et al., *Complementation cloning identifies CDG-IIc, a new type of congenital disorders of glycosylation, as a GDP-fucose transporter deficiency*. Nat Genet, 2001. **28**(1): p. 73-6.
115. Moser, M., et al., *Kindlin-3 is essential for integrin activation and platelet aggregation*. Nat Med, 2008. **14**(3): p. 325-30.
116. Hanna, S. and A. Etzioni, *Leukocyte adhesion deficiencies*. Ann N Y Acad Sci, 2012. **1250**: p. 50-5.
117. Park, C.O. and T.S. Kupper, *The emerging role of resident memory T cells in protective immunity and inflammatory disease*. Nat Med, 2015. **21**(7): p. 688-97.
118. Zhang, Q., et al., *DOCK8 regulates lymphocyte shape integrity for skin antiviral immunity*. J Exp Med, 2014. **211**(13): p. 2549-66.
119. Hernandez, P.A., et al., *Mutations in the chemokine receptor gene CXCR4 are associated with WHIM syndrome, a combined immunodeficiency disease*. Nat Genet, 2003. **34**(1): p. 70-4.
120. Leiding, J.W. and S.M. Holland, *Warts and all: human papillomavirus in primary immunodeficiencies*. J Allergy Clin Immunol, 2012. **130**(5): p. 1030-48.
121. Smith-Garvin, J.E., G.A. Koretzky, and M.S. Jordan, *T cell activation*. Annu Rev Immunol, 2009. **27**: p. 591-619.
122. Tuosto, L. and O. Acuto, *CD28 affects the earliest signaling events generated by TCR engagement*. Eur J Immunol, 1998. **28**(7): p. 2131-42.
123. Viola, A., et al., *T lymphocyte costimulation mediated by reorganization of membrane microdomains*. Science, 1999. **283**(5402): p. 680-2.

124. Yokosuka, T. and T. Saito, *Dynamic regulation of T-cell costimulation through TCR-CD28 microclusters*. Immunol Rev, 2009. **229**(1): p. 27-40.
125. Ha, J.H., et al., *Lysophosphatidic acid stimulates epithelial to mesenchymal transition marker Slug/Snail2 in ovarian cancer cells via Galphai2, Src, and HIF1alpha signaling nexus*. Oncotarget, 2016.
126. Lin, C.H., et al., *Thrombin-induced CCAAT/enhancer-binding protein beta activation and IL-8/CXCL8 expression via MEKK1, ERK, and p90 ribosomal S6 kinase 1 in lung epithelial cells*. J Immunol, 2014. **192**(1): p. 338-48.
127. Nanki, T. and P.E. Lipsky, *Stimulation of T-Cell activation by CXCL12/stromal cell derived factor-1 involves a G-protein mediated signaling pathway*. Cell Immunol, 2001. **214**(2): p. 145-54.
128. Gollmer, K., et al., *CCL21 mediates CD4+ T-cell costimulation via a DOCK2/Rac-dependent pathway*. Blood, 2009. **114**(3): p. 580-8.
129. DeWire, S.M., et al., *Beta-arrestins and cell signaling*. Annu Rev Physiol, 2007. **69**: p. 483-510.
130. Nairismagi, M.L., et al., *JAK-STAT and G-protein-coupled receptor signaling pathways are frequently altered in epitheliotropic intestinal T-cell lymphoma*. Leukemia, 2016. **30**(6): p. 1311-9.
131. Lyons, J., et al., *Two G protein oncogenes in human endocrine tumors*. Science, 1990. **249**(4969): p. 655-9.
132. *NHLBI Exome Sequencing Project (ESP)*. 2015 [cited 2015 6/1/2015]; Available from: <http://evs.gs.washington.edu/EVS/>.
133. Coleman, D.E., et al., *Structures of active conformations of Gi alpha 1 and the mechanism of GTP hydrolysis*. Science, 1994. **265**(5177): p. 1405-12.
134. Noel, J.P., H.E. Hamm, and P.B. Sigler, *The 2.2 A crystal structure of transducin-alpha complexed with GTP gamma S*. Nature, 1993. **366**(6456): p. 654-63.
135. Nishina, H., et al., *Significance of Thr182 in the nucleotide-exchange and GTP-hydrolysis reactions of the alpha subunit of GTP-binding protein Gi2*. J Biochem, 1995. **118**(5): p. 1083-9.
136. Zurita, A., et al., *Obligatory role in GTP hydrolysis for the amide carbonyl oxygen of the Mg(2+)-coordinating Thr of regulatory GTPases*. Proc Natl Acad Sci U S A, 2010. **107**(21): p. 9596-601.
137. Hermouet, S., et al., *Activating and inactivating mutations of the alpha subunit of Gi2 protein have opposite effects on proliferation of NIH 3T3 cells*. Proc Natl Acad Sci U S A, 1991. **88**(23): p. 10455-9.
138. Kaur, K., et al., *RGS-insensitive Galpha subunits: probes of Galpha subtype-selective signaling and physiological functions of RGS proteins*. Methods Mol Biol, 2011. **756**: p. 75-98.
139. Moutsopoulos, N.M., et al., *Defective neutrophil recruitment in leukocyte adhesion deficiency type I disease causes local IL-17-driven inflammatory bone loss*. Sci Transl Med, 2014. **6**(229): p. 229ra40.
140. Berman, D.M., T.M. Wilkie, and A.G. Gilman, *GAIP and RGS4 are GTPase-activating proteins for the Gi subfamily of G protein alpha subunits*. Cell, 1996. **86**(3): p. 445-52.
141. Flanagan, S.E., et al., *Activating germline mutations in STAT3 cause early-onset multi-organ autoimmune disease*. Nat Genet, 2014. **46**(8): p. 812-4.

142. Barren, B. and N.O. Artemyev, *Mechanisms of dominant negative G-protein alpha subunits*. J Neurosci Res, 2007. **85**(16): p. 3505-14.
143. Marivin, A., et al., *Dominant-negative Galpha subunits are a mechanism of dysregulated heterotrimeric G protein signaling in human disease*. Sci Signal, 2016. **9**(423): p. ra37.
144. Bacart, J., et al., *The BRET technology and its application to screening assays*. Biotechnol J, 2008. **3**(3): p. 311-24.
145. Lippert, E., Y. Jacques, and S. Hermouet, *Positive regulation of human T cell activation by Gi2 proteins and interleukin-8*. J Leukoc Biol, 2000. **67**(5): p. 742-8.
146. Huang, T.T., et al., *TCR-mediated hyper-responsiveness of autoimmune Galphai2(-/-) mice is an intrinsic naive CD4(+) T cell disorder selective for the Galphai2 subunit*. Int Immunol, 2003. **15**(11): p. 1359-67.
147. Mosenden, R. and K. Tasken, *Cyclic AMP-mediated immune regulation--overview of mechanisms of action in T cells*. Cell Signal, 2011. **23**(6): p. 1009-16.
148. Lucas, C.L., et al., *Dominant-activating germline mutations in the gene encoding the PI(3)K catalytic subunit p110delta result in T cell senescence and human immunodeficiency*. Nat Immunol, 2014. **15**(1): p. 88-97.
149. Lucas, C.L., et al., *Heterozygous splice mutation in PIK3R1 causes human immunodeficiency with lymphoproliferation due to dominant activation of PI3K*. J Exp Med, 2014. **211**(13): p. 2537-47.
150. Angulo, I., et al., *Phosphoinositide 3-kinase delta gene mutation predisposes to respiratory infection and airway damage*. Science, 2013. **342**(6160): p. 866-71.
151. Deau, M.C., et al., *A human immunodeficiency caused by mutations in the PIK3R1 gene*. J Clin Invest, 2014. **124**(9): p. 3923-8.
152. Fox, C.J., P.S. Hammerman, and C.B. Thompson, *Fuel feeds function: energy metabolism and the T-cell response*. Nat Rev Immunol, 2005. **5**(11): p. 844-52.
153. Carneiro-Sampaio, M. and A. Coutinho, *Tolerance and autoimmunity: lessons at the bedside of primary immunodeficiencies*. Adv Immunol, 2007. **95**: p. 51-82.
154. Notarangelo, L.D., E. Gambineri, and R. Badolato, *Immunodeficiencies with autoimmune consequences*. Adv Immunol, 2006. **89**: p. 321-70.
155. Bjursten, M., O.H. Hultgren, and E. Hultgren Hornquist, *Enhanced pro-inflammatory cytokine production in Galphai2-deficient mice on colitis prone and colitis resistant 129Sv genetic backgrounds*. Cell Immunol, 2004. **228**(2): p. 77-80.
156. Cho, H., et al., *The loss of RGS protein-Galphi(i2) interactions results in markedly impaired mouse neutrophil trafficking to inflammatory sites*. Mol Cell Biol, 2012. **32**(22): p. 4561-71.
157. Derry, J.M., H.D. Ochs, and U. Francke, *Isolation of a novel gene mutated in Wiskott-Aldrich syndrome*. Cell, 1994. **78**(4): p. 635-44.
158. Takenawa, T. and S. Suetsugu, *The WASP-WAVE protein network: connecting the membrane to the cytoskeleton*. Nat Rev Mol Cell Biol, 2007. **8**(1): p. 37-48.
159. Arason, G.J., G.H. Jorgensen, and B.R. Ludviksson, *Primary immunodeficiency and autoimmunity: lessons from human diseases*. Scand J Immunol, 2010. **71**(5): p. 317-28.
160. Saifi, M. and C.A. Wysocki, *Autoimmune Disease in Primary Immunodeficiency: At the Crossroads of Anti-Infective Immunity and Self-Tolerance*. Immunol Allergy Clin North Am, 2015. **35**(4): p. 731-52.

161. Uzel, G., et al., *Dominant gain-of-function STAT1 mutations in FOXP3 wild-type immune dysregulation-polyendocrinopathy-enteropathy-X-linked-like syndrome*. J Allergy Clin Immunol, 2013. **131**(6): p. 1611-23.
162. Rudolph, U., et al., *Gi2 alpha protein deficiency: a model of inflammatory bowel disease*. J Clin Immunol, 1995. **15**(6 Suppl): p. 101S-105S.
163. Jameson, E.E., et al., *Real-time detection of basal and stimulated G protein GTPase activity using fluorescent GTP analogues*. J Biol Chem, 2005. **280**(9): p. 7712-9.
164. Sprang, S.R., *Invited review: Activation of G proteins by GTP and the mechanism of Galpha-catalyzed GTP hydrolysis*. Biopolymers, 2016. **105**(8): p. 449-62.
165. Global Burden of Disease Study, C., *Global, regional, and national incidence, prevalence, and years lived with disability for 301 acute and chronic diseases and injuries in 188 countries, 1990-2013: a systematic analysis for the Global Burden of Disease Study 2013*. Lancet, 2015. **386**(9995): p. 743-800.
166. Heikkinen, T. and A. Jarvinen, *The common cold*. Lancet, 2003. **361**(9351): p. 51-9.
167. Makela, M.J., et al., *Viruses and bacteria in the etiology of the common cold*. J Clin Microbiol, 1998. **36**(2): p. 539-42.
168. Greenberg, S.B., *Update on rhinovirus and coronavirus infections*. Semin Respir Crit Care Med, 2011. **32**(4): p. 433-46.
169. Jain, S., et al., *Community-acquired pneumonia requiring hospitalization among U.S. children*. N Engl J Med, 2015. **372**(9): p. 835-45.
170. Hasegawa, K., J.M. Mansbach, and C.A. Camargo, Jr., *Infectious pathogens and bronchiolitis outcomes*. Expert Rev Anti Infect Ther, 2014. **12**(7): p. 817-28.
171. Pavia, A.T., *Viral infections of the lower respiratory tract: old viruses, new viruses, and the role of diagnosis*. Clin Infect Dis, 2011. **52 Suppl 4**: p. S284-9.
172. Gaunt, E.R., et al., *Disease burden of the most commonly detected respiratory viruses in hospitalized patients calculated using the disability adjusted life year (DALY) model*. J Clin Virol, 2011. **52**(3): p. 215-21.
173. Gitlin, L., et al., *Essential role of mda-5 in type I IFN responses to polyriboinosinic:polyribocytidylic acid and encephalomyocarditis picornavirus*. Proc Natl Acad Sci U S A, 2006. **103**(22): p. 8459-64.
174. McCartney, S.A., et al., *RNA sensor-induced type I IFN prevents diabetes caused by a beta cell-tropic virus in mice*. J Clin Invest, 2011. **121**(4): p. 1497-507.
175. Wang, J.P., et al., *MDA5 and MAVS mediate type I interferon responses to coxsackie B virus*. J Virol, 2010. **84**(1): p. 254-60.
176. Jin, Y.H., et al., *Melanoma differentiation-associated gene 5 is critical for protection against Theiler's virus-induced demyelinating disease*. J Virol, 2012. **86**(3): p. 1531-43.
177. Wang, Q., et al., *MDA5 and TLR3 initiate pro-inflammatory signaling pathways leading to rhinovirus-induced airways inflammation and hyperresponsiveness*. PLoS Pathog, 2011. **7**(5): p. e1002070.
178. Slater, L., et al., *Co-ordinated role of TLR3, RIG-I and MDA5 in the innate response to rhinovirus in bronchial epithelium*. PLoS Pathog, 2010. **6**(11): p. e1001178.
179. Wang, Q., et al., *Role of double-stranded RNA pattern recognition receptors in rhinovirus-induced airway epithelial cell responses*. J Immunol, 2009. **183**(11): p. 6989-97.

180. Triantafilou, K., et al., *Human rhinovirus recognition in non-immune cells is mediated by Toll-like receptors and MDA-5, which trigger a synergetic pro-inflammatory immune response*. *Virulence*, 2011. **2**(1): p. 22-9.
181. Delaloye, J., et al., *Innate immune sensing of modified vaccinia virus Ankara (MVA) is mediated by TLR2-TLR6, MDA-5 and the NALP3 inflammasome*. *PLoS Pathog*, 2009. **5**(6): p. e1000480.
182. Pichlmair, A., et al., *Activation of MDA5 requires higher-order RNA structures generated during virus infection*. *J Virol*, 2009. **83**(20): p. 10761-9.
183. Wu, B., et al., *Structural basis for dsRNA recognition, filament formation, and antiviral signal activation by MDA5*. *Cell*, 2013. **152**(1-2): p. 276-89.
184. Rice, G.I., et al., *Gain-of-function mutations in IFIH1 cause a spectrum of human disease phenotypes associated with upregulated type I interferon signaling*. *Nat Genet*, 2014. **46**(5): p. 503-9.
185. Oda, H., et al., *Aicardi-Goutieres syndrome is caused by IFIH1 mutations*. *Am J Hum Genet*, 2014. **95**(1): p. 121-5.
186. Rutsch, F., et al., *A specific IFIH1 gain-of-function mutation causes Singleton-Merten syndrome*. *Am J Hum Genet*, 2015. **96**(2): p. 275-82.
187. Van Eyck, L., et al., *IFIH1 mutation causes systemic lupus erythematosus with selective IgA-deficiency*. *Arthritis Rheumatol*, 2015.
188. Siren, J., et al., *Retinoic acid inducible gene-I and mda-5 are involved in influenza A virus-induced expression of antiviral cytokines*. *Microbes Infect*, 2006. **8**(8): p. 2013-20.
189. Benitez, A.A., et al., *In Vivo RNAi Screening Identifies MDA5 as a Significant Contributor to the Cellular Defense against Influenza A Virus*. *Cell Rep*, 2015. **11**(11): p. 1714-26.
190. Ciancanelli, M.J., et al., *Infectious disease. Life-threatening influenza and impaired interferon amplification in human IRF7 deficiency*. *Science*, 2015. **348**(6233): p. 448-53.
191. Arora, R., M. Kaplan, and M. Nelson, *Enterovirus-specific IgG in intravenous immunoglobulin preparations*. *Ann Allergy Asthma Immunol*, 2011. **106**(6): p. 544-5.
192. Galama, J.M., M. Gielen, and C.M. Weemaes, *Enterovirus antibody titers after IVIG replacement in agammaglobulinemic children*. *Clin Microbiol Infect*, 2000. **6**(11): p. 630-2.
193. Jaidane, H., et al., *Enteroviruses and type 1 diabetes: towards a better understanding of the relationship*. *Rev Med Virol*, 2010. **20**(5): p. 265-80.
194. Rodriguez-Calvo, T. and M.G. von Herrath, *Enterovirus infection and type 1 diabetes: closing in on a link?* *Diabetes*, 2015. **64**(5): p. 1503-5.
195. Wiszniewski, W., et al., *TM4SF20 ancestral deletion and susceptibility to a pediatric disorder of early language delay and cerebral white matter hyperintensities*. *Am J Hum Genet*, 2013. **93**(2): p. 197-210.
196. Bochkov, Y.A., et al., *Improved molecular typing assay for rhinovirus species A, B, and C*. *J Clin Microbiol*, 2014. **52**(7): p. 2461-71.
197. Case, D.A., et al., *AMBER 2015*. 2015: University of California, San Francisco.
198. Salomon-Ferrer, R., et al., *Routine microsecond molecular dynamics simulations with AMBER – Part II: Particle Mesh Ewald*. *Journal of Chemical Theory and Computation*, 2013. **9**(9): p. 3878-3888.
199. Hornak, V., et al., *Comparison of multiple Amber force fields and development of improved protein backbone parameters*. *Proteins*, 2006. **65**(3): p. 712-25.

200. Meagher, K.L., L.T. Redman, and H.A. Carlson, *Development of polyphosphate parameters for use with the AMBER force field*. J Comput Chem, 2003. **24**(9): p. 1016-25.
201. Li, P., et al., *Rational Design of Particle Mesh Ewald Compatible Lennard-Jones Parameters for +2 Metal Cations in Explicit Solvent*. Journal of Chemical Theory and Computation, 2013. **9**(6): p. 2733-2748.
202. Jing, H., et al., *Somatic reversion in dedicator of cytokinesis 8 immunodeficiency modulates disease phenotype*. J Allergy Clin Immunol, 2014. **133**(6): p. 1667-75.
203. de Chasseval, R. and J.P. de Villartay, *High level transient gene expression in human lymphoid cells by SV40 large T antigen boost*. Nucleic Acids Res, 1992. **20**(2): p. 245-50.
204. Chappier, A., et al., *Human complete Stat-1 deficiency is associated with defective type I and II IFN responses in vitro but immunity to some low virulence viruses in vivo*. J Immunol, 2006. **176**(8): p. 5078-83.
205. Reynolds, S.D., et al., *Airway Progenitor Clone Formation is Enhanced by Y-27632-dependent Changes in the Transcriptome*. Am J Respir Cell Mol Biol, 2016.
206. Poole, A., et al., *Dissecting childhood asthma with nasal transcriptomics distinguishes subphenotypes of disease*. J Allergy Clin Immunol, 2014. **133**(3): p. 670-8 e12.
207. Suprynowicz, F.A., et al., *Conditionally reprogrammed cells represent a stem-like state of adult epithelial cells*. Proc Natl Acad Sci U S A, 2012. **109**(49): p. 20035-40.
208. Lin, R., et al., *Selective DNA binding and association with the CREB binding protein coactivator contribute to differential activation of alpha/beta interferon genes by interferon regulatory factors 3 and 7*. Mol Cell Biol, 2000. **20**(17): p. 6342-53.
209. Hanawa, H., et al., *Efficient gene transfer into rhesus repopulating hematopoietic stem cells using a simian immunodeficiency virus-based lentiviral vector system*. Blood, 2004. **103**(11): p. 4062-9.
210. Lee, W.M., et al., *Growth of human rhinovirus in H1-HeLa cell suspension culture and purification of virions*. Methods Mol Biol, 2015. **1221**: p. 49-61.
211. Lee, W.M., et al., *Infectivity assays of human rhinovirus-A and -B serotypes*. Methods Mol Biol, 2015. **1221**: p. 71-81.
212. Lee, W.M., et al., *Molecular identification and quantification of human rhinoviruses in respiratory samples*. Methods Mol Biol, 2015. **1221**: p. 25-38.
213. Stewart, S.A., et al., *Lentivirus-delivered stable gene silencing by RNAi in primary cells*. RNA, 2003. **9**(4): p. 493-501.
214. Kingston, R.E., C.A. Chen, and H. Okayama, *Calcium phosphate transfection*. Curr Protoc Cell Biol, 2003. **Chapter 20**: p. Unit 20 3.
215. Balish, A.L., J.M. Katz, and A.I. Klimov, *Influenza: propagation, quantification, and storage*. Curr Protoc Microbiol, 2013. **Chapter 15**: p. Unit 15G 1.
216. Munir, S., et al., *Nonstructural proteins 1 and 2 of respiratory syncytial virus suppress maturation of human dendritic cells*. J Virol, 2008. **82**(17): p. 8780-96.
217. Wong, Y.H., et al., *Mutant alpha subunits of Gi2 inhibit cyclic AMP accumulation*. Nature, 1991. **351**(6321): p. 63-5.
218. Pace, A.M., M. Faure, and H.R. Bourne, *Gi2-mediated activation of the MAP kinase cascade*. Mol Biol Cell, 1995. **6**(12): p. 1685-95.
219. Bryant, V.L. and C.A. Slade, *Chemokines, their receptors and human disease: the good, the bad and the itchy*. Immunol Cell Biol, 2015. **93**(4): p. 364-71.
220. Corbisier, J., et al., *Biased signaling at chemokine receptors*. J Biol Chem, 2015. **290**(15): p. 9542-54.

221. Hwang, I.Y., et al., *An essential role for RGS protein/Galphai2 interactions in B lymphocyte-directed cell migration and trafficking*. J Immunol, 2015. **194**(5): p. 2128-39.
222. Todoric, K., et al., *Autoimmunity in immunodeficiency*. Curr Allergy Asthma Rep, 2013. **13**(4): p. 361-70.
223. Moulding, D.A., et al., *Actin cytoskeletal defects in immunodeficiency*. Immunol Rev, 2013. **256**(1): p. 282-99.
224. Bour-Jordan, H., et al., *Intrinsic and extrinsic control of peripheral T-cell tolerance by costimulatory molecules of the CD28/ B7 family*. Immunol Rev, 2011. **241**(1): p. 180-205.
225. Harris, N.L. and F. Ronchese, *The role of B7 costimulation in T-cell immunity*. Immunol Cell Biol, 1999. **77**(4): p. 304-11.
226. Stanners, J., et al., *Interaction between G proteins and tyrosine kinases upon T cell receptor.CD3-mediated signaling*. J Biol Chem, 1995. **270**(51): p. 30635-42.
227. Ngai, J., et al., *Interplay between the heterotrimeric G-protein subunits Galphaq and Galphai2 sets the threshold for chemotaxis and TCR activation*. BMC Immunol, 2009. **10**: p. 27.
228. Rozengurt, E., *Mitogenic signaling pathways induced by G protein-coupled receptors*. J Cell Physiol, 2007. **213**(3): p. 589-602.
229. Frauwirth, K.A., et al., *The CD28 signaling pathway regulates glucose metabolism*. Immunity, 2002. **16**(6): p. 769-77.
230. Hirahara, K., et al., *Helper T-cell differentiation and plasticity: insights from epigenetics*. Immunology, 2011. **134**(3): p. 235-45.
231. Milner, J.D., et al., *Impaired T(H)17 cell differentiation in subjects with autosomal dominant hyper-IgE syndrome*. Nature, 2008. **452**(7188): p. 773-6.
232. Holland, S.M., et al., *STAT3 mutations in the hyper-IgE syndrome*. N Engl J Med, 2007. **357**(16): p. 1608-19.
233. Minegishi, Y., et al., *Dominant-negative mutations in the DNA-binding domain of STAT3 cause hyper-IgE syndrome*. Nature, 2007. **448**(7157): p. 1058-62.
234. Koskela, H.L., et al., *Somatic STAT3 mutations in large granular lymphocytic leukemia*. N Engl J Med, 2012. **366**(20): p. 1905-13.
235. Pilati, C., et al., *Somatic mutations activating STAT3 in human inflammatory hepatocellular adenomas*. J Exp Med, 2011. **208**(7): p. 1359-66.
236. Ram, P.T., C.M. Horvath, and R. Iyengar, *Stat3-mediated transformation of NIH-3T3 cells by the constitutively active Q205L Galphao protein*. Science, 2000. **287**(5450): p. 142-4.
237. Yuen, J.W., et al., *Activation of STAT3 by specific Galpha subunits and multiple Gbetagamma dimers*. Int J Biochem Cell Biol, 2010. **42**(6): p. 1052-9.
238. Ozen, M., et al., *Recurrent Salmonella bacteremia in interleukin-12 receptor beta1 deficiency*. J Trop Pediatr, 2006. **52**(4): p. 296-8.
239. Bustamante, J., et al., *Mendelian susceptibility to mycobacterial disease: genetic, immunological, and clinical features of inborn errors of IFN-gamma immunity*. Semin Immunol, 2014. **26**(6): p. 454-70.
240. Puel, A., et al., *Inborn errors of human IL-17 immunity underlie chronic mucocutaneous candidiasis*. Curr Opin Allergy Clin Immunol, 2012. **12**(6): p. 616-22.
241. Cohen, J.I., *Primary Immunodeficiencies Associated with EBV Disease*. Curr Top Microbiol Immunol, 2015. **390**(Pt 1): p. 241-65.
242. Zhang, S.Y., et al., *TLR3 immunity to infection in mice and humans*. Curr Opin Immunol, 2013. **25**(1): p. 19-33.

243. Zhang, S.Y., et al., *TLR3 deficiency in patients with herpes simplex encephalitis*. *Science*, 2007. **317**(5844): p. 1522-7.
244. Casanova, J.L., L. Abel, and L. Quintana-Murci, *Human TLRs and IL-1Rs in host defense: natural insights from evolutionary, epidemiological, and clinical genetics*. *Annu Rev Immunol*, 2011. **29**: p. 447-91.
245. Yao, H., et al., *ATP-dependent effector-like functions of RIG-I-like receptors*. *Mol Cell*, 2015. **58**(3): p. 541-8.
246. von Bernuth, H., et al., *Pyogenic bacterial infections in humans with MyD88 deficiency*. *Science*, 2008. **321**(5889): p. 691-6.
247. Picard, C., et al., *Pyogenic bacterial infections in humans with IRAK-4 deficiency*. *Science*, 2003. **299**(5615): p. 2076-9.
248. Ferkol, T. and D. Schraufnagel, *The Global Burden of Respiratory Disease*. *Annals of the American Thoracic Society*, 2014. **11**(3): p. 404-406.
249. Hnin, K., et al., *Prolonged antibiotics for non-cystic fibrosis bronchiectasis in children and adults*. *Cochrane Database Syst Rev*, 2015(8): p. CD001392.
250. Chiu, C. and P.J. Openshaw, *Antiviral B cell and T cell immunity in the lungs*. *Nat Immunol*, 2015. **16**(1): p. 18-26.
251. Mukherjee, S. and N.W. Lukacs, *Innate immune responses to respiratory syncytial virus infection*. *Curr Top Microbiol Immunol*, 2013. **372**: p. 139-54.
252. Zeng, M., et al., *MAVS, cGAS, and endogenous retroviruses in T-independent B cell responses*. *Science*, 2014. **346**(6216): p. 1486-92.